LIGHT SCATTERING SIMULATIONS USING COMPLEX

SURFACE MICROSTRUCTURE MODELS

by

MORGAN THOMAS SCHRAMM

A THESIS

Presented to Department of Computer and Information Science
and to Graduate School of the University of Oregon
in partial fulfillment of the requirement
for the degree of
Master of Science

August 1995

"Light Scattering Simulations Using Complex Surface Microstructure Models," a thesis prepared by Morgan Thomas Schramm in partial fulfillment of the requirements for the Master of Science degree in the Department of Computer and Information Science. This thesis has been approved and accepted by:

_____

Dr. Gary W. Meyer, Advisor

7/19/95

_____

Date

Committee in charge: Dr. Gary W. Meyer

Accepted by:

_____

Vice Provost and Dean of the Graduate School

An Abstract of the Thesis of

Morgan Thomas Schramm   for the degree of   Master of Science

in the Department of Computer and Information Science

to be taken   August 1995

Title: LIGHT SCATTERING SIMULATION USING COMPLEX SURFACE

MICROSTRUCTURE MODELS

Approved: _____

Dr. Gary W. Meyer

Models of surface and subsurface microstructure were created and Monte Carlo light scattering simulations were performed to generate accurate surface reflectance functions. Iridescent hummingbird feathers and paper sheets were studied in order to obtain detailed information about their morphology. It is known that measured spectral response curves of hummingbird feathers deviate from those of corresponding ideal thin films. The reflectance functions generated showed similar deviations. For paper, a simple layered model was constructed and the resulting reflectance functions compared favorably with theoretical calculations used to determine diffuse reflectance. Measurements of the spatial scattering of light from paper revealed that a significant amount of back scatter was present in some cases and that a certain amount of anisotropy was also present. By constructing models of the paper web and its coatings, these effects were reproduced and possible origins of these effects were indicated.

CURRICULUM VITA

NAME OF AUTHOR: Morgan Thomas Schramm

PLACE OF BIRTH: Fresno, California

DATE OF BIRTH: March 1, 1969

GRADUATE AND UNDERGRADUATE SCHOOLS ATTENDED:

> University of Oregon
> University of California at Santa Barbara

DEGREES AWARDED:

> Master of Science in Computer Science, 1995, University of Oregon
> Bachelor of Science in Electrical Engineering, 1991, University of California

AREAS OF SPECIAL INTEREST:

> Computer Graphics
> Audio/Image Processing
> Human Computer Interaction

PROFESSIONAL EXPERIENCE:

> Graduate Research/Teaching Fellow, Department of Computer and Information Science, University of Oregon, March 1993-June 1995

> CAD Design Engineer, National Semiconductor, Sunnyvale, California, July 1991-September 1993

ACKNOWLEDGMENTS

TABLE OF CONTENTS

LIST OF TABLES

LIST OF FIGURES

CHAPTER I

INTRODUCTION

Realistic synthetic images are generated by simulating the interaction of light with the objects modeled in a scene. An image is constructed by determining the light scattering events that take place in the scene and then calculating the characteristics of the light that reaches the eye of an observer or synthetic camera placed in the environment. A global illumination model, such as raytracing, is used to describe the way light scatters from surface to surface. Local illumination models describe the specific characteristics of the light scattered from a point on a given surface. A primary focus of research in the field of realistic image synthesis has been the determination of appropriate local reflectance functions for a large variety of materials. A software tool recently developed by Gondek, Meyer, and Newman (1994) allows for the determination of general surface reflectance functions based on computer simulations of the interaction of light with morphological models of the microstructure of these surfaces. This software tool simulates the operation of goniospectrophotometer, which is a measurement instrument used to record the complete spectral and spatial characteristics of light scattered from a surface. This thesis explores the application of this tool in the determination of accurate reflectance functions for two different complex surfaces.

In computer graphics, reflectance functions are described by various local illumination models. These models are designed to calculate the appearance of a object given the spatial orientation and spectral intensity of the light incident upon its surfaces. Some of the phenomenon light may undergo when it is incident upon a object include: reflection from the object's surfaces, transmission through the object, and absorption by the object. When light interacts with complex surfaces, such as the ones we will be

studying in this work, it may be subject to all three phenomena. These three mechanisms contribute to the overall scattering characteristics of a material. The spectral characteristics of this scattering define such attributes as the color or hue of an object whereas the spatial characteristics of this scattering define the gloss or luster of the object. By capturing these effects, a local reflectance function can be thought of as a mathematical description of these optical characteristics. Given the spectral and spatial properties of the incident illumination, a local reflectance function will describe the spectral and spatial distribution of the light scattered from a given surface.

One of the most widely used local illumination models is the one developed by Phong Bui-Tou in 1975. This model describes the light scattered from a surface in terms of two distinct components, a specular and a diffuse component. In practice, a third component is also added to account for the ambient lighting conditions of a scene. While the Phong model provides an easy method for representing the scattering function for a broad class of surfaces, it is difficult to find the appropriate parameters for a given surface in anything but an ad-hoc fashion. There is no way to link the model's parameters to measurable characteristics of a real object since this model is not physically based. Developing reflectance models that are more physically valid has been an area of ongoing research in the field of computer graphics.

An alternative to the Phong model was proposed by Blinn (1977). The Blinn model includes a more accurate specular term than the one used in the Phong model. This new specular term incorporates the Fresnel equations in order to calculate the reflectivity for uniform, optically smooth surfaces. The resulting reflectance function captures some of the subtle effects produced by polished metal and also represents the specular lobe at glancing angles in a more accurate fashion.

Another improvement in the accuracy of reflectance functions was realized in the model developed by Cook and Torrance (1982). This model uses an energy based approach to derive the reflectivity of a surface and is based upon earlier work on physically based reflectance functions done by Torrance and Sparrow (1966, 1967). The specular term is computed by modeling the surface as a collection of optically smooth microfacets. The distribution and orientation of these facets are controlled statistically by functions that represent the roughness of real surfaces. This model also included a wavelength based Fresnel term which correctly modeled the shift in color of the specular reflection relative to the incident angle of illumination and was absent in both the Phong and Blinn models. The Cook-Torrance functions were also fully bidirectional as they were dependent on both the incident and exitance directions.

In order to accurately represent the scattering of light from a surface, a reflectance function must relate the ratio of incoming light to exiting light for all angles both in the incidence and exitance directions. In addition, these ratios should be separately available across the entire spectrum of visible light in order to accurately represent the reflectance properties of surfaces whose spatial and specular characteristics are intertwined. The specular composition of light scattered from surfaces such as thin films, for example, is directly related to the spatial geometry of the illumination and viewing conditions. In order to capture the effects from such a surface, the reflectance function must be able to represent the spectral composition of the scattered light for all directions relative to the surface normal. The bidirectional reflectance distribution function (BRDF) introduced to the computer graphics community by Kajia (1986) is such a representation. The BRDF description specifies the ratio of reflected radiance to incident flux density for all incident and reflected directions. In the most general form of the BRDF, this ratio is separately recorded for all wavelengths across the spectrum.

Kajia showed that previously developed local illumination models could be recast as special cases of the BRDF. He also used the BRDF representation to capture anisotropic reflectance functions, which are the result of preferential orientation in the microgeometry of a surface. Materials such as cloth, or brushed metal, have microfeatures that are preferentially oriented in the plane of their surfaces and thus will produce reflectance functions which are not symmetric about the normal of these surfaces. This anisotropy in the reflectance function can only be represented by a bidirectional function such as the BRDF. Through this work, Kajia was able to broaden the class of surfaces that could be accurately represented by reflectance functions used in computer graphics.

Cabral et al. (1987) used a BRDF to represent the scattering function of the light reflected from an explicit surface model. In this approach an array of triangular microfacets was used to represent a surface and a reflectance function was then computed by considering the self-shadowing and masking effects that a beam of light covering a significant area of this surface would be subject to. The resulting reflectance distribution is captured in a hemisphere which has been discretely divided into a number of cells and positioned atop the surface. A spherical harmonic representation of the BRDF is computed from the reflectance values of these cells. The characteristics of the resulting reflectance function are controlled by the nature of the triangular microfacets used to represent the surface. Cabral, for example, used a white noise distribution to control the height of the triangles used in one of the surfaces studied in their work. Anisotropic reflectance functions can also be generated by constructing a microstructure which has a preferential orientation.

Research done by Westin et al. (1992) extended the work of Cabral with a more elaborate surface representation which involved directly computing the spherical harmonic function during a ray casting simulation. Westin used this new approach to

produce realistic reflectance functions for anisotropic surfaces such as brushed aluminum and textiles. He also showed how a hierarchical approach could be used to develop reflectance functions for complex surfaces. He incorporated reflectance functions calculated for primitive elements in the models of larger structures composed of these elements; this allowed for a more efficient computation of the reflectance functions of these larger structures.

The spherical harmonics representation of the BRDF used in both of these previous studies is useful in characterizing the entire spatial distribution of the light scattered from a surface. However, it does not contain a provision for the spectral component of this scattering. A separate spherical harmonic function must be used for each wavelength in order to capture the spectral aspect of the scattering from a surface. This hinders the efficiency of the representation and complicates its calculation. A BRDF representation presented by Gondek, Meyer, and Newman (1994) addresses this issue. This representation integrated the spectral and spatial characteristics of the BRDF in a single data structure which was then used in a Monte Carlo raytracer to generate realistic images of a broad variety of complex surfaces. The reflectance functions for these surfaces were precomputed by simulating the interaction of light with accurate geometric models of the surfaces. These simulations incorporated both the surface reflectance, and subsurface scattering from the materials in question. This latter aspect of the interaction of light with a material had not been addressed by either previous method. The software developed for these simulations represents a virtual goniospectrophotometer. An actual goniospectrophotometer is a device which is used to measure the spectral and spatial scattering of light from a surface.

The method used in the virtual goniospectrophotometer is similar to the one employed by Westin to generate reflectance functions for explicitly modeled surfaces.

Numerous light rays are shot into a model from a given incident direction, and their scattering is captured in order to calculate the reflectance function for the model. The modeled surface can be composed of various semi-opaque geometric primitives and tessellated height fields. Wavelength dependent indices of refraction and absorption can also be specified for these objects, with the goal being to model the actual structure under consideration as accurately as possible. The rays shot at these models contained polarization and phase information and could represent either a single wavelength or an array of wavelengths along the visible spectrum. A technique similar to raytracing was used to track each ray as it interacted with the structures in the surface model and a variety of optical effects were captured this way. The behavior of a ray at any given optical interface is governed by the wavelength dependent indices of refraction at the interface and the polarization state of the ray. Depending on user defined parameters, a statistical approach can also be used to control ray branching at an interface. Absorption is accounted for by specifying wavelength dependent absorption coefficients for the elements of the model and then using these to calculate ray attenuation according to the Bouger-Beer laws. Interference effects were also accounted for by keeping track of phase information as rays were transported through the model. Rays that exited the surface model in parallel (within a small tolerance) were summed according to the Fresnel-Arago laws, as described in Gondek (1994). This allowed the effects of thin film interference to be captured. The software could also be run in a mode that detected the existence of multiple thin films and analytically calculated the reflectance for these structures. This approach avoiding the exponential ray branching that would occur if conventional techniques were used.

The scattering that results from the interactions of these multiple rays with the surface model is captured by a novel data structure which is well tailored for this type of

simulation. A geodesic sphere is used to represent the exiting directions above and below the surface, with each facet of this sphere designed to capture the exiting rays over a discrete range of possible exit directions. The sphere dynamically subdivides during the course of the simulation so that regions containing high degrees of variation are more finely discretized than more uniform regions. The rays captured in each facet of the dome are then used to calculate and store the spectral reflectance ratio with respect to the incident direction. This ratio represents the spectral reflectance for the range of exit angles that the facet covers. Spectral transmitance ratios are similarly created by capturing the rays exiting the bottom of the model. Since the work presented in this thesis relies only on the reflectance ratios, references to the transmittances are left out of the following discussions.

The data structure as described is adequate enough to represent the spectral reflectance ratios for one incident angle across all exitance directions; however, in order to represent the full BRDF, this simulation must be re-run for a number of incident directions. Rather than creating a separate data structure for each incident angle sampled, the same data structure is reused and further elaborated by simulating subsequent sets of rays at other incident directions. The spectral reflectance ratios recorded in the structure are tagged in order to keep track of which incident direction they belong to. Using this single unified data structure has the drawback that the area of highest variance, which in turn causes the greatest degree of elaboration in the structure, is in the specular direction. For surfaces that exhibit significant specular reflection, the structure is very inefficient since it is highly elaborated across the entire structure when multiple incident directions are sampled. In order to avoid this inefficiency, the entire data structure is rotated for each incident angle such that the specular direction is coincident for all the incident angles sampled. This effectively concentrates the portion of the data structure that has to be

highly subdivided, thereby saving significant amounts of space at run time. This technique also eases the interpolation necessary during rendering in order to produce a smooth reflectance function from the discretely sampled incident directions.

Each simulation run thus produces the spectral reflectance ratios for a family of discrete incident directions. A set of ratios for a given arbitrary incident angle is then generated by interpolating the ratios across the four nearest discrete angles which were sampled in the simulation. This data is used to represent the BRDF of the modeled surface in a Monte Carlo raytracer which enables synthetic images of these surfaces to be generated. The virtual goniospectrophotometer was used by Gondek et al. to generate realistic surface reflectance functions for such materials as pigmented plastic, thin-films, and interference paint. Gondek later enhanced the tool in order to generate reflectance functions for multiple thin films and Christensen filters.

This thesis extends the previous work by concentrating on two complex surfaces and uses the tool in conjunction with carefully constructed models of these surfaces to generate accurate reflectance functions for them. A biologically occurring and a man-made structure were chosen for this study. Both of these surfaces exhibit unique optical properties which are directly related to their structure. Accurate models for these materials are created by employing morphological data gathered by previous researchers. Simulations on these models are shown to generate reflectance functions that exhibit the same characteristics as their empirically observed counterparts. It is also shown that these synthesized reflectance functions compare favorably with both theoretical reflectance models and empirically measured reflectances for these surfaces.

This thesis is divided into three subsequent chapters. The next chapter reviews the causes of thin film interference and discusses how this relates to the iridescence found in certain hummingbird feathers. Theoretical models that account for this phenomenon

are also discussed. The structure that produces this effect is detailed along with the models that were constructed to simulate this surface. Reflectance functions generated from these models are compared with the previously developed theoretical results. The third chapter covers a similar study which was undertaken on the man-made structure of paper. A review of the composition and manufacture of paper is presented, with concentration on how these factors affect the optical characteristics of the end product. Test standards used in the industry to measure some of these pertinent properties are briefly discussed in the Appendix. Theoretical treatments used in the paper industry to account for these properties are also overviewed in the third Chapter. The results of laboratory measurements and light scattering simulations conducted on models of the paper structure are also presented. The final chapter ties together the conclusions generated by this work, and offers suggestions for future work.

CHAPTER II

THE IRIDESCENT HUMMINGBIRD

One encounters an astonishing variety of color in the natural world: a circumstance which is complimented by the equally versatile purposes for which color is used in nature. Colorants in the animal world, for instance, have been attributed to such disparate purposes as camouflage from predators and as eye catching displays for potential mates (Land 72). This latter example is most likely the reason for the rare colors found in some species of hummingbirds. Because these "jewels of flight" have long been noted for their striking iridescent feathers, these feathers are a particularly interesting surface for our type of optical study. Portions of these surfaces display rare iridescent colorings, which we now know to be the result of sub-microscopic structures embedded in the surface of the feather. These feathers have been of interest to ornithologists, biologists, and optical scientists alike because of these unique qualities. The results of their studies provide a knowledge basis from which we can develop a model of the feather surfaces for use in the virtual goniospectrophotometer. The existing research also provides us with a metric by which to compare the resulting reflectance functions from our simulations. We will show that by using a carefully reproduced model of the microstructure of these iridescent feathers in conjunction with the virtual goniospectrophotometer, we can synthesize a reflectance function that reasonably matches that which is observed. In the next section, we will review the some of the mechanisms by which color is produced, and then contrast this to the production of color by the complex structure embedded in the hummingbird feather.

Colorings in Animals

In order to understand the unique intricacies of the hummingbird's feather, we must first review how color is produced. Color can be thought of as the subtraction of portions of the visible spectrum from light reflected from a surface. Thus when an object appears blue when illuminated by a white light, we know that the green through red portion of the spectrum have been somehow minimized in the reflected light that reaches our eye. There are a number of ways these portions of the spectrum could be suppressed.

By far the most common phenomenon by which color is produced is selective absorption. In this case, certain portions of the incident spectrum are absorbed by the object while the rest of the spectrum is reflected, thus producing the color of the object. This type of color is called pigmentary color, and it is responsible for the colorings found in most animals including the hair and skin color of humans. In bird species, pigmentary color accounts for the red, yellow, gray, and brown hues found in their feathers. Pigments suspended in the transparent feather barbule selectively absorb only discrete portions of the visible spectrum to produce these colors. In the unique case of the African Touraco, the red pigment of the feather will actually wash off in water, and feathers immersed in water will even become transparent (Simon 71). The Touraco is also noted for the fact that it is the only known bird species that produces green pigments. While green colorings are not uncommon to birds, it is normally the result of a combination of colors. Green is most often found in birds as the result of adding the pigmentary produced color yellow, to the *structurally* produced color blue.

Structural color arises from the spatial organization of a material. The primary difference between structural color and pigmentary color lies in the fact that there is no explicit absorption in the former case. Structural color involves either the spatial
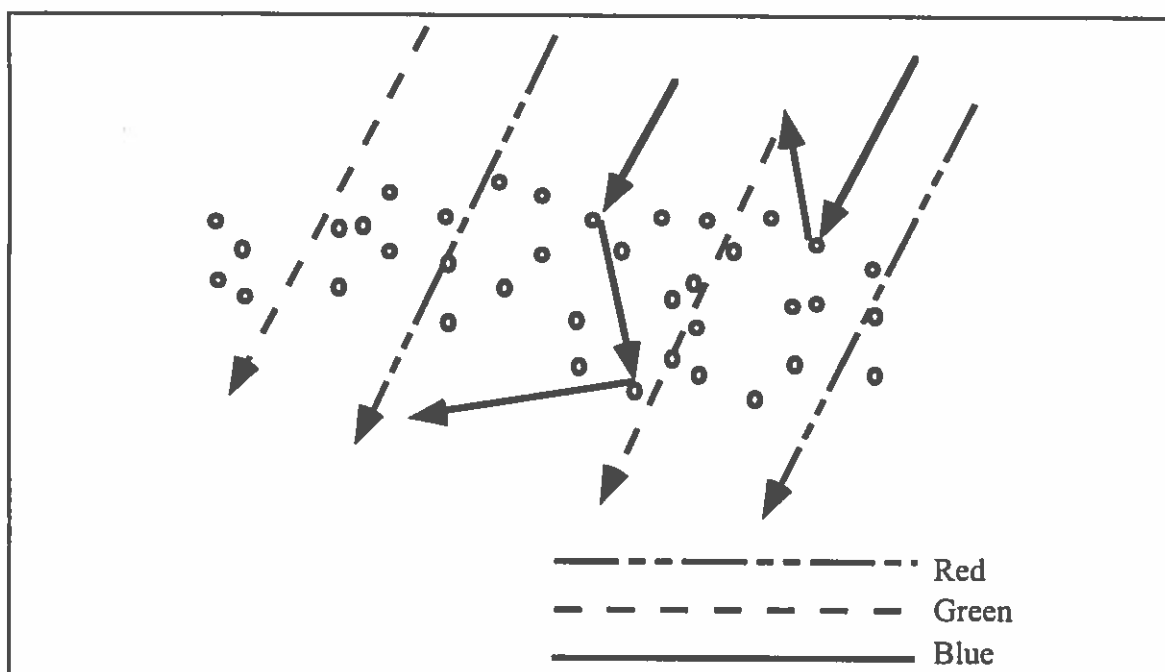
Figure 1: Tyndall scattering. The blue portion of the spectrum is scattered while the other portions are unaffected.

diversion of portions of the spectrum, or extinction of regions of the spectrum through interference and diffraction. For instance, the blue hues found in most birds and in most animals (including the eyes of humans), is produced by a form of structural color called diffusion or Tyndall scattering. This phenomenon occurs when the blue portion of incident light is scattered by tiny particles in the medium, while the other portions of the spectrum are not effected. The multiple scattering of light in the blue region results in a portion of the energy in this region being reflected back while the rest of the spectral energy is transmitted directly through the medium. This type of structural color is most familiar to us as the blue of the sky. Tiny particles in the atmosphere refract and reflect only the blue portion of the incident sunlight while the rest is transmitted through, as shown in Figure 1.

A second type of structural color involves the reinforcement of certain wavelengths of light through a process of interference. Certain structures such as thin

films and diffraction gratings will scatter light in specific polarization states such that some wavefronts will constructively interfere, while others will interfere destructively and extinguish portions of the spectrum. Interference colors are differentiated from their pigmentary counterparts by the purity of their spectral hues, their metallic sheen, and by the play of color as the viewing angle is changed. This latter effect is most marked in thin film type interference, which is displayed in such diverse species as insects, fish, reptiles, and birds. Certain types of bird feathers have been noted for this unique effect, even in the earliest optics literature. Newton, for instance, in his landmark Treatise on Optiks (1704), noted with interest the change in hue of peacock feathers as the incident viewing angle was changed. The association of this effect with thin film interference lead early researchers to theorize that these colors were the result of structural anomalies well before experimental tools were available to confirm this fact. The advent of the electron microscope provided proof that the fine structure required for such phenomenon was present in these cases.

Electron microscope studies of iridescent hummingbird feathers have shown that a precise array of cells exists below the surface of the feather that approximates the structure of multiple thin films. These results support the early theories regarding the nature of the coloring produced by these feathers. The following sections will explain in greater detail the process of thin film interference and how this relates to the structure of certain hummingbird feathers and the models of these structures used in our simulations.

Thin Film Interference and the Hummingbird Feather

Even the earliest theories developed to account for the iridescence of certain bird feathers considered this phenomenon to be the result of interference effects. The similarities between the optical character of these feathers and the observed characteristics
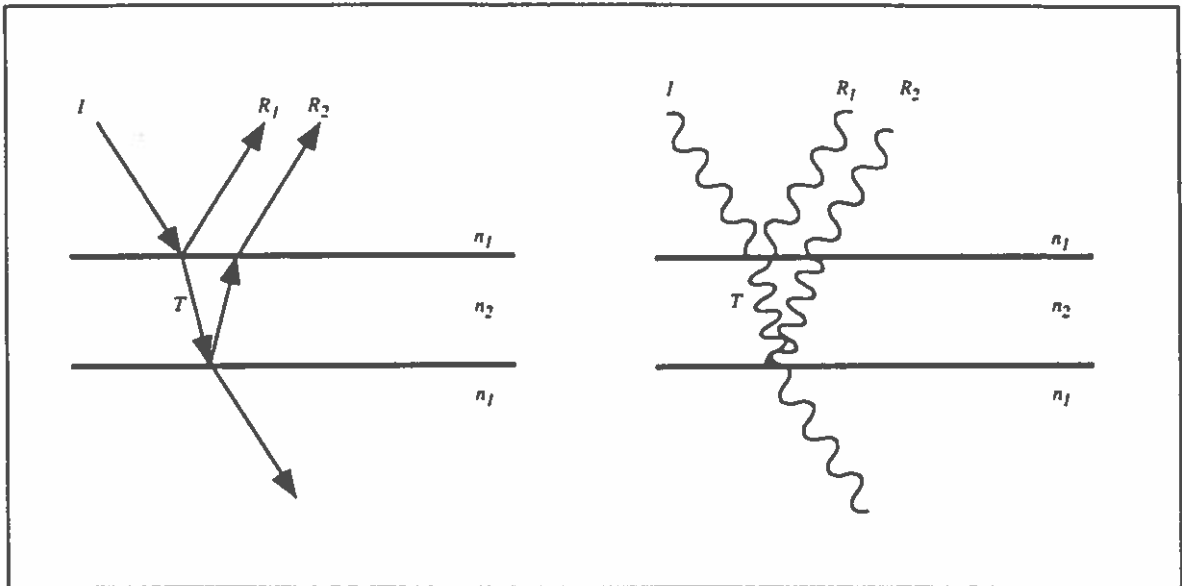
Figure 2: The geometry of thin film interference. Represented both as rays and as wavefronts.

of known interference structures, such as soap bubbles and oil slicks, are what lead these early researchers to this conclusion. More recent researchers (Greenwalt et al. 1960) have found through electron microscopy that, at least in the case of hummingbirds, the iridescent color is most likely the result of multiple stacks of thin films embedded in the feather. In order to fully appreciate the physical intricacies of these structures, we will briefly review thin film interference and show how the structures found by Greenwalt et al.'s investigations lend credence to the theory that these colors are in fact the result of thin film interference.

Thin film interference results from the phase differences in the multiple wavefronts of light reflected from the two interfaces of a thin transparent substance. The geometry for this situation is shown in Figure 2. An incoming wavefront, I, is incident upon a thin film with an index of refraction n_2. In this case, we consider I to be monochromatic, at a wavelength λ. A portion of the incident wavefront is reflected at the top interface as shown by R_1, and a portion is transmitted, shown by T in the figure.
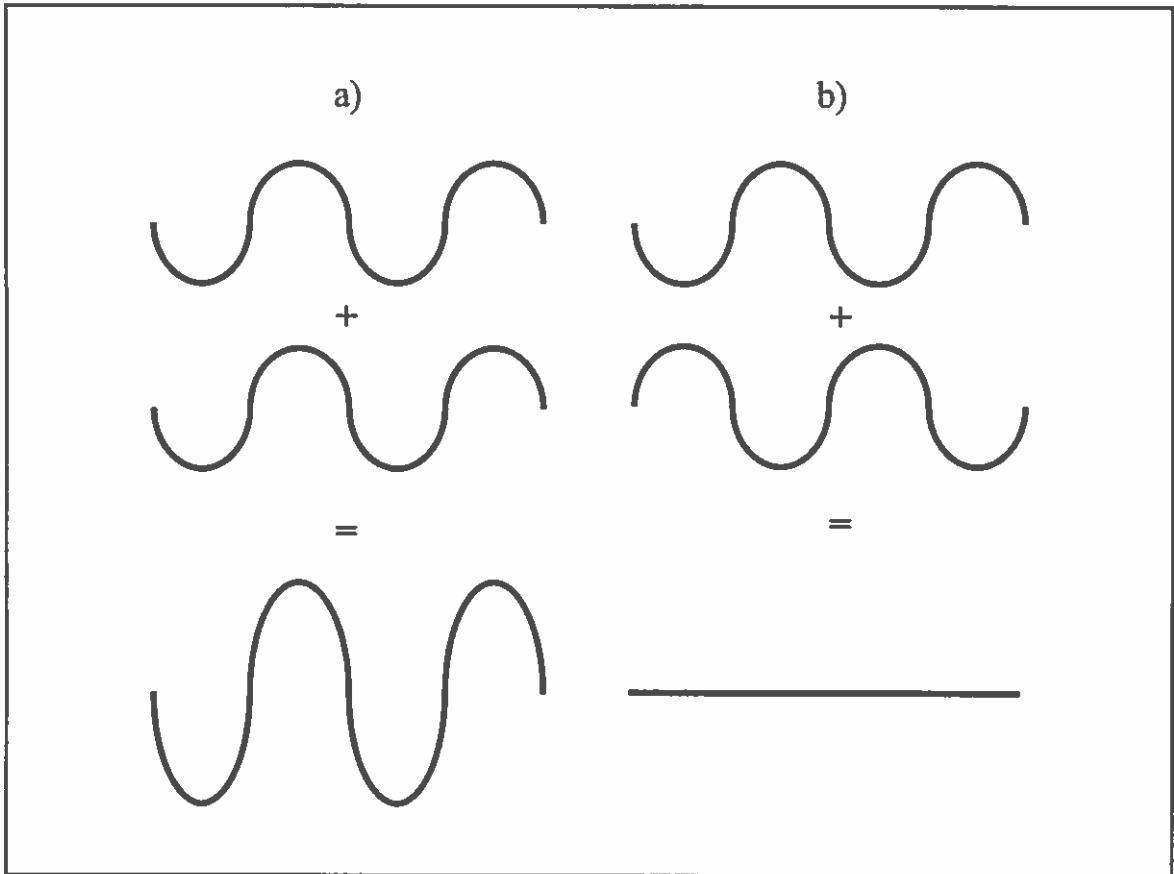
Figure 3: The summation of waves. a) exactly in phase, and b) 1/2 wavelength out of phase.

The relative amplitudes of T and R_1 are a function of the incident angle and the indices of refraction, as predicted by the Fresnel equations (Hect 79). The transmitted wavefront is subject to a similar splitting at the bottom interface of the film, and the reflected wavefront at this interface is shown as R_2. In the diagram, we have shown R_2 transmitting through the top interface oriented in parallel to R_1. In fact R_2 will again split into two components: an internally reflected component, and the transmitted component which is shown. The internally reflected wavefront is omitted in this diagram for clarity, however this splitting process will proceed until all the energy in T has been transmitted through one of the interfaces, or absorbed. Since R_1 and R_2 exit the film in parallel and originate from the same source, their field components can be superimposed according to

the Fresnel-Arago laws. Because of the wave-like properties of light, the two wavefronts R_1 and R_2 may have phase differences which causes them to interfere. If the two wavefronts have a phase difference of exactly half λ, then they will destructively interfere and cancel each other out as shown in Figure 3b. If the two wavefronts are exactly in phase, the case shown in Figure 2, then they will reinforce each other as shown Figure 3a. The conditions under which this summation can occur and the exact nature of this process is described in more detail in (Gondek 94) and (Hect 79).

The relative phase of the two wavefronts in our example is related to the optical path length that R_2 travels through the film. The optical path length is defined as the product of the physical path length and the index of refraction n_2. We know that a wavefront reflected from a low-to-high (index of refraction) interface will undergo a phase shift of 180°. If we assume $n_1 < n_2$ for our example, then we know that at the initial interface, the two wavefronts T and R_1 are 1/2 λ out of phase. We can then calculate the phase difference of R_1 and R_2 by adding the optical path length through the film to this amount. Using these relationships, we can calculate the optimal path length for constructive interference. If the path length is 1/2 λ (or alternately 3/2 λ, 5/2 λ, etc.) then the two wavefronts will be in phase. Path lengths of 1/4 λ, (or 3/4 λ, 5/4 λ, etc.) will cause the two wavefronts to cancel each other and extinguish.

The characteristic change in hue of thin films that comes about by changing the incident or viewing angle is also related to the optical path length. As the incident or viewing angle is changed, corresponding changes in the optical path length shift the wavelength of maximum coherence. In Figure 4 we see three different viewing situations associated with increasing angles of incidence. Each ray has a different optical path length through the film, and thus will have different phase relationships to it's initially reflected counterpart (which are not shown in this diagram). When the film is subject to white
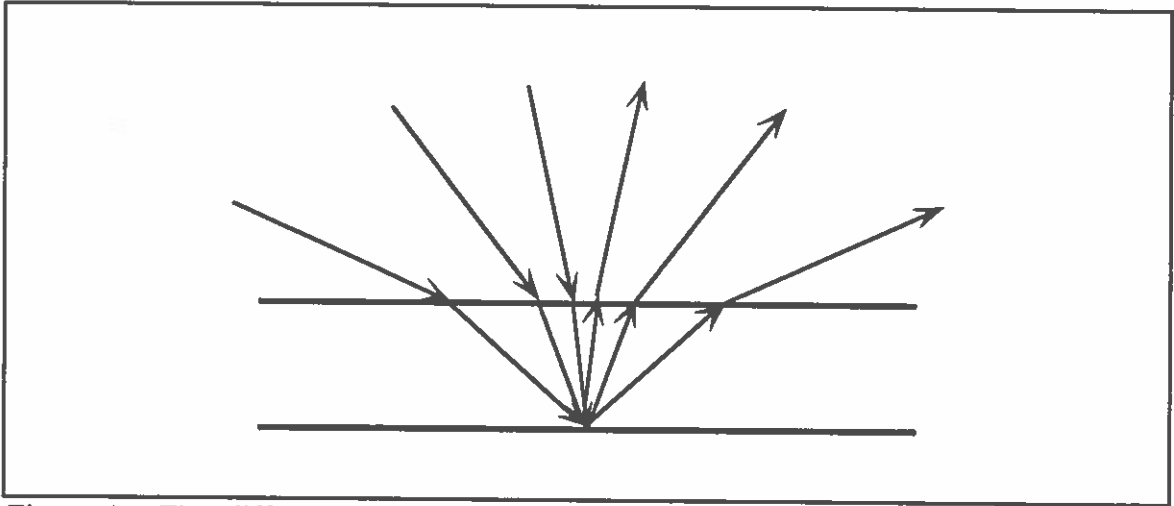
Figure 4: The difference in optical path length through a thin film associated with incident/viewing angle.

incident illumination, this change in the optical path length shifts the wavelengths that are constructively and destructively interfering, which effectively shifts the perceived hue. One color will be perceived at normal incidence which corresponds to the wavelength of maximum coherence; as we rotate the film away from normal, the optical path length changes and the wavefronts of this initially coherent wavelength fall out phase, while another portion of the spectrum falls into phase. This shift in hue will occur as long as the optical path length is 1/2, 3/2... of some wavelength of the visual spectrum.

For a single thin film, the process of reinforcement will produce a broad flat peak in the spectral reflectance curve as shown by curve a) in Figure 5. By stacking up a number of thin films atop each other, the reinforcement of the wavelength of maximum coherence will be enhanced. Curve b) in Figure 5 represents a surface consisting of a seven layered film. Curve c) in this figure represents the spectral reflectance for a Calypte Anna or Red Gorget species of hummingbird. As we noted previously, early researchers theorized that these feather colors were structural because of the similar qualities they shared with known structural surfaces. Empirical data like that shown in Figure 5 lead these early researchers to realize that the colors observed in these feathers
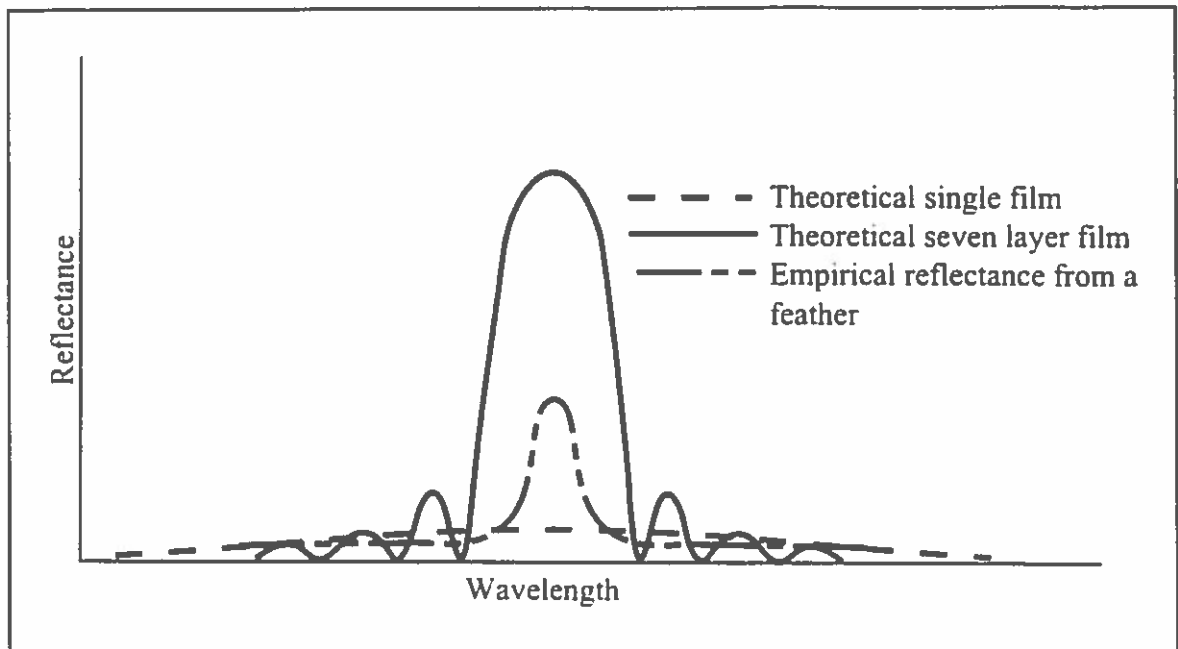
Figure 5: Comparison of reflectance functions for ideal thin films and an iridescent hummingbird feather. (From Greenwalt, 1960)

could not be the result of a single thin film, but must be the consequence of multiply stacked films. These structures are too small to be seen by the naked eye or even with the aid conventional microscopes, and thus for a long period the existence of these structures could not be confirmed.

A study done by Greenwalt, Brandt and Friel in 1960 finally confirmed these theories by using electron microscopy to map the structure of iridescent hummingbird feathers. They found the iridescent barbules contained multiple layers of thin platelets stacked in a very regular fashion as shown in Figure 6 b). These flattened, elliptically shaped plates consisted of a high refractive material, melanin with an index of refraction of 2.0, which were embedded in a transparent medium of keratin with an index of refraction of 1.56. These platelets were distributed in a mosaic pattern as shown in Figure 6a). Further examination of the platelets revealed that they have foam-like air pockets in their center as shown in Figure 6 b) and c). Similar platelets were also found in non-iridescent
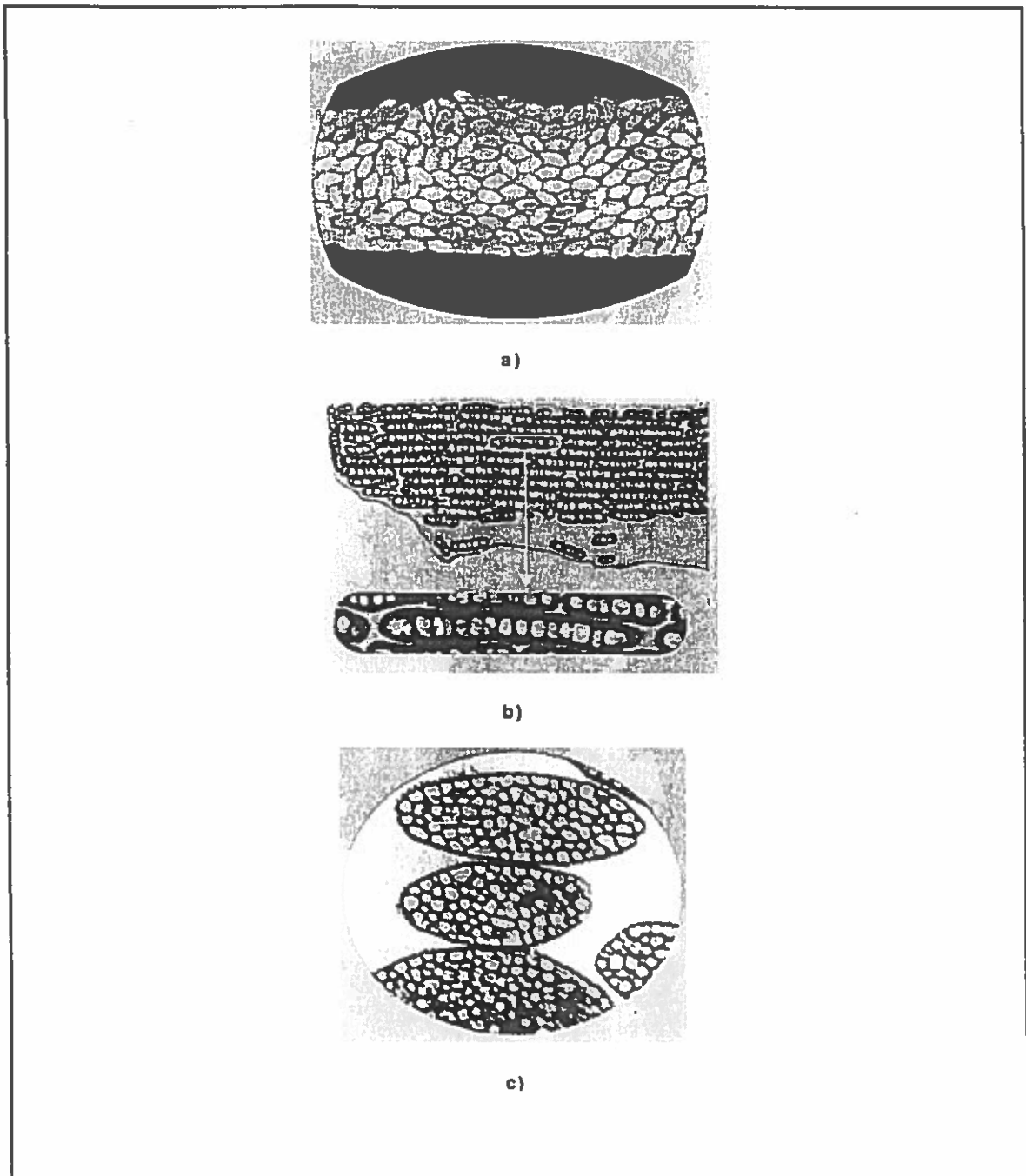
Figure 6: The structure of an iridescent feather barbule. a) Top view of an iridescent feather barbule from an optical microscope. The mosaic of platelets from the top layer can clearly be seen. b) An electron photomicrograph of a cross section of an iridescent barbule. A regular layering pattern of the platelets is evident. c) An electron photomicrograph of a cross section of individual platelets seen from the top. The light oblongs are air pockets embedded in the melanin material that makes up the plates. (From Greenwalt, 1960)
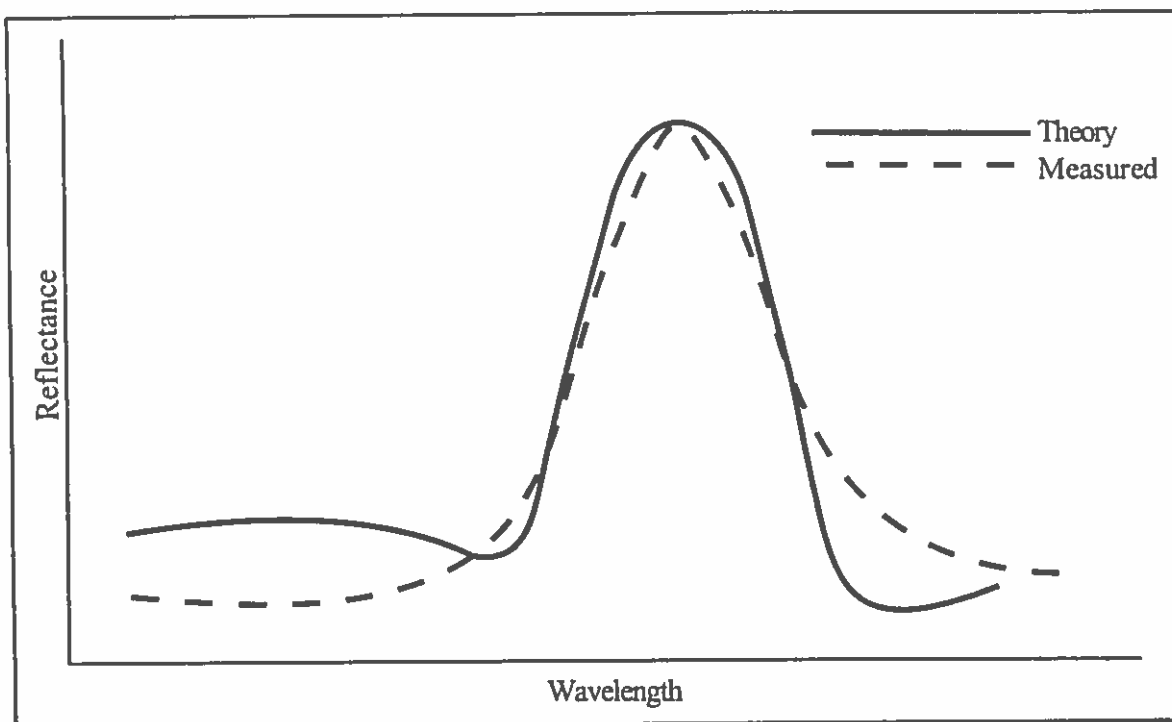
Figure 7: Comparison of Greenwalt et al.'s theoretical solution with observed spectra for a Green Gorget (Topaza Pyra) hummingbird. (From Greenwalt, 1960.)

portions of the feather, however these neither contained the air pockets nor were arranged in the regular fashion that was characteristic of the iridescent portion of the feather.

The periodic nature of this structure suggests a situation in which thin film interference could take place. The dimensions of the regular intervals of high and low indices of refraction are of the proper magnitude for interference to take place, however comparisons of the theoretical curves for ideal thin films and those observed in the iridescent feathers revealed some anomalies. An example comparison for these cases is shown in Figure 5. Curve b) is the theoretical curve of an ideal 7 layer stack of alternating high and low index of refraction materials. This is compared to curve c) which is the empirical reflectance curve for the iridescent feather from a Red Gorget hummingbird, which was found to have 7 layers of platelets of similar dimensions to those used for the curve in b). The first thing one notices upon examination of these

curves is that there are no secondary peaks in the empirical case. Greenwalt et al. attribute this absence to "surface fluctuations in the platelets" without elaboration.

The second discrepancy involves the width of primary peak in the theoretical and empirical curves. The empirical curve shows a much sharper peak than the theoretical one. To account for this, Greenwalt et al. developed a theoretical model for inference of optically *non-homogenous* materials. Up until this point, analytic solutions for interference structures only existed for homogeneous materials, i.e. materials with a constant index of refraction. Greenwalt et al. argued that the structurally reinforced air pockets in the platelets caused a transitional increase in the index of refraction as a function of the distance along the z axis from the center of the plate. In this way, the index of refraction of the platelets could be represented by a smoothly varying function which could then be integrated over the thickness of the platelets. By some particularly complex differential calculus, which will not be repeated here, the authors were able to generate approximate analytical solutions for this model of the platelets that better agreed with the empirical curves. Their solution involves replacing the non-homogenous portions of the platelets, namely the center sections with the air pockets, with a homogenous mass that has the effective refractive index calculated by integrating over the non-homogenous areas. The results of their theoretical solution are shown in Figure 7. While their new analytical solution was much closer in shape to the empirical results, the issue of the absence of secondary peaks remained unresolved.

Surface Modeling and Simulations

Progressively refined models of an iridescent Calypte Anna, or Green Gorget hummingbird feather, were developed for use in the virtual goniophotometer. The surface reflectance functions that were generated from these simulations were then compared with
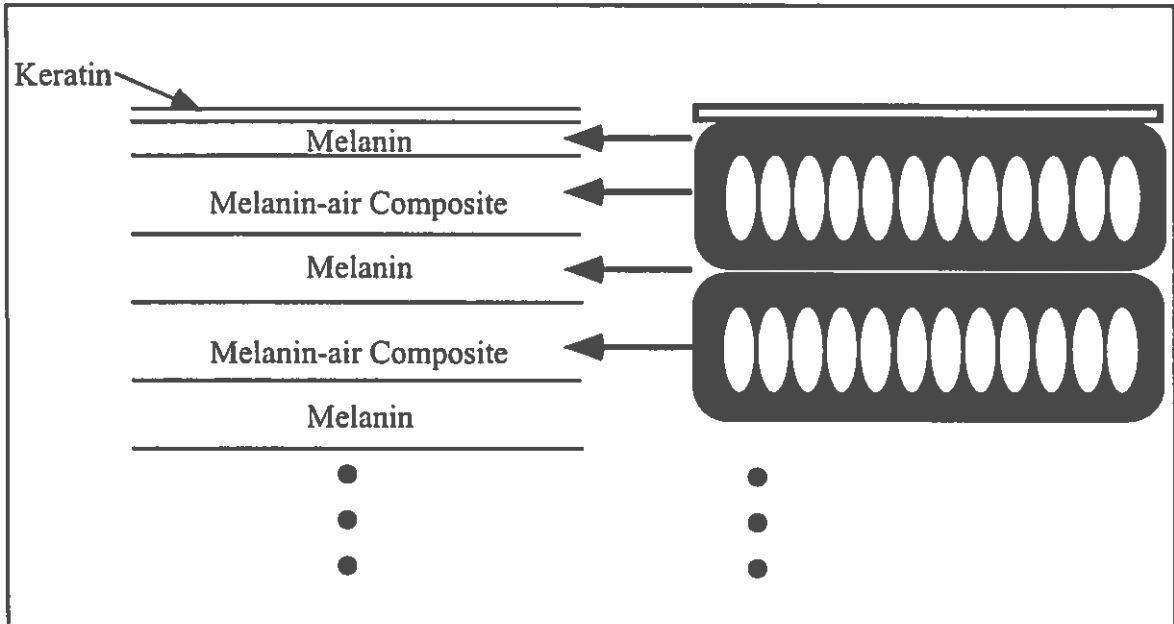
Figure 8: Cross section of ideal thin film model and corresponding platelets.

those found by Greenwalt et al. By adopting an approach that progressively refined the model in order to more accurately represent the microgeometry of the feather, we were able to generate surface reflectance functions with similar characteristics to those found in the study. The stages of this refinement included modeling the feather as:

- A collection of ideal thin films.

- A stack of broad rectangular plates.

- An array of interlocking bricks.

- A mosaic of pseudo-randomly oriented flattened spheres.

While we did not employ the theoretical solutions of Greenwalt et al. in our simulations, we did however use one of their techniques to simplify the model. Instead of developing a model of the platelets in which the internal air pockets are explicitly included, we chose to replace them with uniform sub-regions of the same optical thickness reported in the Greenwalt et al. study. Without this simplification, the running time of the simulations would have been unreasonably long due to the complexity of the geometry.
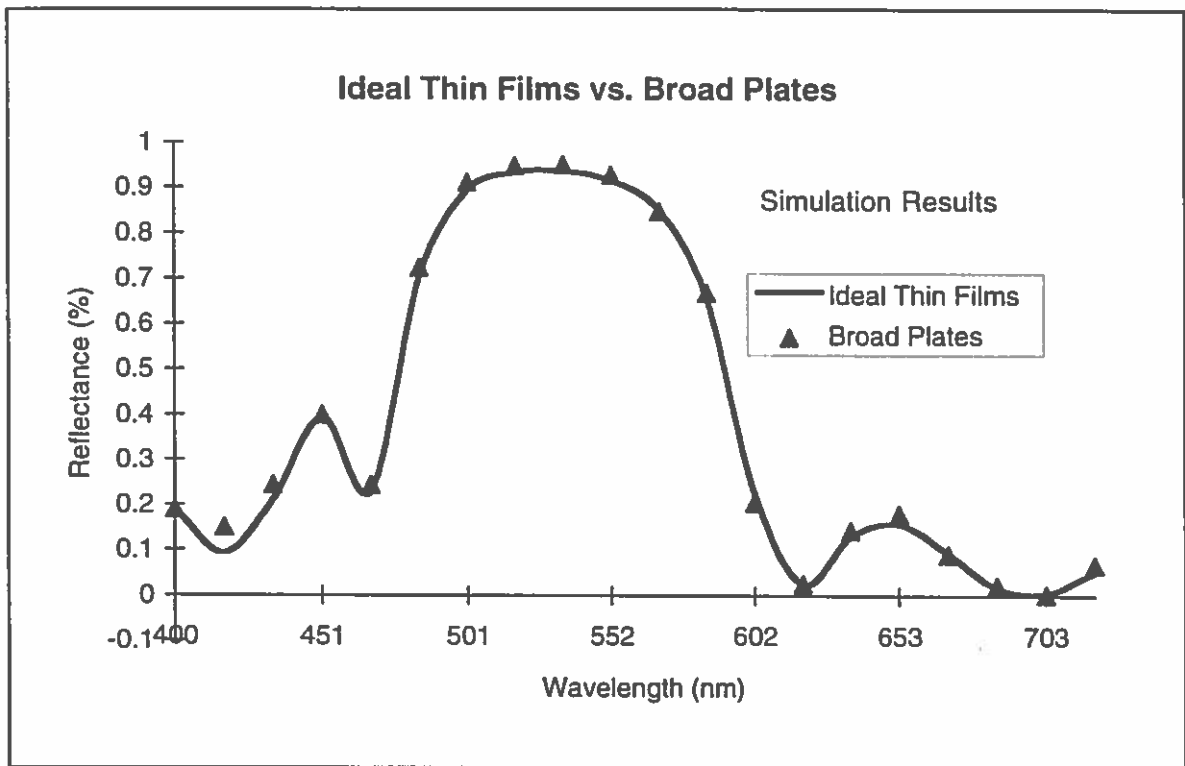
Figure 9: Comparison of simulation results for ideal thin film model and broad plate model.

The first approximation to the feather structure was constructed with ideal thin films. 14 layers of alternating high and low refractive materials were used to represent the seven layers of platelets in a Green Gorget feather. A thin layer (10 *nm*) of low refractive material preceded these layers in the model, which represented the thin keratin skin found in the feather. The index of refraction for this layer was 1.56 corresponding to keratin. The high refractive layers, which were meant to represent the melanin body of the platelets, were given an index of 2.0, and the low reflective layers, which represented the air pockets, were assigned an index of 1.50 in accordance with the values found by Greenwalt et al. The high index layers were 148 *nm* thick, except for the first and last layers which were half that, or 74 *nm* thick. The low index layers all had a thickness of 98 *nm*. These values were arrived at by using the mean dimensions reported by Greenwalt et. al. Figure 8 shows a cross section of this geometry and how it is meant to
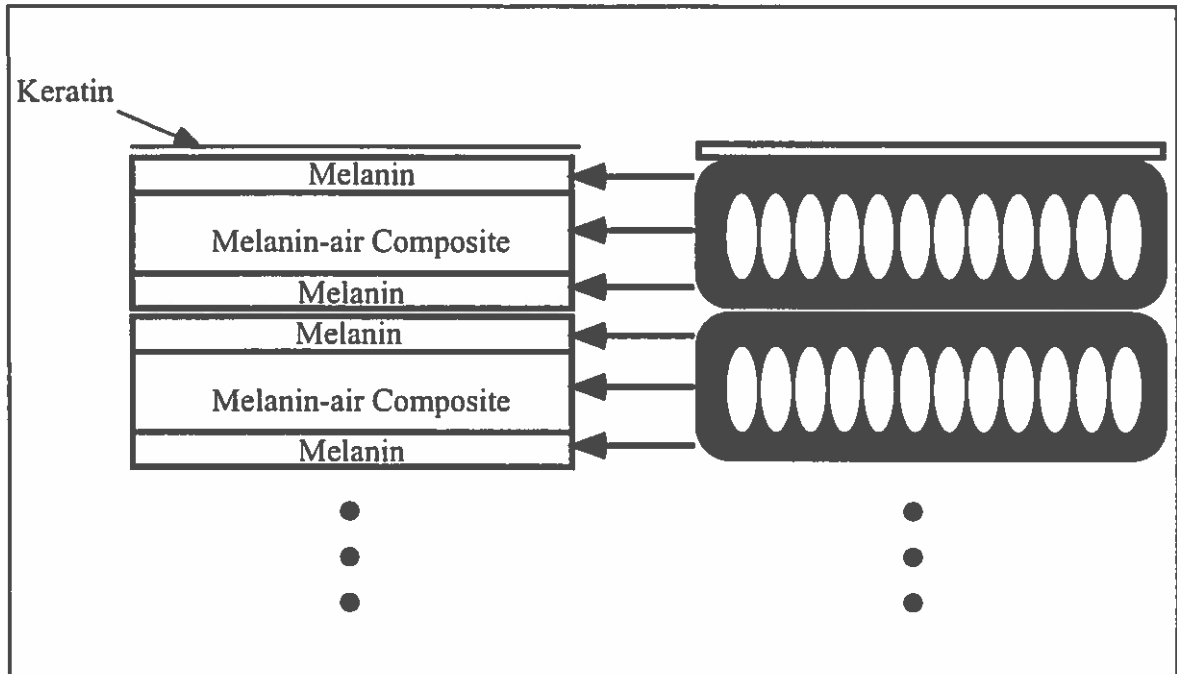
Figure 10: Cross section of broad plate model and corresponding platelets.

represent the platelet mosaic of the feather. As expected, this model produced reflectance functions which were identical to an ideal multi-thin film system as shown in Figure 9. Note the broad primary peak and visible secondary peaks.

The next stage of refinement involved replacing the ideal thin films with broad high index boxes embedded with low index centers. This intermediate model provides a logical transition between the ideal thin films used in the previous case and the geometric-primitive based approach used in the following models. By confirming the results generated at this level of refinement, we were assured that the geometric primitives were being processed correctly. Seven of these broad plates were stacked atop each other in order to match the geometry of the thin films as shown in Figure 10. An arbitrary space of 1 *nm* was inserted between each plate in order avoid discrepancies in processing the geometry during simulation. The plates were 172 *nm* thick and contained rectangular cores of a 98 *nm* thickness. The identical indices of refraction used in the thin film model
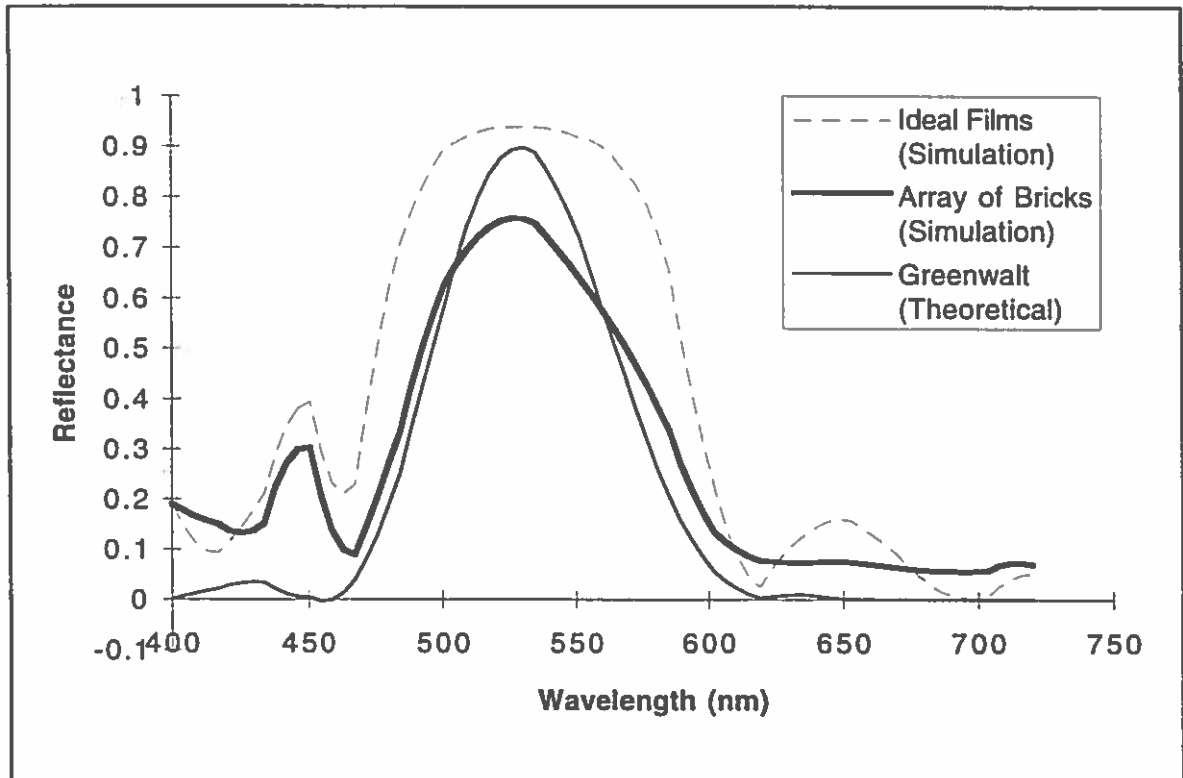
Figure 11: Comparison of reflectance functions for array of bricks model.

were used here, and the simulation results shown in Figure 9 show these two models produced matching reflectance functions.

Both of the models up to this point had not represented the individual platelets found in the feather. All the platelets on one level were represented only as a conglomerate film or box. Both resulting reflectance functions exhibited the characteristic broad primary peak and significant secondary peaks associated with ideal thin films, which were not found in the reflectance functions of the feathers. By further refining the model to include the individual platelets, reflectance functions with better correlation to those observed in Greenwalt et al.'s study were generated. Each of the broad plates of the previous model were broken into an array of interlocking bricks. Seven layers of these bricks were used as before, corresponding to the seven layers of platelets. The horizontal

dimensions of the bricks were set equal to the average dimensions of the platelets as reported in the study: 1500 *nm* by 2000 *nm*. As was the case for the previous model, a space of 1 nm was inserted between neighboring bricks. The thickness of the bricks and their low index core were also the same as the previous model. The reflectance functions generated by the simulations are shown in Figure 11. This reflectance function shows similar characteristics to the one generated by the Greenwalt theory. The bandwidth of the primary peak has narrowed and the secondary peaks, while still visible, have been attenuated.

Additional refinement of the model was undertaken in the hopes of generating reflectance functions that further matched those found in the study. In this final model, the bricks were replaced by flattened spheres of equivalent dimensions. This immediately introduced difficulties, for while the optimal packing arrangement of regularly shaped boxes is trivial to determine, the case for spheres is somewhat less tractable. The packing of spheres has been studied in the context of computer graphics by Pickover 89, and in general by Gardener 68, and Boyd 73. In these previous studies, the spheres were all uniformly scaled along the coordinate axes, however the spheres used in our model were more radically scaled along the z axis since we were using them to represent flat platelets. A further complication was introduced by our desire to control the horizontal orientation of the spheres to be consistent with that found in the actual feather. Orientation was not addressed in the previous sphere packing works since uniformly scaled spheres are isotropic with regard to all three coordinate axes. Rather than trying to use an optimal algorithm for our packing problem, we choose to use a more flexible genetic-type algorithm to build the mosaic of platelets.

Each layer of platelets was constructed by recursively *growing* adjoining platelets around a seed that was randomly placed in the layer. Each resulting platelet had a set of

growth rules which were applied to grow further adjoining platelets. These rules incorporated the statistical information that was provided by the Greenwalt et al. study regarding the orientation of the platelets in the actual feather structure. The dimensions of the platelets were also reported statistically, and this information could have been incorporated into the model in a similar fashion as was used for the orientation data. For our initial attempts, only the orientation was allowed to vary and the scaling dimensions were set to the mean recorded in the study. A total of seven layers of platelets were generated and each layer was grown in a depth first manner until a predefined area was filled. Figure 12 shows the development of the platelet model in succeeding steps of the algorithm. As shown by the figure, there is a local consistency in the orientation of the platelets, whereas there is little correlation between the orientation of platelets that are farther apart. This characteristic is similarly observed in the platelet mosaic of the actual structure, as was shown in Figure 6.

The reflectance functions generated through simulations with this model were disappointing. We had hoped for results which would better match the observed and theoretical reflectance functions found in the Greenwalt et al. study, namely a further decrease in the bandwidth of the primary peak and further dampening of the secondary peaks . Instead the resulting functions were found to be erratically shaped with multiple peaks. By further examination of the model and by observing the simulations as they ran, it was found that these puzzling results were the consequence of the curvature of the sphere geometry chosen to represent the platelets. This geometry is shown in Figure 13. It was initially thought that the curvature, or change in the surface normal of the platelets relative to the vertical axis would be very slight due to the fact that the spheres were dramatically flattened along this direction. For rays emanating from the surfaces of a single platelet, shown as R_1 through R_4 in the figure, the change in the surface normal was
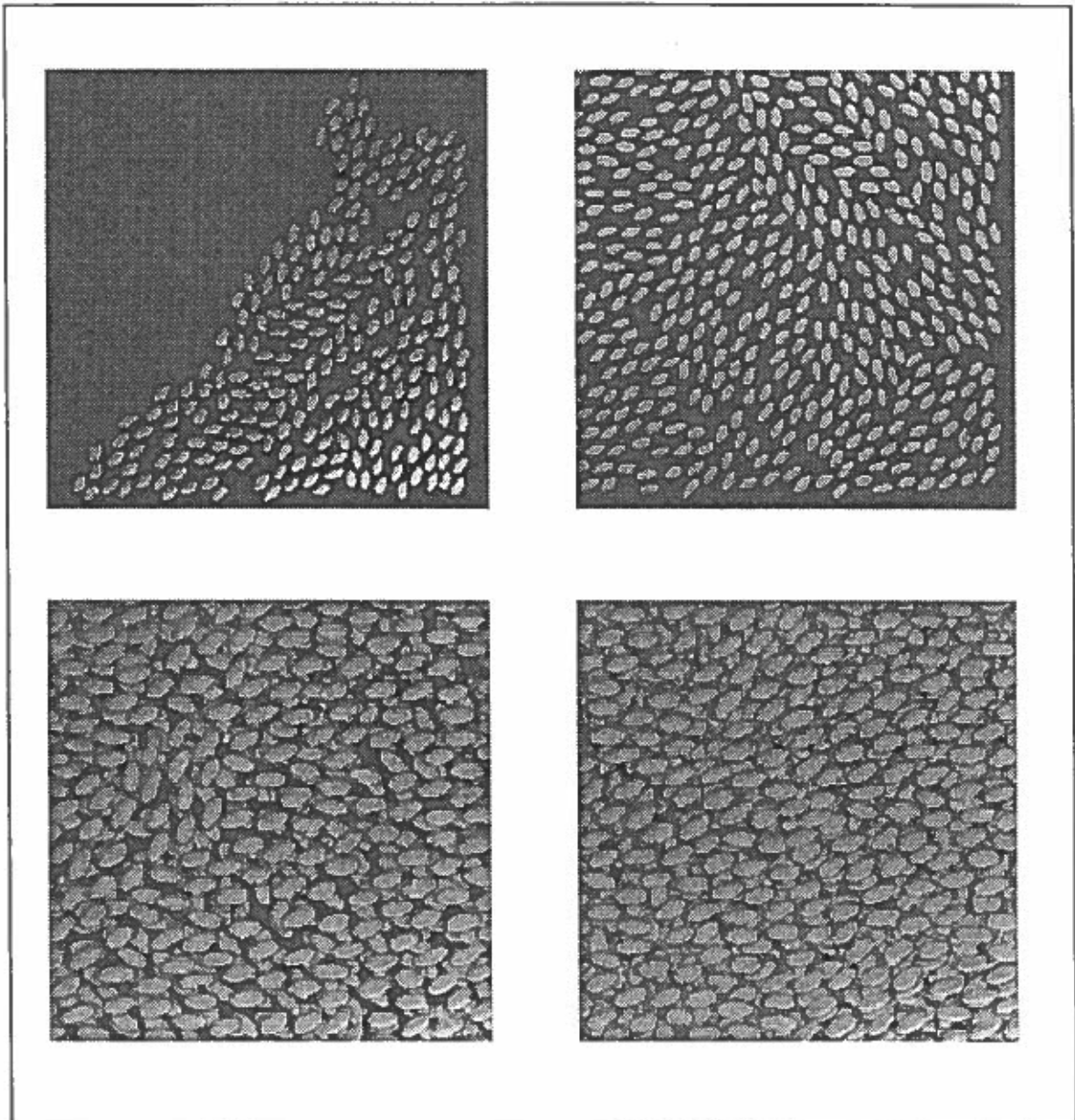
Figure 12: Generation of the flattened spheres model. Successive steps in the algorithm shown from left to right, top to bottom.

small enough for them to be considered parallel and candidates for interference. Rays which were reflected from platelets in subsequent layers, shown as R_5 in the figure, often times were not similar enough in direction for them to be considered parallel with reflected rays from preceding platelets. This situation resulted in rays passing through fewer
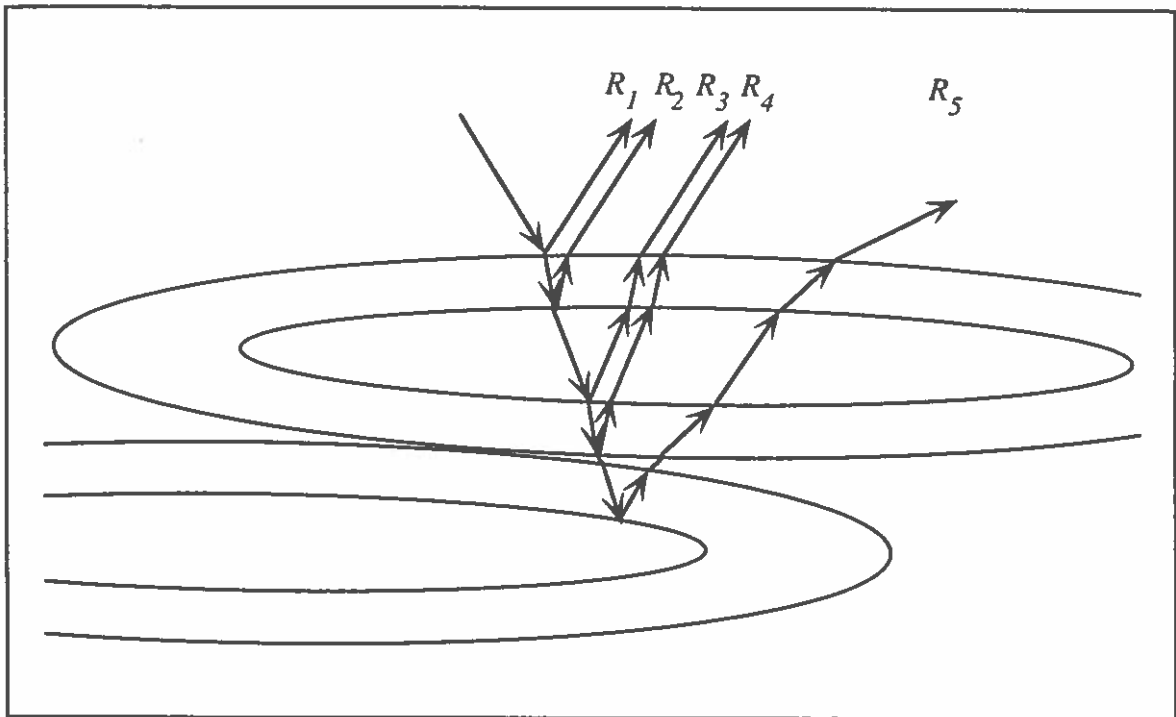
Figure 13: Cross section of the flattened spheres model.

multiple thin films than in the previous model. The results were further degraded by the fact that the thickness of the plates changed over the area, with thinner regions of material located at the edges. This effectively changed the wavelength of maximum coherence so that there was no single region of the spectrum that was reinforced for a given viewing orientation. Because of these two factors, the poor results of the flattened sphere model are attributed to the inconsistencies between the model and the feather, and not as shortcomings of either the methodology or the simulation tool. A better model of the feather, such as one that employs flattened cylinders or higher order primitives, should produce more satisfying results.

Despite the poor correlation between the reflectance functions generated by the flattened spheres model and those expected, it has been shown that by progressively refining the model of the feather we can approach reasonable approximations to the reflectance functions found by Greenwalt et al. The reflectance functions generated by

the brick model began to show some of same characteristics that distinguish Greenwalt et al.'s results from that predicted by ideal thin films. Further refinement of this model such that it more closely resembles the actual feather structure should produce more accurate surface reflectance functions. It was found that the refinements attempted with the flattened spheres model deviated too significantly from the original structure for accurate results to be obtained. A different modeling approach is suggested, possibly involving more complex geometries, which would produce better results.

CHAPTER III

PAPER

The visual appearance of paper results from the interaction of light with the complex surface and subsurface of the paper material. Incident wave fronts of light are reflected from and transmitted into the body of the sheet. Depending on the optical characteristics of the paper, the light entering the surface may be re-emitted thereby contributing to the overall appearance of the sheet. The optical characteristics of the surfaces in question are influenced by both the type of materials used and by the process in which the paper was produced.

The variety of substances employed in the modern day production of paper is quite large. Materials used just in the base stock include bulk fiber (normally organic pulp) in addition to bleaches, dyes, and filler material, which are all added to improve the optical characteristics of the sheet. In addition to materials in the base stock, there are frequently materials deposited over the outer surface of the formed web to improve the optical or mechanical properties of the paper. Aside from the raw materials, there are also a number of finishing techniques that are applied to the sheet in order to influence the optical properties of the paper.

There is currently no comprehensive theoretical model that is able to adequately link all the competing factors that contribute to the optical characteristics of paper. There exist, however, a number of theories that have proven to be of value in predicting how changes in either composition or production methods affect these optical properties.

Most of these theories are derived from, or closely resemble, the Kubelka and Munk formulations that describe the diffuse reflectance and opacity of semi-opaque films (Kubelka and Munk 31). Our purpose in this document is to present an overview of the relationships between the various materials, production processes and the optical characteristics of paper, and to link these relationships with the theoretical models that are used in the industry. Using this background as a basis, we will then focus on a few specific phenomena that will be explored through examining optical measurements and simulations of a few selected classes of sheets.

The chapter is divided into 4 subsequent sections. First we will precisely define the optical properties of interest in the industry. The next section is devoted to developing the theoretical background by which paper appearance is analyzed. The third section will discuss the factors in the composition and production that effect the optical characteristics of a sheet. The final section will discuss the optical measurements and simulation results of a number of carefully selected paper specimens.

Definition of Optical Properties

The visual appearance of a sheet can be described by such properties as its color, gloss, brightness, whiteness, and its opacity (the degree to which it is able to hide what is printed underneath.) These terms all have familiar meanings and we would be able to subjectively determine these properties by visual inspection; however there are defined standards used in the paper making industry that are designed to provide an empirical basis by which to compare these properties. Since subsequent discussions will refer heavily to these properties, a brief overview of them is in order. We will also note the various TAPPI (Technical Association of the Pulp and Paper Industry) and ISO

(International Standards Organization) standards where applicable. A brief overview of these relevant standards is included in the Appendix.

Color

The color of a sheet is one of the most readily apparent optical properties of it. However color is also one of the most difficult characteristics to properly define and measure. From a subjective standpoint, color can be equated with the dominant hue of the sheet. The spectral hue that most closely matches the perceived hue is then referred to as the "color" of the sheet. In a more formal fashion, color is related to the spectrally selective absorption of the sheet. The reflected incident light that is *not* absorbed then defines the color of the sheet. In this sense color is not a scalar, but is the wavelength profile of the sheet across the visible spectrum. There are a number of methods used in the paper making industry to evaluate color, ranging from visual comparison to complex experimental procedures. This section will describe these methods and the role they play in the manufacture process.

The determination of color, whether defined subjectively or formally, is inherently related to the light source under which the specimen is viewed. The spectral composition of the illuminating source will affect the spectral characteristics of the light reflected from the surfaces in question. TAPPI standard T 515 (TAPPI T 94) specifies the spectral characteristics of standard illuminates to be used in color determination and matching applications. When conducted by trained individuals, visual comparisons under these careful conditions can produce surprisingly accurate results. However this process is time consuming and relies on the availability of skilled personnel and thus is not generally appropriate for a production environment where a more automated method is desired.

Color measurement devices can alternatively be employed to determine the spectral response of a sheet. These measurements can then be integrated into the production process to insure that color tolerances are met. Such devices are available and have been used in a variety of industries for color matching purposes.

The mechanics of color measurement devices are based upon knowledge of the human visual system gathered through extensive experiments conducted by color scientists. These experiments sought to relate human observers responses to carefully controlled mixtures of colored lights. The knowledge of these relationships are necessary to accurately specify color since the human visual system does not respond in a linear fashion to changes in spectral excitation (Judd and Wyszecki 75). A color scale based upon the human visual system evolved from these experiments and is specified by the CIE Standard Observer. The CIE Standard Observer is defined by three color matching functions $\bar{x}$, $\bar{y}$, and $\bar{z}$, which are related to the response of the human eye to spectral excitation and were determined by experiment. These functions can be in integrated into a triplet, the XYZ tristimulus values, through the following set of equations (Hunter and Harold 87):

$$X = k\int_{\lambda} (S_\lambda \cdot \bar{x}_\lambda \cdot R_\lambda)d\lambda \qquad (III.1)$$

$$Y = k\int_{\lambda} (S_\lambda \cdot \bar{y}_\lambda \cdot R_\lambda)d\lambda \qquad (III.2)$$

$$Z = k\int_{\lambda} (S_\lambda \cdot \bar{z}_\lambda \cdot R_\lambda)d\lambda \qquad (III.3)$$

where:

$$k = \frac{100}{\int_{\lambda} (S_\lambda \cdot \bar{y}_\lambda)d\lambda} \qquad (III.4)$$

$R_l =$ The spectral reflectance of the sample at wavelength l.

$S_l =$ The relative power of the illuminant at wavelength l.

The use of colorimeters based upon CIE XYZ tristimulus values, or derivatives of CIE XYZ, is described in TAPPI standard T 524 and T 527 (TAPPI T94). These procedures provide a method of characterizing the color of a sheet in one of the 3-dimensional color spaces that are commonly used in color science applications. Other tristimulus spaces, such as Lab and Luv, are used in the paper making industry according to TAPPI standard T 524. These spaces are noted for the special property that equal Cartesian distances in these spaces represent perceptually uniform changes in color. Scales with this uniformity property are useful in color matching applications.

A different approach to the characterization of color involves determining the wavelength dependent reflection from a sheet with spectrophotometer. This device measures the reflectance from a sample at discrete wavelengths throughout the visual spectrum. For each wavelength sampled, the ratio of reflected light (over an ideal reflector) is recorded. Spectral response curves like those in Figure 14 can then be constructed from this data. Color characterizations of this type are actually a super-set of the tristimulus formulations discussed above, and there are mathematical transformations that allow tristimulus parameters to be derived from the spectral reflectance curves.

While the spectral reflectance is a complete representation of the sheet's color, tristimulus measurements are more often used as these measurements are easier to make and thus more appropriate for production environments (Bureau 89). The use of the more cumbersome spectrophotometer measurements has been limited to special instances when the color under a variety of lighting conditions must be known. The procedure for making such measurements is specified in TAPPI T 442 (TAPPI T 94). This standard
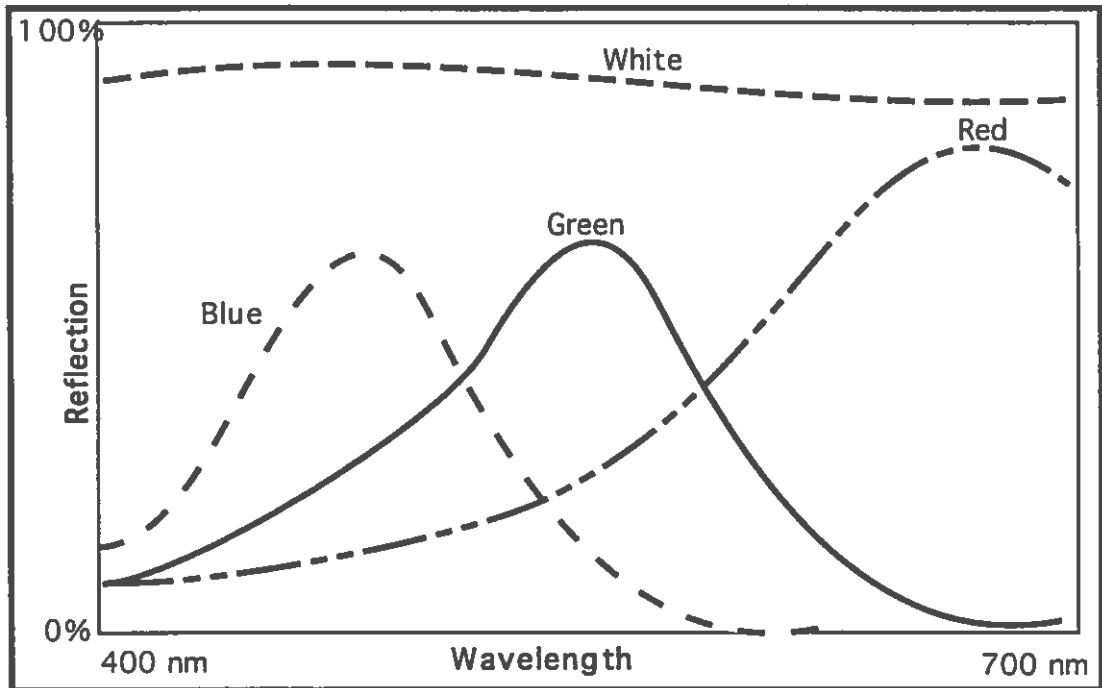
Figure 14: Color as a Wavelength Profile.

describes the strict spectral, geometric and photometric requirements that must be maintained for the accuracy of this type of measurement.

Other properties of interest that are related to color are *brightness* and *whiteness*. In the case of color we found that a variety of general purpose measurement devices have been adopted by the industry to determine this property. This solution is appropriate as color is a property that is ubiquitous in many industries. The properties of brightness and whiteness are of unique importance to the paper industry, and in contrast to the case with color, a number of specialized instruments have been developed to determine these properties.

Brightness and Whiteness

When paper is manufactured for printing applications, the contrast between the printed image and the paper substrate is an important factor. The properties that relate to the substrate's contrast quality are its whiteness and brightness. While these two terms may seem identical at first glance, these properties have distinct meanings in the paper industry.

Whiteness is the name given to the property that describes the uniformity of a sheet's reflectance curve, whereas brightness refers to the reflectivity of the sheet specifically in the blue region. These properties are important for printing and writing sheets, which can both be characterized as white in color. The importance of these properties lies in the fact that the quality of a printed page is related to the contrast of the ink vs. the substrate.

Whiteness refers to both the uniformity in the spectral response curve, and the relative magnitude of the reflectivity. A paper's whiteness, as opposed to its color, indicates that the absorption of light is non-selective. Absolute reflectance also plays a role in the determination of a sheet's whiteness, in that papers with higher overall reflectance are considered whiter. While both "white" and "gray" sheets have uniform reflectance curves, the former would have a greater whiteness value than the latter. The white sheet in this case would have an overall greater reflectivity than the gray sheet, and as a result its whiteness value would be higher.

The related property of brightness refers to the relative hue of the sheet. Brightness is defined as the percentage reflectance of blue light and is measured by determining the reflectance at a wavelength of 457 nm. The underlying impetus for this

measurement is that the reflectance in this area of the spectrum is related to the relative whiteness or yellowness of the paper. "Cold white" sheets have a bluish tint due to more energy in the blue region, and provide a higher print contrast than "warm white" sheets, which have a slightly yellow cast. TAPPI T 452 and T 525 specify the standard methodologies for determining brightness.

Depending on the application, high brightness is not always desirable. High brightness, high contrast sheets are appropriate when trying to capture the readers attention. These colder sheets tend to produce more eye strain, but for applications where the readers attention is only needed for a short time, this is not a problem. Warmer sheets may be desired for books where there will be extended exposure and less eye strain is desired.

Gloss

Color, whiteness and brightness are all properties associated with the spectral distribution of reflected light. In all the cases we have looked at so far, the methods for measuring these properties have included descriptions of the geometric conditions under which the measurements take place; however none of these properties are themselves directly related to the *spatial* distribution of scattered light. The only property that can be attributed primarily to the spatial distribution of the reflected light is gloss. Gloss is related to the tendency of the sheet to reflect incident light in the mirror direction.

Glossy sheets exhibit a shine or luster that is the result of reflection concentrated around the specular direction. A more matte surfaced paper reflects light diffusely, or uniformly throughout all exitance directions. The spatial distribution of the reflected light is a function of both the surface roughness and the index of refraction of the surfaces in question. Sheets with rough or non-uniform surfaces will often exhibit a more diffuse

scattering tendency than smooth surfaced papers. The roughness of paper sheets is governed by such factors as the materials applied to the surface and the mechanical finishing processes, as will be discussed later. The role of the index of refraction is also important in that surfaces with high indices of refraction have more scattering potential since these surfaces reflect and refract light more dramatically. This implies that the spatial tendency, whether diffuse or specular, will be enhanced. The index of refraction becomes especially pertinent when evaluating various coatings, as we will see in later discussions.

As was the case with brightness, there are special purpose measuring devices used in the paper making industry to determine gloss. The standard equipment and procedures used in making these measurements are described in TAPPI T 480 and T 653 (TAPPI T 94). Gloss is specified by on a scale of 0 to 100 *gloss units*. Typical values for matte finished papers range from a few to 20 gloss units. Gloss is imparted to sheets mainly through a mechanical process that smoothes their surfaces. Sheets that have gone through these special finishing processes have gloss readings ranging from 20 to 40 gloss units, with higher values attained in special cases such as cast-coated, lacquered, or waxed sheets.

High gloss is desirable in some of the same instances as high brightness, namely where capturing the readers attention is paramount. Glossy paper has a visually appealing property similar to a photograph. Depending on the ink formulations used, glossiness can also increase the intensity and brilliance of printed sheets. For these reasons, high gloss is appropriate for printed images. Gloss tends to increase eye strain, so it may not be desirable for applications where extended reading is required.

Reflectance

The properties of gloss, brightness, whiteness, and color are all special cases of the more universal property: reflectance. In its most general form, reflectance is defined as the ratio of diffusely reflected light over the incident illumination, integrated over the visible spectrum. This value represents only the gross reflectance and does not take into consideration either the spatial, or the spectral characteristics of the sample. Incident light that is not accounted for in the measured reflectance is either absorbed into the body of the sheet, or transmitted through the sheet and escapes out the other side. The general definition of reflectance can then be narrowed by constraining such parameters as the wavelength of light measured, as in brightness determination, or the geometry of the measurement, as is done for gloss determination.

The reflectance measurements most often used in the paper industry are defined by the backing material used when taking the measurement and are given in Table 1. The reflectance value is widely used in theoretical treatments of the optical properties of a sheet, but is not generally used directly in production environments. Reflectance is used in this context mainly in calculations to determine the various opacity values used in the industry. Brightness and whiteness are the properties that are more often used to describe the reflective properties of a sheet.

Opacity

Opacity relates to the ability of a sheet to hide what is underneath or printed on the reverse side of the page. This value can be derived from the sheet's reflectance values. It is important for printing and writing papers because increased show-through will

Table 1: Reflectance Definitions.		
R_0	=	The reflectance of a sheet when backed by an ideal black absorber.
R_{100}	=	The reflectance of a sheet when backed by an ideal 100% reflector.
$R_{.89}$	=	The reflectance of a sheet when backed by an 89% reflector.
R_∞	=	Visual Efficiency: The reflectance of an (infinite) pile of sheets such that all light is either reflected or absorbed (none transmitted.) In practice this measurement is taken on a finite sized pad, the number of sheets in the pad being determined experimentally by noting when changes in the reflection incurred by adding more sheets becomes non-detectable.

reduce the print contrast and degrade the perceived quality of the printed material. Opacity is also important for a number of paper applications, such as packaging, where show-through is not desirable. Sheets with higher opacity values are more appropriate for these applications.

As we noted earlier, light entering a sheet can undergo a number of phenomenon: it can be absorbed into the sheet, reflected back from the surface/subsurface, or transmitted through the sheet. The opacity of a sheet specifies the amount of light that is transmitted through it. There are many factors affecting the transmittance. Papers with greater thickness or higher basis weights tend to be more opaque, as less light passes through the bulk of the sheet due to greater scattering and more absorption.

Aside from thickness, the absorption properties of the sheet also play a role. Higher absorption causes less light to pass through the sheet, raising the opacity.

Absorption is related to the composition of the sheet: what type of fibrous materials, fillers, and coatings are used. Opacity is also related to the color of a sheet through absorption. Colored sheets will tend to be more opaque as the dyes and pigments added to the sheets will absorb greater amounts of light and decrease the amount of light transmitted. While higher absorption rates enhance opacity, they reduce the reflectivity, and thus caution is used when attempting to increase opacity by increasing absorption. Increasing the reflectivity of a sheet will also enhance the opacity, and may be a better approach to increase the opacity. We will explore this trade off further in later sections.

Since opacity is related to the translucency of a sheet, it can be derived from two dissimilar reflectance values. In the case of one form of opacity, called the *contrast ratio* in the industry, the value is defined as the ratio of the reflectance of a sheet on top of a black backing (R_0) over the reflectance on top of an ideal reflector (R_{100}). (See Table 2.) In this case, the two reflectance values are different due to the fact that light must be transmitted through the sample twice for the R_{100} value, whereas the R_0 value ideally contains only reflected and no transmitted light. As the opacity increases, transmission is lowered, and the value of R_{100} will be closer to that of R_0. A number of opacity values are defined in a similar fashion and are listed in Table 2.

The primary characteristic that the opacity value of sheet should capture is its show-through. The Printing Opacity (C_0) version of opacity is believed to be the most representative of this important characteristic (Bureau 89). The Contrast Ratio ($C_{.89}$) value is used more often however, because it is an easier measurement to make. Another factor in show-through not directly related to opacity, is strike-through. Strike-through is the result of ink penetration into the paper which makes the paper more transparent in these regions. Strike-through is not readily measured and is sometimes not apparent until well after the printing process has been completed.

Table 2: Opacity Definitions.

$C_0 = R_0/R_{100}$ Contrast Ratio (ideal): This opacity value relies on having an ideal backing and is rarely used because of this fact. The following formulation for $C_{.89}$ is what is used in practice to determine the contrast ratio.

$C_{.89} = R_0/R_{.89}$ Contrast Ratio: This specification for opacity involves measuring the reflectance over a black backing and then over a white body having an absolute reflectance of 89%. The black backing must have less than 0.05% reflectance. TAPPI T 425 specifies the methodology for determining this value.

$C_\infty = R_0/R_\infty$ Diffuse Opacity: (Also called Printing Opacity) is specified in TAPPI T 425 and T 519. This procedure replaces the 89% white reflective backing with a (theoretically infinite) pad of sheets of the paper being measured. The R_0 measurement is still done with a single sheet, however the backing for the R_∞ measurement is now a stack of sheets such that increasing the thickness of the pile would not change the measurement (corresponding to the Visual Efficiency value as defined in Table 1). There are two TAPPI specifications that describe the procedure for taking this measurement. The main difference between these specifications is the illumination source in the first case is at a 15° incident angle, whereas it is at normal (0°) incidence for the second. Since opacity does not relate to any spatial characteristics of the reflected light, the diffuse reflectance is measured in both cases.

A number of opacity values are defined in a similar fashion and are listed in Table 2. The primary characteristic that the opacity value of sheet should capture is its show-through. The Printing Opacity (C_0) version of opacity is believed to be the most representative of this important characteristic (Bureau 89). The Contrast Ratio ($C_{.89}$)

value is used more often however, because it is an easier measurement to make. Another factor in show-through not directly related to opacity, is strike-through. Strike-through is the result of ink penetration into the paper which makes the paper more transparent in these regions. Strike-through is not readily measured and is sometimes not apparent until well after the printing process has been completed.

Theoretical Treatments

There are a wide variety of factors both in the composition and the production process of paper that come to bear on the optical characteristics of the final product. We have defined the various properties of interest in the industry and described how values for these properties are empirically determined. No currently existing theories are able to adequately link all the variables of composition and production to the resulting optical properties. There are however, theoretical treatments that have proven useful in predicting how some of the more gross optical properties are affected by changes in these variables. The main properties these theories are concerned with are reflectance (R_0, $R_{.89}$, R_∞) and opacity ($C_{.89}$). None of the theoretical treatments we encountered in the literature dealt specifically with the spatial characteristics of the light scattered from a sheet. The two primary theories only dealt with the diffuse optical characteristics. The two theories and their strengths and weaknesses will be described in this section.

Kubelka and Munk Theory

The primary theoretical model used in the paper industry is based on the work of Kubelka and Munk (Kubelka, Munk 31). This model was originally developed to describe the reflectance and transmittance of semi-opaque films such as paints. The original formulations relate diffuse reflectance and transmittance to the thickness of the film (X),

and to two parameters that are defined as the scattering coefficient (S) and the absorption coefficient (K). The scattering coefficient is defined as the change in reflectance as the thickness of a thin film is increased (Judd 38):

$$\text{Scattering Coefficient: } S = \frac{dR_0}{dX} \qquad \text{(III.5)}$$

The coefficient of absorption is similarly defined as the change in transmittance due to decreasing thickness:

$$\text{Absorption Coefficient: } \qquad K = \frac{dT}{dX} \qquad \text{(III.6)}$$

Slightly modified versions of these coefficients are used in the paper industry and are called the *specific* scattering coefficient (s) and the *specific* absorption coefficient (k). The difference between the modified coefficients and those used in the pure form of the Kubelka-Munk formulations lies in the fact that thickness is an awkward parameter for paper, and basis weight is used in its place. In the most general case, the value of these two coefficients is wavelength dependent and the subsequent equations are assumed valid only for that wavelength.

Given the above definitions, two simultaneous differential equations can be derived describing the transport of light through a very thin layer. The geometry for this situation is shown in Figure 15, in which a turbid media has been applied in a uniform film over a substrate with reflectance C. The incident light which is transmitted down through the media is represented by i, while the light which is transmitted up back toward the surface (as result of scattering from lower layers) is represented by j. The incident light which will be reflected from the media is then the integration of the scattering from i,
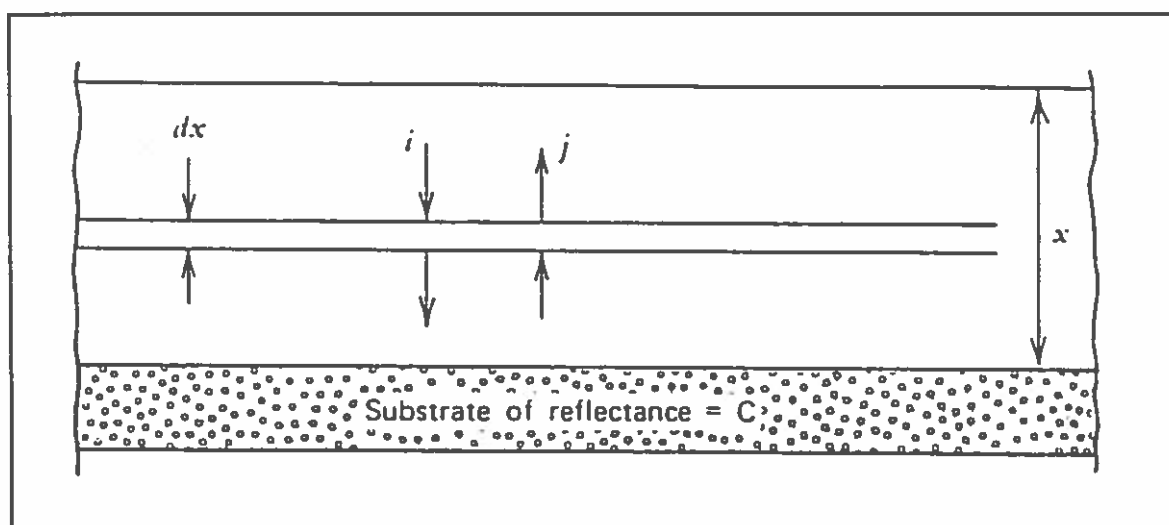
Figure 15: The transport of light through a turbid media (Mitton 73).

minus the absorption from j, integrated over the thickness x of the material in question. A particularly accessible derivation of the Kubelka-Munk equations can be found in (Haase 91), to which the reader is referred for further insight.

In the basic Kubelka Munk formulation, reflectance is related to the ratio of the two parameters s and k:

$$R_{\infty} = 1 + \frac{k}{s} - \sqrt{2\frac{k}{s} + (\frac{k}{s})^2} \qquad \text{(III.7)}$$

Equation III.7 allows the reflectance of a pad of sheets to be calculated given the ratio of the coefficients for the sheets. According to equation III.7, the reflectance is a function of the ratio k over s such that increases in s will increase the reflectance, if k is held constant. This corresponds to an increase in reflectivity with increased scattering. If s is held constant and k is increased, we will see a lower reflectance due to increased absorption. These tendencies are shown graphically in Figure 16, where the visual efficiency calculated in equation III.7 is plotted vs. the coefficients k and s.

Note that thickness (X) is absent in Equation III.7 since we are calculating reflectance for an infinitely thick pad of sheets in this case. Subsequent Kubelka Munk equations use thickness as one of the primary parameters. The thickness of a sheet is often difficult to determine, and varies with humidity and external force (a sheet of paper is readily compressed.) While this parameter was used directly in the early applications of the Kubelka-Munk theory to paper by (Steele 35) and (Judd 38), it has since been abandoned in favor of basis weight (W). The substitution of W for X was first proposed in (VandenAkker 49) and has been used ever since. Basis weight is the weight per unit area of a sheet and is determined by the weight of a ream of (500) sheets of pre-defined dimensions, as specified in TAPPI T 410. Basis weight is a commonly used value in the industry and thus is better suited for use in the Kubelka-Munk formulations.

As was shown above, R_∞ is related to the ratio k over s and it is common practice to derive and use this ratio independently of specific values for s and k. Another composite value that is useful when applying the Kubelka-Munk equations to paper, is the product sW. Given sW and R_∞ the reflectance ($R_{.89}$, R_{100}, R_0) can be calculated by:

$$R_g = \frac{(g-R_\infty)\big/R_\infty - R_\infty(g-1/R_\infty)a}{(g-R_\infty)-(g-1/R_\infty)a} \tag{III.8}$$

$$a = e^{sW(1/R_\infty - R_\infty)} \tag{III.8a}$$

Where g in equation III.8 represents the reflectance value of the backing used. The contrast ratio can also be calculated given sW and R_∞ :

$$C_{.89} = \frac{(-1+a)[0.89 - R_\infty - (0.89-1/R_\infty)a]}{(-R_\infty + a/R_\infty)[0.89/R_\infty - 1 - R_\infty(0.89-1/R_\infty)a]} \tag{III.9}$$
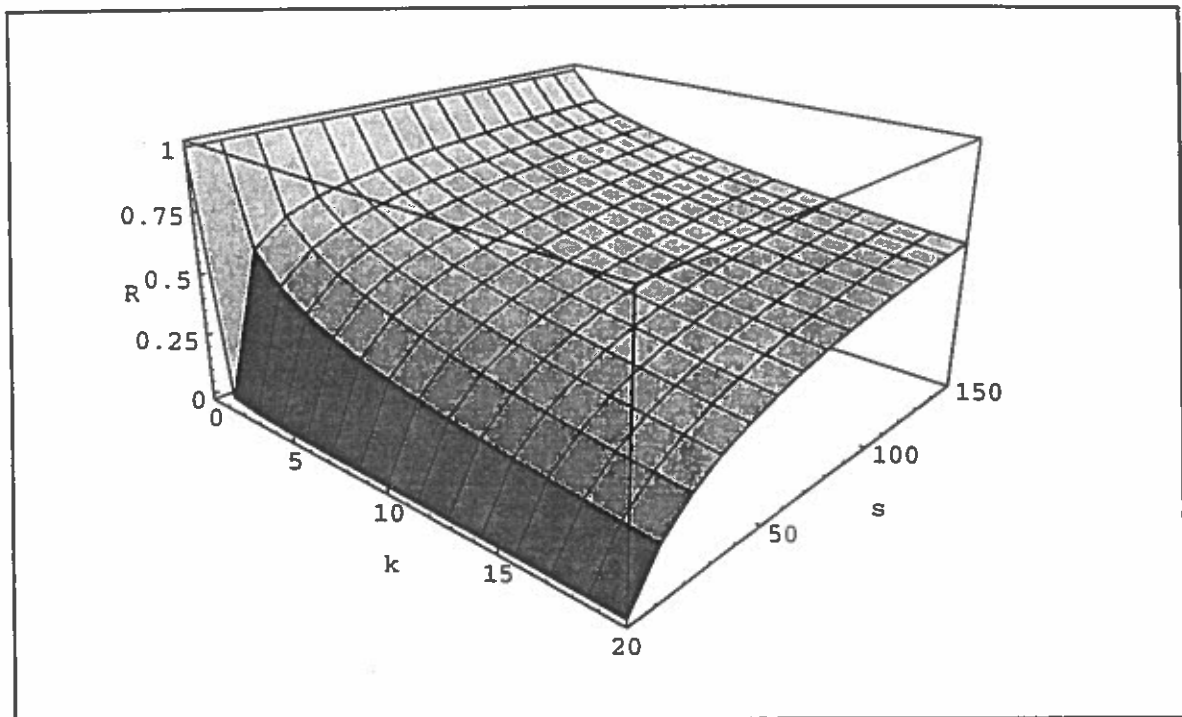
Figure 16: The visual efficiency *R0* plotted against the scattering coefficient *s* and the absorption coefficient *k* according to equation III.7.

Both equation III.8 and III.9 are part of a complete overview of the Kubelka-Munk equations for paper found in (Robinson 75). This reference contains permutations of theequations solved for the various parameters in terms of various known values, and also describes the methods used in determining the *s* and *k* coefficients for a sheet.

One of the primary benefits of the Kubelka-Munk formulations is its predictive power in determining the optical behavior of multi-ply or conglomerate sheets. Once the values of *s* and *k* have been derived for specific materials, the optical properties for sheets composed of the two materials can be determined. Given a composite sheet with known percentages of the materials, the composite *s* and *k* can be found by:

$$s_{comp} = s_1 W_1 + s_2 W_2 \qquad \text{(III.10)}$$

$$k_{comp} = k_1 W_1 + k_2 W_2 \qquad \text{(III.11)}$$

where W_1 is the basis weight of material 1, and W_2 is the basis weight of material 2 such that:

$$W_{comp} = W_1 + W_2 \qquad \text{(III.12)}$$

where W_{comp} is the entire basis weight of the composite sheet. The new s_{comp} and k_{comp} can then be used in Equations III.7, III.8 and III.9 to predict the optical properties of the composite sheet. This method generalizes to greater than two materials.

Originally this compositional method was applied to multi-ply sheets and sheets composed of pulp mixtures. As production methods advanced, the method was retrofitted to include the various fillers and coatings that are ubiquitous in the industry today (Clark 65, Ramsay 66, Starr 76, Starr 78, Howard 83). The results of these attempts varied as it was found difficult to determine specific s and k values for the materials in question. One observation was that the values of s and k varied both with the concentration of the material, and with the mechanical process employed in the production of the sheet (Paulner 82).

There are a number of possible reasons why the Kubelka-Munk formulations perform poorly in these circumstances. These reasons are primarily related to the assumptions concerning the thickness made in the original Kubelka-Munk formulations. The Kubelka-Munk equations were originally derived for media in which there is significant internal scattering, and little or no direct surface scattering or transmission. Media that is too thin for internal scattering is governed by Lambert's law and is not appropriate for Kubelka-Munk analysis since there may be direct transmission. Thicker

materials are characterized by higher reflectance and low transmittance, and luckily all but the thinnest caliper of paper fall into this range. Coatings however, may be applied in optically thin layers, and may be further compressed by mechanical finishing processes. It is doubtful that coatings in this context fall under the thick film assumptions made in the Kubelka-Munk formulas.

Cases where there is a high degree of surface reflection, such as high gloss sheets, are also not meant for Kubelka-Munk analysis. This deficiency in the Kubelka-Munk equations was noted early on in the pigment industry, and corrections to account for this case were formulated by (Saunderson 42), but were not adopted by the paper industry due to the considerable complexity they added to the solutions.

There is one final deficiency worth mentioning that relates more generally to the application of the Kubelka-Munk equations to paper. The original formulations assume that there is a uniform distribution of scattering material in a given film under consideration. It is well known that there are significant variations in the distribution of mass in a sheet of paper (Jordan 87). The paper industry uses the term *formation* to describe a sheet's uniformity of mass distribution. Sheets with poor formation (highly non-uniform distributions) will exhibit local inconsistencies in scattering and absorption which are not accounted for in the Kubelka-Munk solutions.

Scallan and Borsch Theory

Given the limitations in the Kubelka-Munk formulas, an alternative approach based upon optical considerations of the morphology of a sheet is presented in Scallan and Borsch, (1972). Their theory is based upon a model of paper that consists of multiple layers of the actual fiber cell walls of the sheet and air. The scattering of light is then accounted for by applying the Fresnel laws to the cell wall/air interface. Absorption

is assumed to occur when light travels through cell walls and is governed by the Bouger-Beer laws. In this way, the overall reflectivity and opacity are related to actual physical parameters of the sheet, such as the thickness of the cell walls, the refractive index of the fiber material, and the number of fibers in a cross section of the sheet.

In order to account for the light reflected from a sheet, the sheet is modeled as a series of parallel layers consisting of cell wall material separated by air. The reflectance and transmittance of a single layer are first calculated by (Scallan and Borsch 72):

$$R_1 = r + \frac{r(1-r)^2 f^2}{(1-r^2 f^2)}$$ (III.13)

$$T_1 = \frac{(1-r)^2 f}{(1-r^2 f^2)}$$ (III.14)

where

$$f = e^{-2at}$$

$r =$ A constant corresponding to the reflectivity of the cell wall/air interface.

$t =$ Thickness of a layer.

$a =$ The absorption coefficient of the cell wall material.

Once the values of R_1 and T_1 for a single layer are determined, the number of layers in sheet (n) is calculated using the basis weight (W), specific volume for the cell wall material (V), and the thickness of the layers (t):

$$n = \frac{VW}{t}$$ (III.15)

Using the value obtained for n along with R_1 and T_1 the sheet reflectance R_0 can be calculated from:

$$R_0 = R_n = R_1 + \frac{R_{n-1}T_1^2}{1 - R_1 R_{n-1}} \qquad\qquad \text{(III.16)}$$

The reflectance value R_∞, which is important in some opacity determinations, can be calculated by increasing the value of n until R_n becomes independent to further increases in n.

Scallan and Borsch showed these formulations to agree well with empirical measurements (Scallan and Borsch 72, 74, 76). The theory also performed well in situations where the Kubelka-Munk equations had poorer results, such as with very thin sheets and with sheets with lower reflectivity due to high absorption fiber material. The superior performance of the morphological approach is attributed to the fact that it uses constants (f, n, a) that are based upon measurable physical quantities. The specific scattering and absorption coefficients of the Kubelka-Munk equations do not take into account the actual physical construction of the sheet, nor the optical laws that apply to it. It should be noted that the actual measurement of the constants in the morphological model is experimentally tedious, and for this reason the Kubelka-Munk theory still enjoys the most use in the industry.

The problem of non-uniform mass distribution that was found to plague the Kubelka-Munk assumptions was also addressed by Scallan and Borsch, (1976). By letting the number of layers (n) and the thickness of the layers (t) vary, they were able to integrate the effects of poor formation into the calculation of opacity and reflectance. While the theory proved extensible, these formulations added significantly to its complexity.

Optical Factors in Composition and Production

Now that we have both a clear definition of the optical properties that are of importance, and theoretical models to explain these properties, we would now like to explore the factors in the construction of paper that influence its optical characteristics. There are two primary considerations: what are the materials paper is composed of, and what processes are used to create it. In particular, we are interested in determining how these materials and processes affect the final appearance of the sheet, and how the theoretical approaches account for these relationships.

The manufacture of paper can be decomposed into three stages. First the *base stock* is constructed from a raw fiber source. For all intents and purposes, the base stock alone can be considered paper. In fact this single stage process has been used for hundreds of years to manufacture paper. In the modern process there are two other steps which may follow the construction of the base stock. Mineral pigments in the form of coatings may be applied to the base stock after formation. Additionally the coated, or uncoated, stock may go through a mechanical finishing process which imparts a desired texture to the final product. Each of these stages and the materials involved play a role in the final appearance of the sheet. The next few sections will discuss these stages and their effects of the optical properties of a sheet.

Construction of the Base Stock

The first step in constructing paper involves depositing suspended fibrous raw material onto a moving wire. The liquid solution containing the fiber is allowed to drain away and the fibers randomly interleave which results in the formation of a complex web.

Several layers of fiber are applied to this initial layer in order to build up the thickness of what becomes the base stock. The factors in this stage of the production that influence the optical properties include:

- The source of the raw material.
- The amount of material used.
- The treatment of the raw material.
- The uniformity in the distribution of material (*formation*).
- The isotropic tendencies of the fiber in the web.

After the base stock is formed, coatings or finishing techniques may be applied. Both of theses processes will further contribute to the appearance of the final product.

Source of Raw Materials

The fibrous raw material, or *pulp*, used in the composition of the base stock can come from a variety of sources. Regardless of the source, the pulp consists primarily of cellulose based fibers. Currently the most common source of fibrous raw material for domestic production is wood pulp. Cotton is used to a lesser extent and is noted for the purity of its cellulose content. Exotic sources such as bamboo, bagasse (sugar cane), hemp, and man made polymers are used rarely in the United States, but enjoy wider uses in regions where wood pulp is not readily available. The main optical characteristics affected by the choice of pulp are color and brightness.

Cellulose fibers in their pure form resemble hollow transparent cylinders. During processing the fibers may deform and come to resemble thin ribbons in the web. The cell walls composing a fiber have relatively low, non-selective absorption, and an index of

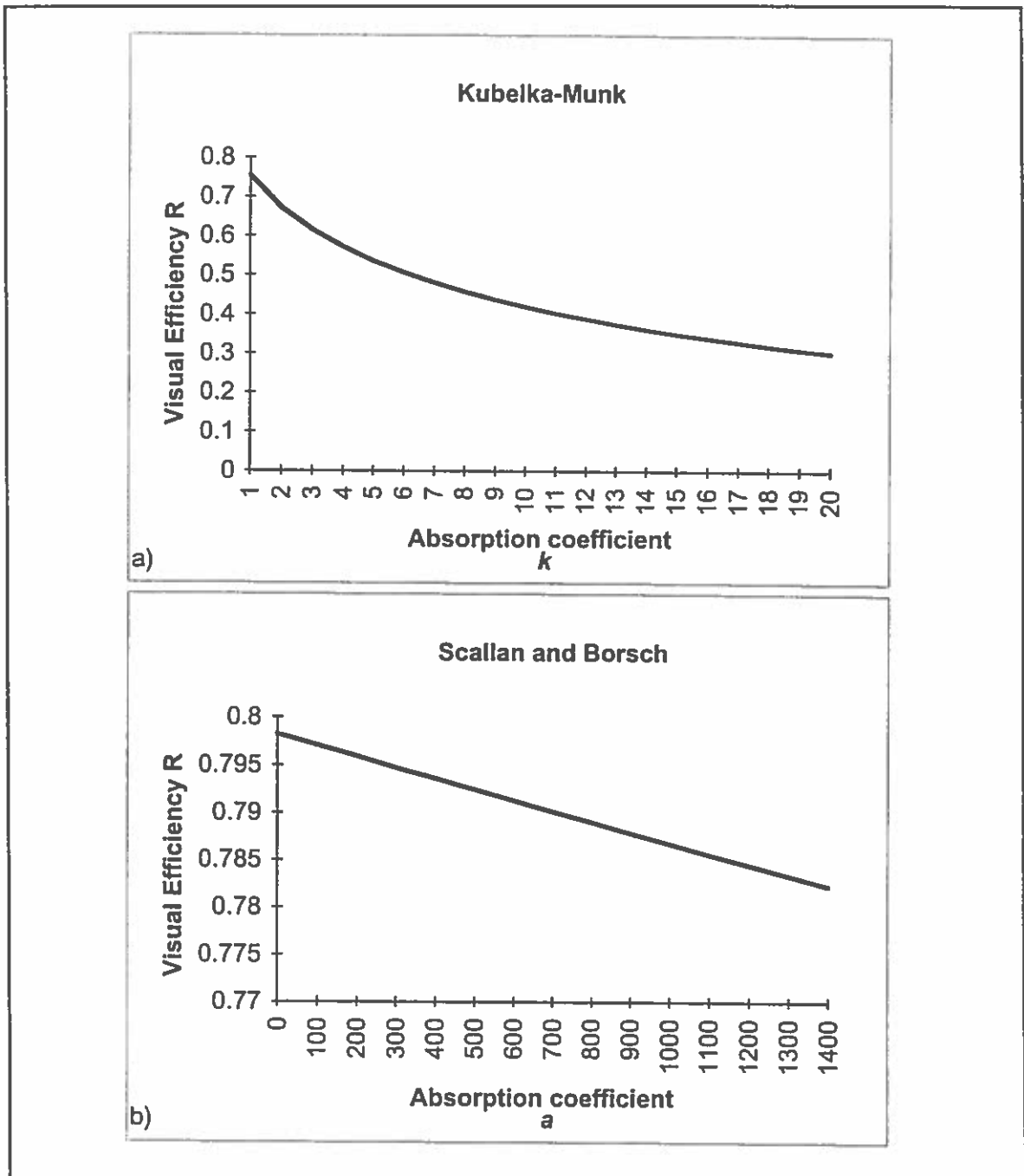Figure 17:   a) The Kubelka Munk solution for R_∞ Equation. III.7 plotted with s held constant and k varying. b) Scallan and Borsch solution, Equation. III.16, plotted with varying a and other parameters held constant.

refraction of 1.56 (Harrison 62). Since pure fibers are transparent, and generally have little absorption, the visual characteristics of the base stock is governed primarily by the

scattering of light from the many air-cell wall interfaces. Given this fact, the main optical effect, that results from the choice of raw pulp, is related to the purity of its fiber content.

Cotton is one of the best known sources for pure cellulose. When cotton is used as the primary fiber source, the resulting stock has uniform reflectance and high brightness. Wood, on the other hand, is composed of both cellulose and lignin, a binding agent. While the wood pulping process is designed to reduce the lignin content in the finished pulp, some still remains. Wood based papers have a reduced reflectance because of their lignin content, since lignin has higher absorption than cellulose. This absorption is more pronounced in the blue range of the spectrum, resulting in lowered brightness and a yellowish cast. These factors can be offset to some extent by treating the pulp with bleach or fluorescent agents.

As we can see, the primary optical effect of different fiber sources lies in the spectral absorption profile of the material. In the context of our two theoretical models, this difference manifests itself in the respective absorption parameters of the formulas. In the Kubelka Munk approach, the specific absorption coefficient (k) will have a wavelength dependence that is proportional to the absorption profile of the fiber source. In the case of wood pulp, we would expect k to be higher in the blue region ($l < 500\ nm$) than the red ($l > 600\ nm$). For cotton fibers, we would expect relatively uniform values for k. The situation is similar in the Scallan and Borsch formulations. In this case the absorption coefficient a in Equation. III.13 and III.14 is also wavelength dependent. The primary difference in the two parameters a and k, is that the a parameter in the Scallan and Borsch equations is a physically based parameter where k in the Kubelka Munk approach is defined only in relation to s and the reflectance. This makes the experimental determination of appropriate k values tedious. In fact, these values can not be directly

measured, but must be calculated from careful reflectance measurements of sheets with known basis weights. The relationship between these parameters and the visual efficiency calculated from the two theories is shown in Figure 17. Part a) of this figure shows how changes in the Kubelka-Munk coefficient k affect the visual efficiency. In contrast to the non-linear relationship between the Kubelka-Munk absorption coefficient and the reflectance shown in part a), the a parameter in the Scallan and Borsch formulas has a linear relationship to the visual efficiency as shown in part b) of this figure. In either case, the choice of pulp is directly related to the values of these respective absorption coefficients.

Amount of Raw Materials (Basis Weight)

A second factor affecting the optics of a sheet is related to the amount of material contained the base stock. The thickness, or bulk of a sheet affects both the optical and mechanical properties of the final product. For instance, both opacity and reflectance are correlated to the bulk of a sheet. It would be useful to have a metric that quantifies this sheet bulk and the *basis weight* of a sheet is such a measure. Basis weight is defined as the weight per unit area and is fundamentally related to the amount of material in a sheet. It is measured by weighing a ream of 500 sheets of pre-defined dimensions. These dimensions, called the *basic size* of the sheet, vary slightly by paper grade and application. As this metric is related to mass, it is also used to specify the content amounts of additives such as fillers and coatings. When basis weight is referred to in the context of the base stock, the value relates to the quantity of fiber in the web. As more raw material is deposited on the web during formation, the basis weight increases. Because of this relationship, the basis weight is also correlated to the thickness of the sheet. The thickness, or *caliper* of a sheet, is sometimes an important measure itself, but

Kubelka-Munk Effects of Basis Weight
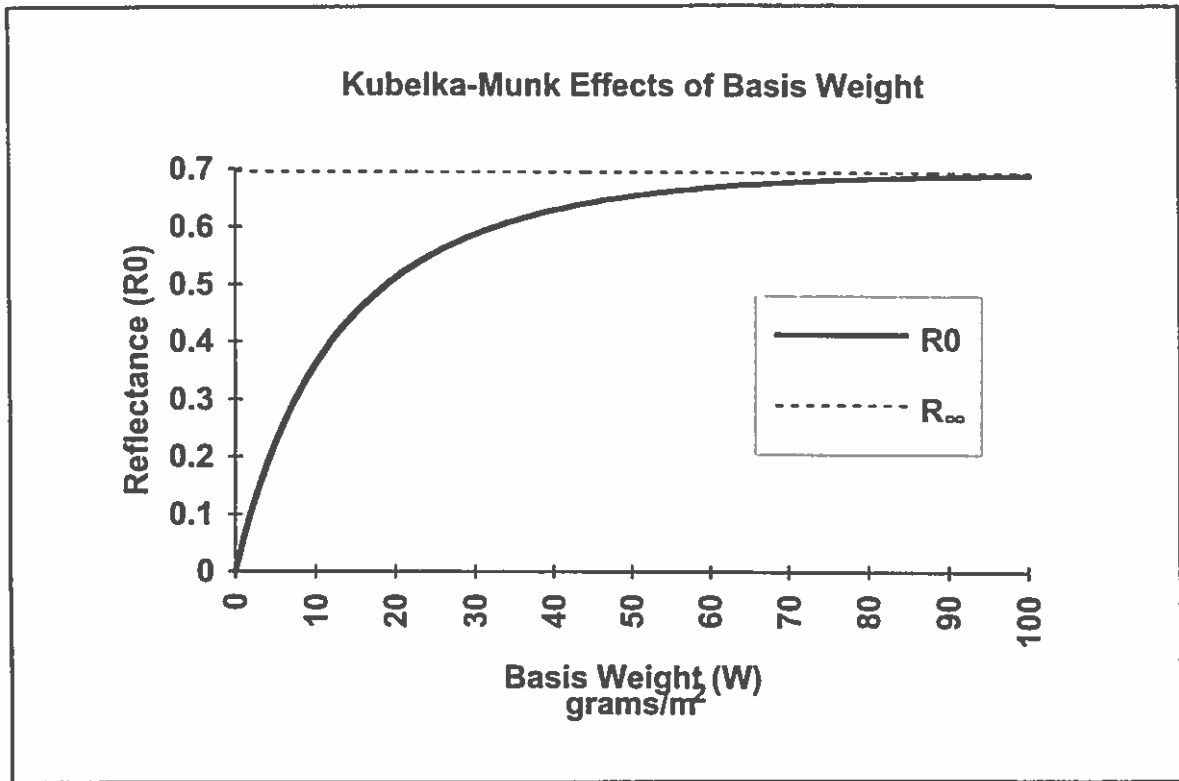
Figure 18: Kubelka Munk solution, Equation. III.8 plotted with s and k held constant and W varying (s and k values are typical for unbleached mechanical pulp, typical reference sheets often have a basis weight of 60 g/m²).

since paper is compressible and sensitive to humidity, the basis weight is the preferred metric.

The primary optical characteristics that basis weight influences are the reflectivity and opacity. Absorption, and to a lesser extent scattering, are amplified as the internal bulk of a sheet is increased. The increase in bulk will raise the opacity as there is less overall transmission of light through the sheet. The effect on the reflectance, however, is more subtle. The increased amount of material provides more surfaces available for scattering, which tends to raise the reflectivity; however this greater bulk of material also introduces more absorption, which will offset the increased reflectivity. Figure 18 shows the effects of changes in the basis weight on the reflectivity as predicted by the Kubelka-Munk equation III.8. As we can see by this figure, the reflectivity asymptotically

approaches the visual efficiency (R_∞) as the basis weight increases. Intuitively this result makes sense, as we would expect an infinitely thick sheet to have the maximum reflectance for a given fiber source or bond type.

In contrast to the Kubelka-Munk approach, the Scallan and Borsch formulations relate basis weight to the number of layers (n) in a sheet through equation III.15. The parameter n in equation III.15 is proportional to the basis weight and is related to the reflectance through equation III.16. This relationship is shown in Figure 19. Figure 19 shows the effects of varying n (proportional to the varying basis weight in Figure 18), while keeping the values of f, a, and t constant. In this approach, the visual efficiency (R_∞) is not explicitly solved for, but is defined as the asymptotic value approached as n is increased without bound.

Treatment of Raw Materials

Before the fibrous raw material is used to construct the web, there are a number of chemical and mechanical treatments it may undergo which will affect the optical properties. The fibrous material is first subject to a process which separates the fibers from their naturally occurring configurations. After the fibers have been isolated, bleaches or dyes may be added to the pulp solution in order to directly influence the optical characteristics. Finally the pulp solution may be augmented with filler material before, or during, the web formation process.

The fibers in a raw material must first be isolated in liquid solution before being applied to the wire. The maximum fiber resolution is desired because if the solution contains multi-fiber flocks, they will show up in the final sheet as dark spots. Isolating and breaking down the fibers before they are applied to the web also increase *bonding,* which is the phenomenon in which fibers are electrostatically coupled in the web. Inter-

Scallan and Borsch Effects of Mass (Basis Weight) on Reflectance

Reflectance (Rn) vs **Number Layers (n) (Proportional to mass)**
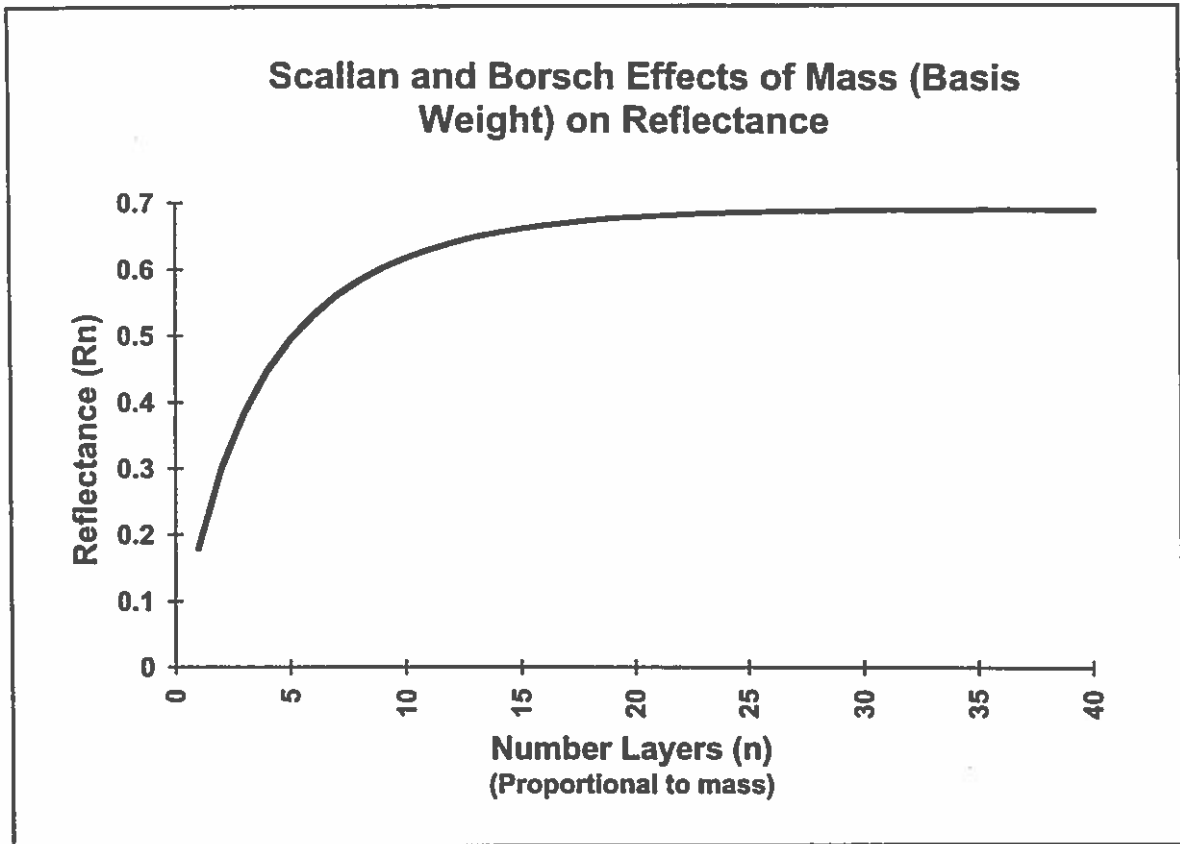
Figure 19: Scallan and Borsch solution, Equation. III.16, plotted with f, a, and t held constant and n varying.

fiber bonding is what keeps the web from falling apart after formation, and is what gives paper is strength and durability. The process that achieves this separation is called *beating*. Beating was originally accomplished by subjecting portions of pulverized raw material to continuous agitation. This constant action, coupled with the addition of a liquid solution, serves to isolate the fibers. More recently this mechanical process has been augmented with chemical processes that produce more uniformly separated and sized fibers.

In addition to isolating the fibers, beating will break fibers down into smaller parts. By decreasing the particle size, more fibers are allowed to occupy the same space, which increases the number of air-cell wall interfaces available for scattering. Since the individual

particles are smaller, there is also a decrease in absorption due to the shorter average path length that the light travels when passing through these smaller particles. This results in a greater ratio of scattering to absorption and in an increase in overall reflectance. This relationship between particle size and reflectance has been explored in simulation work done by Gondek, Meyer, and Newman (1994). This study simulated the effect of decreasing particle size in pigmented plastics. The results of this work support earlier observations that decreasing particle size increases scattering and reflectance. The inverse relationship between particle size and reflectance is known to hold until the particle size is decreased to a size comparable to the wavelength of light. At this point the relationship begins to break down as interference and small-particle effects such as diffraction begin to dominate. In the case of paper, this relationship breaks down much earlier, well before the fiber size approaches this limit (VandenAkker 82). If the fibers are broken up too finely, the small fiber particles will bond into larger homogenous masses when applied to the web. This results in large transparent areas with relatively low scattering, and correspondingly lowered reflectivity. The complex relationship between the degree of beating and the reflectivity is shown in Figure 20.
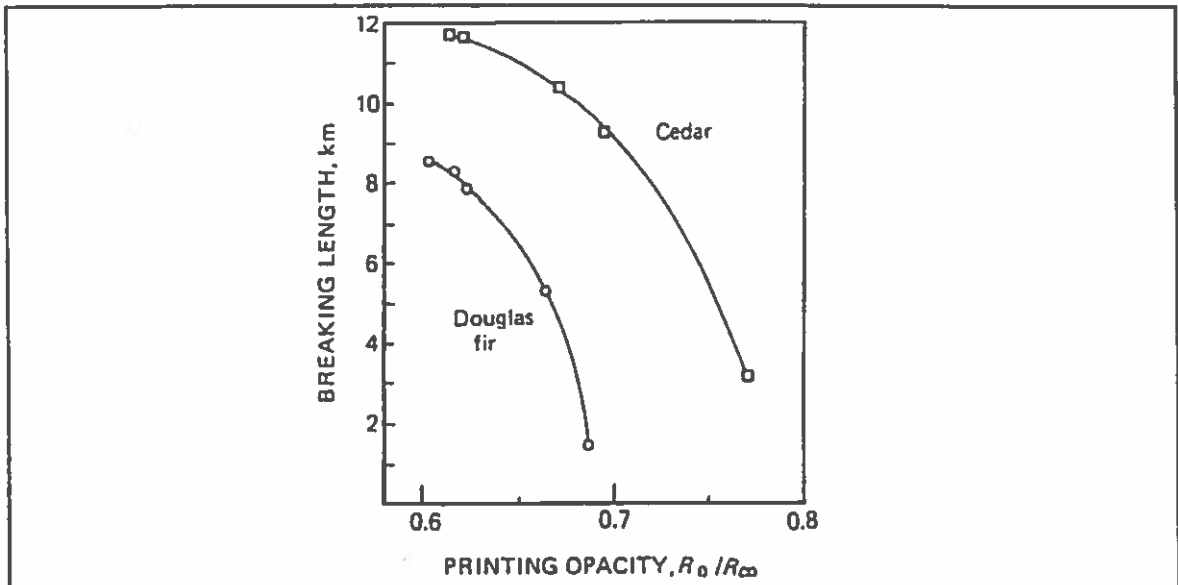
Figure 20: Degree of beating expressed as Breaking Length vs. Opacity. Smaller breaking length corresponds to further beating. Notice that with increased beating the increase in opacity becomes smaller. (From Scallan and Borsch 1974)

The effect shown in Figure 20 is difficult to capture in the theoretical treatments. The only way for the Kubelka-Munk formulations to account for this relationship is through the specific scattering coefficient (s). For a given pulp beaten to the apex of the curve in Figure 20, we would expect Kubelka-Munk analysis to yield a high s value; while a lower s would be expected at any other level of beating. This implies that the specific scattering coefficient is a product of both the pulp source, and the level to which it is beaten. The dependence of s on the degree of beating complicates the application of the Kubelka-Munk equations to paper. In a production environment, the beating level is controlled enough to permit the use of Kubelka-Munk analysis, but this impact on s should be noted.

The Scallan and Borsch formulations deal with this relationship more straightforwardly. In this approach, two parameters: thickness (t) and the number of layers (n), are directly linked to beating. Initially, increased beating causes a decrease in the thickness of the cell wall layers which will result in a rise in n as predicted by

equation III.15. Additional beating will eventually cause a rise in the thickness due to increased inter-fiber bonding. The number of layers for a constant basis weight will then decrease. This effect can been seen in Figure 21 where the reflectivity has been plotted against the layer thickness (t) for a standard 60 g/m^2 sheet.

Pulp Additives

In addition to the beating process, the fiber solution may be augmented with either chemical or material additives before formation of the web. The specific additives we are interested in are those that are designed to impact the appearance of the sheet. These additives include: bleach, dyes, particulate filler, and fluorescent agents. Each of these compounds are used to enhance or change specific optical properties of the final product. The next section will briefly discuss how these agents are used in the production process and to what extent they shape the final appearance of the sheet.

Both bleaching agents and dyes are used to control the absorptive properties of fiber material. Bleaching agents are added to the pulp solution to decrease any influence lignin, or other absorptive impurities may have. Bleached pulp will have a more even spectral response, and generally higher brightness values due to decreased absorption. In contrast, dyes are used primarily to produce colored sheets. As opposed to bleach, dyes will increase absorption and usually are applied to selectively absorb portions of the visual spectrum in order to produce the desired color. Dyed pulps will yield base stock with a lower reflectance than stock of similar pulp that is not dyed. While bleach and dyeing have opposite effects on the absorptive properties of a pulp, they are often used in conjunction, as dye takes much better to pulp that has been previously bleached (Bureau 89).

Effects of Layer Thickness in Scallan and Borsch Eq.
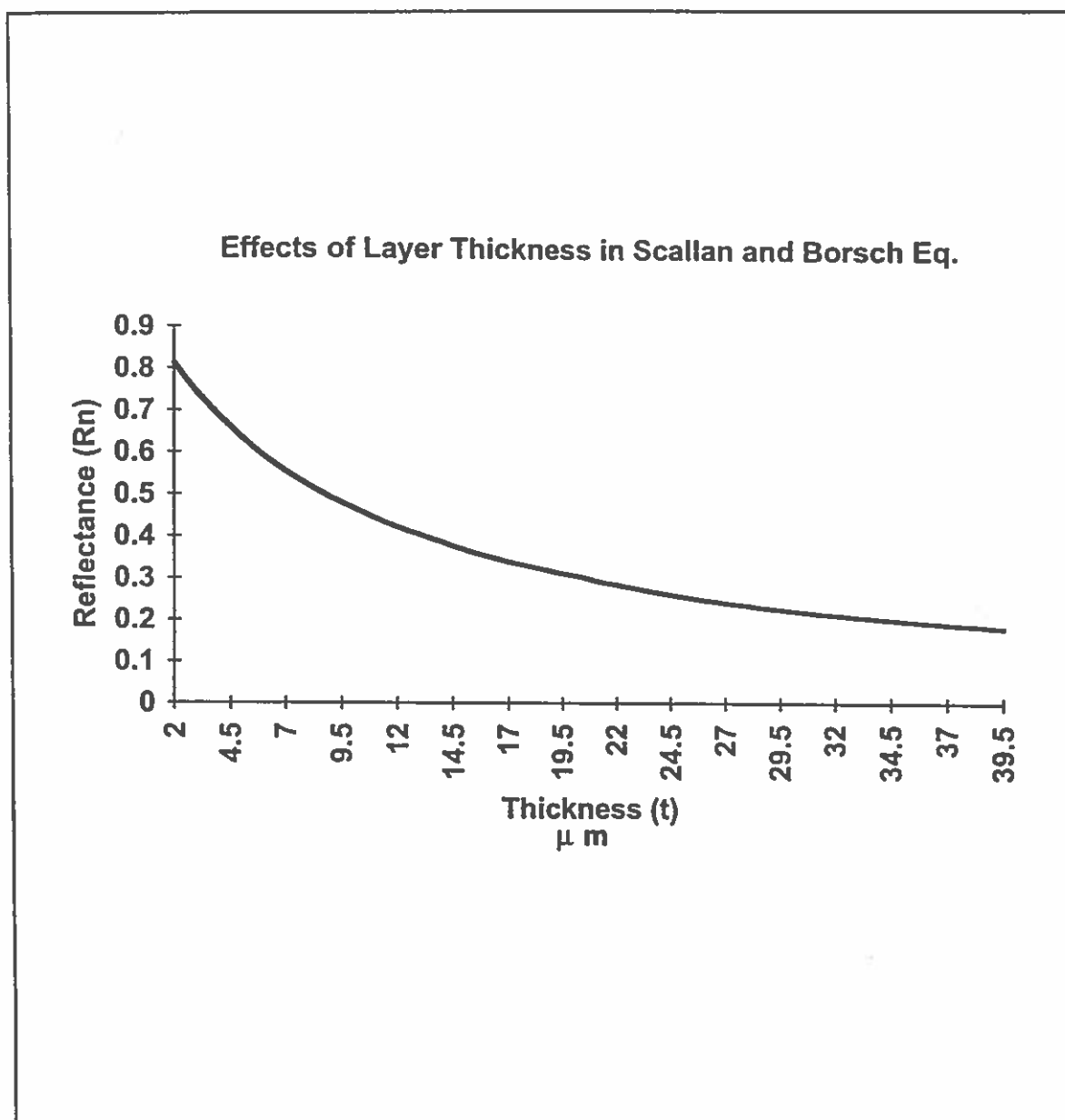
Figure 21: Plot of t vs. reflectivity predicted by equations III.13-III.16. The values of W and a were held constant, while the number of layers n was allowed to vary with t according to equation III.15 (W=60g/m², graph shown is interpolated for non-integer values of n).

Since both bleach and dye are used to control the absorptive properties of the pulp, the theoretical treatments account for these additives in their respective absorption coefficients. Much as was the case with different fiber sources, the wavelength

dependent absorption coefficient will characterize the effects of the dye or bleach. Dyed pulps will have higher non-uniform absorption coefficients, while bleached pulp should have lower, uniform coefficients. It should be noted that the Kubelka Munk formulations are known to perform poorly in ranges of high absorption (Van den Akker 82). This poor performance results from the difficulty in deriving the specific absorption coefficient for dyed papers, and because the effects of non-uniform mass distribution manifest themselves more markedly under these conditions.

A third type of additive to the fiber solution are florescent agents. These materials come in the form of either dyes or optical brighteners, and have the unique property that they absorb ultra-violet light and reflect it back in the visual spectrum. Stock constructed from pulp that has been treated with florescent materials is exceptionally bright and difficult to characterize with either of the theoretical formulations. Because there is no longer a simple one-to-one wavelength correspondence between the incident and reflected light, neither set of equations can successfully be applied. Florescence also complicates accurate color matching because the reflectivity at any point on the spectrum now depends on portions of the spectrum not normally accounted for in the specification of standard illuminates.

The last type of additive that is used to augment pulp are fillers. Fillers are white pigment particles that are added to the pulp before, or during formation in a process called *loading*. The primary purpose of loading is to enhance optical properties such as opacity, brightness, and whiteness through increased scattering. Substances used for this purpose include clay, calcium carbonate, and titanium dioxide powders. The amount of these materials used, or *loading level,* range from a few to 15 percent of the overall mass of the stock. These small particles fill the gaps inside the hollow fibers, and between fibers in the web. Since the addition of these particles increase the number of available

surfaces, the overall scattering of the sheet is increased. This increased scattering will lead to an increase in opacity, as less light finds its way through the web. Brightness and whiteness will generally increase also due to the greater scattering and the spectral nature of the pigments. Since these pigments are also used as coatings, we will forgo any specific discussion of the nature of these substances until the next section. In addition to the optical properties loading affects, it also decreases the influence of humidity on the structural stability of the sheet.

Although based on the morphology of the sheet, the Scallan and Borsch theory does not attempt to account for material additives such as those used in loading or coating of the base stock. The Kubelka-Munk approach characterizes the overall scattering and absorption of a material without regard to internal structure, so in theory, these formulations do not have the same limitations as Scallan and Borsch's. According to Kubelka-Munk analysis, if s and k coefficients can be derived for particular individual substances, then the diffuse reflectivity and opacity can be predicted for composite materials, given the percentages of the individual materials that make up the mixture. Careful studies were undertaken by Starr and Young (1976, 1978) to determine the s and k coefficients for commonly used raw pigments and to establish experimental methodologies for making these measurements. They found that their values did not produce predicted results that agreed with observation for either loadings or coatings. This study further noted that the apparent coefficients resulting from the observed reflectances were not constant for a given material and varied over the loading level. The wide variation in the effects of the loading level on the coefficients led these researchers to suggested that the Kubelka-Munk equations were not adequate and needed revision before being used with loaded or coated sheets.

Formation (Distribution of Mass)

After the raw fibers have been properly prepared and treated, they are applied in multiple layers to the wire to form the base web. Depending on the application method, the fibers may have some directional tendency in the plane of the sheet. We will explore the optical consequences of this angular tendency in the next section. Except for this grain directionality, the fibers can be considered randomly distributed across the area of the sheet. A cross section through any given point on the sheet will cut through a variable number of fibers. This translates into a non-uniform distribution of mass across the sheet. Analogously we could say that there are point to point differences in the basis weight at any point on the sheet. The subjective degree of this non-uniformity is termed *formation*. The statistically determined value is referred to as the *formation index*. A sheet with poor formation has a highly variable distribution of mass, while a sheet with better formation has a more even distribution. Formation affects the optical properties of a sheet because there is a non-linear relationship between mass and both the opacity and the reflectance. The theoretical treatments take two slightly different tacks when approaching this problem.

The effects of formation on the optical characteristics of a sheet can be seen readily by viewing transmitted light through any typical sheet. The apparent light and dark regions correspond to areas of lower and greater mass respectively. The role of mass in the reflectance of paper was shown in Figure 18. Recall that in this figure, the Kubelka-Munk equations were used to predict the reflectivity of sheets with varying basis weights. A similar relationship exists between basis weight and opacity and is shown in Figure 22. As exhibited by this figure, there is a non-linear relationship between the opacity and the basis weight. The opacity is fairly sensitive to changes in basis

Effects of Basis Weight in Kubelka-Munk Eq.
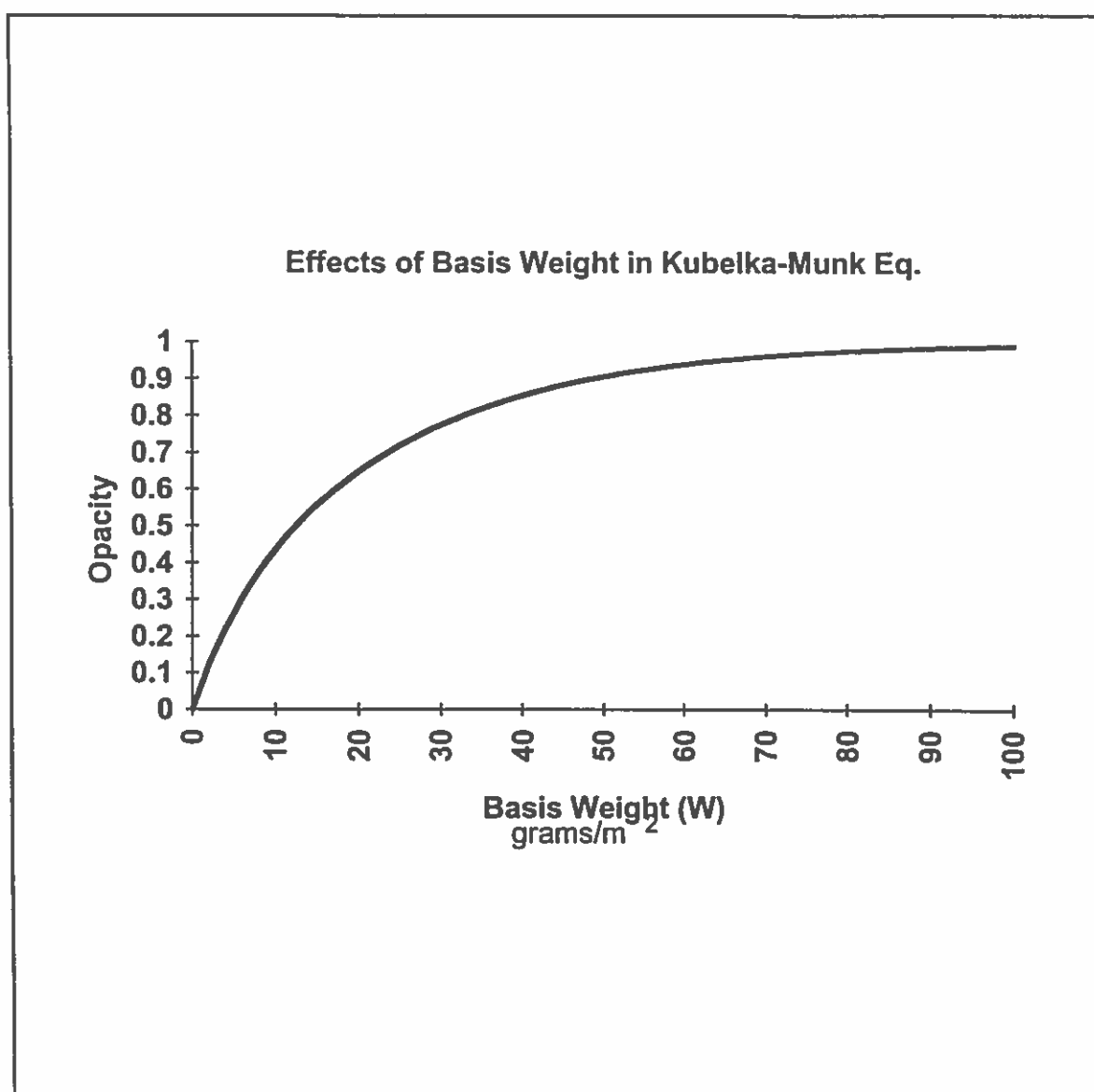
Figure 22: Plot of opacity vs. basis weight as predicted by equation III.9 with all other parameters held constant. Parameter values are the same as those used in Figure 18.

weight in the low regions of the curve, but this dependence levels out in the higher regions. Since in a real sheet there is a non-uniform distribution of mass, the basis weight of the entire sheet is equal to the average of the varying local basis weights. The theoretical opacity values in Figure 22, were obtained from equation III.9 and will not, in

general, agree with the observed opacity of real sheets that have corresponding equivalent average basis weights. When considering a real sheet, the areas of low mass have markedly poorer opacity compared to the average weight of the sheet, than is compensated for by the regions of high mass. Because of the relationship to mass shown in Figure 22, the high mass regions will not make up for the very low opacities in the lower regions, and the resulting mean opacity will be lower than that predicted by equation III.9.

Similar results were observed in work done by Jordan (1987). In this approach, a sheet was modeled as a collection of discrete areas. By considering varying basis weights for these areas, the predicted effects of poor formation were calculated by averaging local opacities derived from the Kubelka-Munk equations. It was observed that real papers showed a Gaussian distribution of mass, so the basis weights for the local areas were distributed in a similar fashion according to:

$$\text{Probability}(w) = \frac{1}{\sqrt{\pi}} exp(-(w - \overline{w})^2 / 2\sigma^2) \qquad \text{(III.17)}$$

where w is the local basis weight, $\overline{w}$ is the average (sheet) basis weight, and s represents the index of formation. This function is plotted for a 60 g/m^2 sheet with a formation index of 0.3 in Figure 23c). A density function for opacity based equation III.17 can then be computed which represents the distribution of local area opacities. This distribution is shown in Figure 23a). When this function is averaged over the area of the sheet, it produces a lower overall opacity than would be predicted for a sheet with the same basis weight but uniform distribution. It was further shown that across sheets with equal average basis weights, the ones with poorer formation had lower opacities. These effects
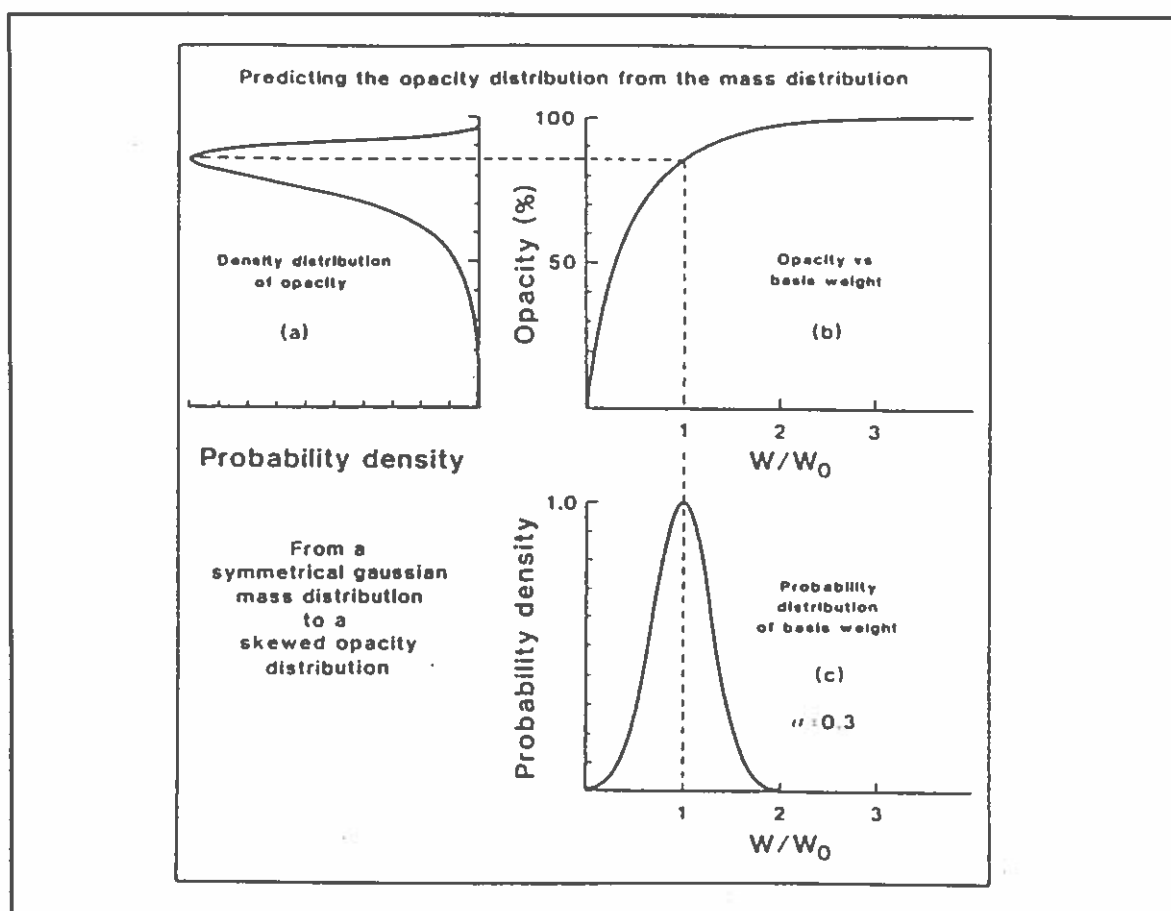
Figure 23a): The distribution of opacities due to the basis weights in part. b) The relationship between basis weight and opacity. See Figure 22. c) The probability distribution of basis weight across a 60 g/m^2 sheet as predicted by equation III.17. Shown as a ratio of local basis weight over average basis weight. (From Jordan 85.)

tend to be more pronounced for sheets with lower average opacities because the sensitivity is much higher in this region of the curve (see Figure 22).

Interestingly enough, this region of lower opacity is where Kubelka-Munk analysis has the worst performance. Jordan's work presents a method for successfully employing the Kubelka-Munk equations for papers that have low opacities. However, a correlation between the specific scattering coefficient (s) and formation was also noted in this work. It was observed that there was a large variation in the s values of papers with different indices of formation, even though they were composed of the same material and
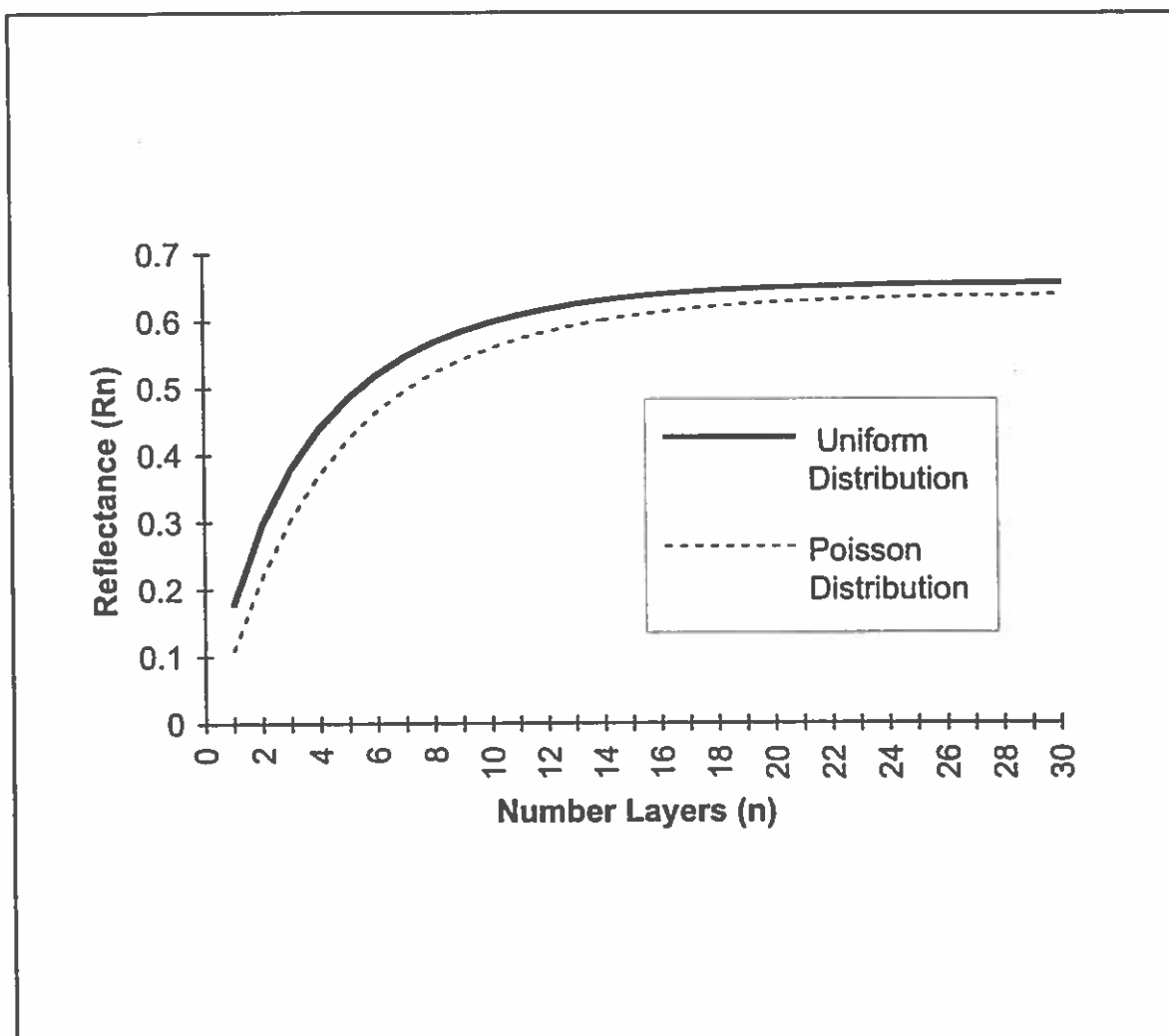
Figure 24: Plot of reflectance vs. number of layers as predicted by equation III.16 and III.18. Constant parameters *a*, *r* and *t*, were chosen to represent paper with relatively high absorptance, the region in which the effect of non-uniform distribution of mass is most pronounced.

had the same basis weight. The value of *s* was determined to have an even more pronounced relation to formation than that of opacity. This result further underlines the difficulty in pinning down appropriate values for the Kubelka-Munk coefficients.

Scallan and Borsch (1976), were able to integrate the effects of formation into their layered theory using a technique similar to Jordan's. They reasoned that the overall reflection of a sheet could be calculated by taking a weighted sum of point reflectances.

Each point reflectance was calculated according to equation III.16, considering the number of layers present in the cross section at that specific point. The overall reflectance is then (by Scallan and Borsch 76):

$$R_{\bar{n}} = F_1 R_1 + F_2 R_2 + F_3 R_3 + \ldots \qquad \text{(III.18)}$$

where $R_1, R_2, R_3, \ldots$ are the reflectances of sheets composed of 1, 2, 3,... layers respectively, and $F_1, F_2, F_3, \ldots$ are the fraction of the total area that is composed of these numbers of layers. By assuming that the number of layers across a sheet follows a Poisson distribution, equation III.18 can be re-written as:

$$R_{\bar{n}} = e^{-\bar{n}} \left[R_1 \frac{\bar{n}^1}{1!} + R_2 \frac{\bar{n}^2}{2!} + R_3 \frac{\bar{n}^3}{3!} \ldots \right] \qquad \text{(III.19)}$$

where $\bar{n}$ is the average number of layers across the entire sheet. Figure 24 graphically shows the difference between this formulation and the previous one. In this plot, the reflectivity as a function of n ($\bar{n}$) is shown as calculated both from the original Scallan and Borsch equation III.16, and the new equation III.19. Scallan and Borsch found that these corrections for formation produced results very close to observed experimental results. These results also held up under conditions of high absorption; a situation in which the Kubelka-Munk formulation produced notoriously poor results.

Fiber Orientation

Most mechanically produced papers have anisotropic properties that are associated with the direction in which the fibers are oriented in the plane of the sheet.

When raw fibers are applied to the wire, they tend to align themselves parallel to the direction the wire is moving. This direction is termed the *grain* or *machine* direction. A variety of mechanical characteristics show anisotropic tendencies related to the machine direction. It is well known that such characteristics as the dimensional stability and the tensile strength of the sheet are different in the machine and cross-machine directions. Paper manufactures and industrial consumers are well aware of these anisotropic tendencies, and care is taken in applications such as printing to account for these mechanical differences when processing. While the consequences of fiber orientation have been well studied for the mechanical properties of the sheet, little research has been done into how the optical properties are affected.

Given the interest in the effects of fiber orientation on the mechanical properties of paper, there have been a number of studies on how to quantitatively characterize the degree of orientation in manufactured sheets. Dodson and Fekih (1991), examined the effects of fiber orientation on formation. In this study, orientation was defined statistically as the distribution of angular directions in which the fibers were oriented in the plane of the sheet. The intensities of this distribution function were parameterized by the *eccentricity e*, which could be experimentally determined for a given sheet. The eccentricity value is correlated to the randomness or irregularity of the web and is influenced by such factors as production method and quality of raw material. It was found that there was a linear relationship between the *e* value and the formation. The greater the tendency for fibers to orient in the machine direction, the greater the variance in the sheet's point-to-point mass distribution. A separate study by Yuhara et. al. (1991), supports these findings with empirical evidence. In this latter study, the basis weight variance and fiber orientations were determined experimentally and by simulation. The results of this work confirmed the link between orientation and formation. As was

seen in the previous section, formation, or variance in the basis weight, has consequences on opacity and reflectivity. While this fact was alluded to in both studies, the specific optical effects of orientation were not explicitly mentioned.

Aside from the optical influence orientation has through its role in basis weight variations, there is reason to believe that fiber orientation also contributes to a spatial variation in the scattered light. One possible reason for the omission of studies on the optical effects of orientation, is that the optical properties of most interest, namely opacity and reflectance, are not related to the spatial distribution of scattered light. Any anisotropic effects that the fiber orientation would have on the optical properties would, by definition, manifest themselves in the spatial distribution of the scattered light. Neither of the theoretical treatments account for the spatial characteristics of opacity or reflectance, and the only optical property that includes spatial information is gloss.

Coatings and Sizings

After the base stock has been formed, the second stage in the modern paper making process involves applying materials to the surface of the stock which are designed to enhance its mechanical and optical properties. These materials come in the form of *coatings* and *sizings*, and are differentiated by their intended purpose. Coatings consist of a layer of mineral pigments that are deposited and bound to the outer surfaces of the sheet. The addition of these white pigments enhance the opacity, brightness, whiteness, and reflection of the final product. Sizings on the other hand, are chemical substances that are applied to the sheet in order to smooth the surface, make it more water resistant, and increase its strength. Both of these processes have specific effects on the optical characteristics of the resulting sheet. This next section will explore how these process influence the final optical characteristics.

Coatings

Coating materials are added on top of the base stock primarily to enhance the optical properties of the sheet. The source materials used in coatings are the same materials used in fillers. The most often used materials in coatings are clay, calcium carbonate, and titanium dioxide. Coatings are used to improve brightness, whiteness, reflectivity, opacity, and in some cases effect gloss. These effects are the result of the small pigment particles filling in the voids on the surface of the base stock web and increasing the amount of scattering. The attributes of a particular pigment that relate to its optical effects include:

- size,

- shape,

- index of refraction,

- binding agent.

We will discuss each of these factors and their role in the optics of a coating in turn.

The size of the pigment particles that compose a particular coating has an effect on the degree of scattering it will provide. As was discussed with reference to beating in section 3.1.3, the smaller the particles, the greater the scattering and subsequent enhancement of the relevant optical properties. Most pigments used in coatings come in a powdered form. These powders may be subject to some processing, analogous to the beating process in the case of fibers, which serves to break up the particles before application to the surface of the base stock. Clay for instance, is often put through a de-laminating process before it used as a coatings. Aggregate booklets of material that occur naturally in clay are broken up into small individual platelets. This process serves to increase the number of surfaces available for scattering when the clay is applied as a coating.

The degree of scattering a pigment material will provide is also related to its index of refraction. For our purposes here we can roughly define the degree of scattering as the ratio of reflected over transmitted light at an air-pigment interface. The behavior of incident wave fronts of light at such an interface can be described by the Fresnel laws. Given the index of refraction and the incident angle of the incoming light, the Fresnel equations will yield the intensities of the transmitted and reflected light. Specific details of the Fresnel equations are beyond the scope of our current discussion; the reader is referred to Hect and Zajac (1979) for a detailed overview of these equations. These equations reveal that a material with a higher index of refraction (relative to air) will have a greater ratio of reflected to transmitted light. Thus pigments with higher indices of refraction will have a higher degree of scattering. Titanium dioxide, for example, is known in the paper manufacturing industry to be one of the best coating materials available due to the unexcelled brightness and whiteness it produces. Not surprisingly, the index of refraction for titanium dioxide (2.55 or 2.7 depending on the type) is higher than that of other commonly used coatings (VandenAkker 77) The effects of the index of refraction on the degree of scattering are somewhat mitigated by the use of *binding* agents. Bindings are chemical adhesives that are applied to the coated stock in order to keep the coating attached to the web. The addition of these adhesives reduce the number of air-pigment interfaces and dilute the scattering potential of the coating. The informal analysis used above to account for the influence of the index of refraction on scattering, was done under the assumption that the particles were isolated and that the majority of the particle's surface area represented an air-pigment interface. Pigments in real coatings are characterized by a number of pigment-pigment and pigment-fiber interfaces as shown in
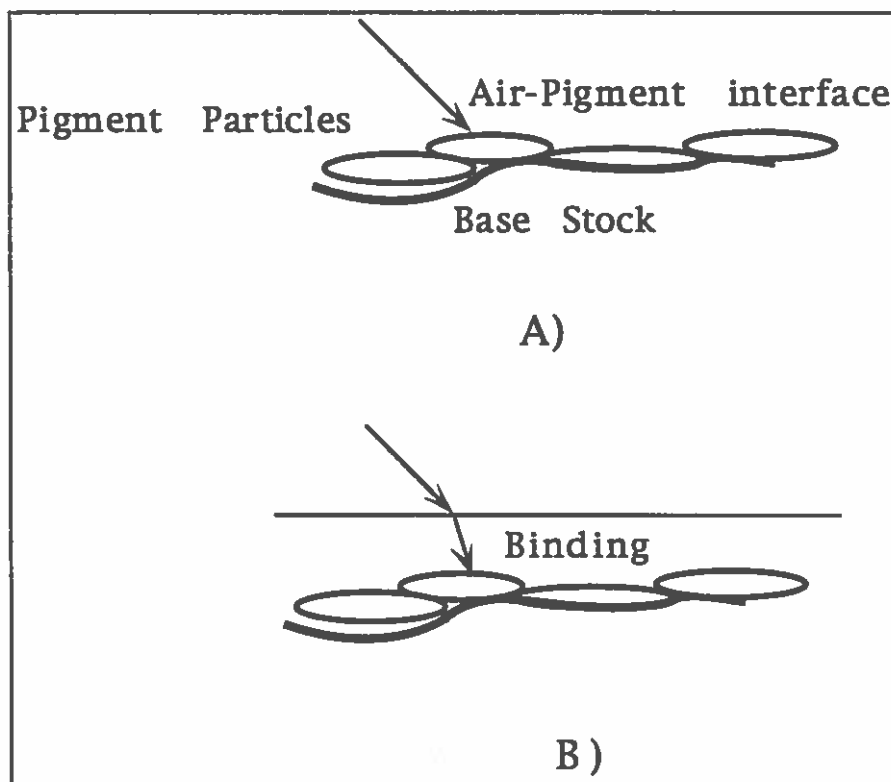
Figure 25: a) The high index interface between air and the pigment particles. b) Two lower index interfaces, first air-binding, and then binding-pigment.

Figure 25. These interfaces have a lower mean refractive index and produce inferior scattering than that of pure air-pigment interfaces. The introduction of bindings adds another intermediate substance between the air and pigment particles. There will be less scattering in light that makes the transition through an air-binding-pigment interface than light passing directly through an air-pigment interface. The paper manufacturer must carefully weigh the mechanical benefits of bindings vs. their interference with the optical enhancements of the coatings that they are meant to secure to the base stock. As a result, much care is taken in finding the proper balance of bindings to coating material which produces the best optical results while maintaining the stability of the coating.

The spatial characteristics of the scattered light for a given coating is related to the shape the pigment particles used in the coating. Irregularly or spherical shaped particles

will produce a more diffuse scattering effect, while laminar particles will tend to enhance the specular nature of a sheet. Papers coated with calcium carbonate for instance, will often have a more matte appearance than similar stock that has been coated with clay, or laminar titanium dioxide. The flat rectangular shape of the latter pigments tend to add a specular tendency to the scattered light, whereas the spheroid shape of the calcium carbonate will scatter light in all directions. The increase in gloss related to the use of platelet shaped particles can be further enhanced by coupling it with a finishing process. These processes are discussed in later in this chapter.

Sizings

Most manufactured paper receives an application of *sizing*, regardless of whether or not coatings have been applied to its base stock. Sizings are chemical treatments that are applied to the outer surfaces of a stock in order to reduce its absorption of liquids and increase its strength. Sizings can also be added to the fiber solution before the formation of the web. Commonly used materials include starch and alkaline based solutions. Surface sizing cements down the top layer of fibers and seals off the capillaries leading to the interior bulk of the sheet. This effectively increases the surface stiffness, tensile strength, and retards the penetration of liquids into the sheet.

While sizings are used for a vastly different purpose than bindings, their optical effects are similar. The application of sizing substances reduce the number of air-cell wall interfaces and may subsequently reduce the overall scattering of a sheet. As was discussed with reference to bindings, this reduced scattering can have negative effects on both the opacity and reflectance. Another optical property affected by the use of sizings is gloss. By cementing down the surface fibers, sizings serve to smooth the sheet and enhance is glossiness. This side effect may be very subtle depending on the amount of

sizing used and is often minimized by other factors. As we will see in subsequent sections, the control of the gloss of a sheet is accomplished mainly through finishing techniques.

Finishing Techniques

The geometry of the particles that a coating is composed of plays some role in the spatial aspect of light scattered from a sheet, however the main factor affecting this aspect of the scattered light is the finishing technique employed on the sheet. Finish techniques are mechanical processes which are applied to paper in order impart a particular texture or finish to the final product. These techniques are used to produce high gloss, or uniquely textured papers. The three techniques used to this end include: calendering, supercalendering, and cast coating.

Calendering is a process in which the base stock is run through two metal rollers after it is formed in order to mechanically alter the structure of the web. This action is used to increase the smoothness of the top surfaces of the stock, compress the fibers, and reduce the stiffness of the stock. The smoothing that normally results from calendering will enhance the gloss of a sheet, however the compression which also results may have adverse effects on the opacity and reflectance of a sheet by compacting the fibers such that the light scattering ability of the sheet is reduced.

The process of supercalendering is similar to calendering except that this process is used on both base stock and coated stock. Another difference is that instead of two metal rolls, one of the rollers used in this case is resilient and formed of either highly compressed fabric, or very smooth paper. Stock run through this machine is subject to a mechanical polishing action which smoothes the sheet and in the case of coated stock, aligns the particles in the coating. The gloss produced by supercalendering is far superior

to that produced by calendering alone, and most high gloss sheets are produced by this method or by cast coating. In some cases the surface of the metal roller used in this process may be engraved to produce embossing, patterning, or some other unique texture in the final product.

Cast coating is distinct from the other processes in that it is applied only to coated stock. This process consists of running the coated stock through a heated drum immediately after the coating has been applied to the base stock. The wet coating is quickly dried on the drum and an image of the highly polished drum is cast onto the sheet. Sheets finished in this fashion have extremely high gloss and superior ink holdout. Premium and high-grade glossy papers are produced in this manner.

Measurement and Simulation Results

Given that the factors governing the optical characteristics of paper are quite numerous, we would now like to focus our discussion on a few specific optical phenomena that we found to be of interest for our study. We hope to provide some insight into the mechanics of these specific effects by investigating them through the use of both optical measurements and geometric models used in conjunction with our virtual goniophotometer tool. The phenomena of particular interest that were well suited for this type of exploration included:

- the effect of formation (mass distribution) on overall reflectance,
- anisotropic reflectance functions caused by fiber orientation,
- retro-reflectance in the incident direction (back-scatter).

The optical effects we chose to focus on were of interest for a number of different reasons. The effects of non-uniform mass distribution have been noted in the literature

and theoretical models have been developed to account for it, thus it makes for an interesting case to compare with our simulated models. The second phenomenon, anisotropic reflectance functions, are not directly noted in the literature, but can logically be extrapolated from work that has previously been done regarding the effects of fiber orientation on formation. This effect was also discovered in our measurements and therefore was an interesting case to simulate. Accounts of the last phenomenon, back-scatter, were not found anywhere in our literature review, but were noted after the first measurement results were studied. We had no immediate explanation for this surprising result, and thus felt it would be a unique effect to attempt to reproduce in our simulations.

In the process of having optical measurements performed, paper samples from a variety of bond grades and types were gathered with the help of individuals in the paper industry. From these samples, representative specimens were chosen based on such criterion as their similarity to printing papers (those used in the labeling applications for example) and their ability to display the phenomenon we are investigating. The chosen specimens were sent to a third party laboratory for optical profiling. This process involved measuring their reflectance functions under the illumination of a 670 *nm* laser for a number of different spatial orientations.

In addition to the measurement results, geometric models were carefully constructed in software for use with our virtual goniophotometer. Reflectance functions, similar in form to those of the measurements, were generated by simulations and were compared to both the measurement results and the theoretical formulations discussed in earlier chapters. The models and the simulation results provide some insight into the mechanics of the specific optical effects we choose to concentrate on in this study.

The remainder of this section is divided into four subheadings. First we will overview the paper samples and the general results of the optical measurements performed on them. Next we will detail our exploration of formation effects and compare the results of our models with the established theories which were discussed previously in this chapter. The third subsection of this section overviews the degree to which anisotropic tendencies were found in our measurements and our reproduction of these effects in simulation. Finally we will discuss the significant back-scattering phenomenon which were found in our measurements. We postulate that this effect may partially be the result of the geometry of specific materials used in the coatings of the samples displaying this effect.

<div align="center">Paper Samples and Measurement Results</div>

A broad range of paper samples were donated by individuals in the paper manufacturing and distribution industries for this study. These samples included sheets constructed with a variety of pulp materials, coatings, and processes. Information regarding the composition and manufacture were provided along with the samples. The two specimens from this lot chosen for measurements were singled out because they were representative of sheets used in applications in which their optical properties are important. The two sheets also provided contrasting cases with the regard to the effects we are investigating.

The first specimen selected was, by visual inspection, very similar in look and feel to paper used in printing applications such as the labeling of canned goods. This sample was machine manufactured, provided by Unisource Worldwide Inc. OR., and goes by the name of "Mountie Matte." The sample was smooth, white, and somewhat glossy in appearance. The basis weight of the sheet was 60 g/m^2. It was composed of a bleached

ground-wood pulp substrate with a calcium carbonate/clay coating, an industrial standard polystyrene binder, and an alkali sizing (Murray , 95). The ratio of coating to substrate weight was not available, nor were the relative amounts of materials used in the coating, as this information is viewed as proprietary by the manufacturer. Normally coatings account for 10 to 15% of the overall basis weight of a sheet (Bureau 89). Since this sample was machine manufactured, it was one of the candidates we predicted would display anisotropic tendencies in its reflectance functions, and it was therefore an appropriate choice for our investigation of this effect. This sample also showed a significant amount of retro-scatter, which was also of interest to us.

The second specimen was typical of writing grade bond or paper that is used for important printed documents. This sample was more roughly textured than the previous, slightly yellow in hue, and diffuse in appearance. The sheet was composed of 97% unbleached softwood pulp (Jack Pine and Red Pine), 3% hardwood pulp (Minnesota Aspen), and contained no fillers, coatings, or sizings (Peterson, 95). This sheet provided an excellent contrast to the previous specimen because it was *hand* formed by Potlatch Industries Cloquet MN. and did not contain any secondary materials. Because the sheet was not manufactured by machine, we expected to see no anisotropic tendencies in its reflectance functions. This specimen also benefited from the fact that it was composed only of pulp and thus was easier to accurately model than the previous specimen. Since this sheet was uncoated, it would also provide us with an opportunity to confirm our speculation regarding the role of coatings in the back-scatter phenomenon which was discovered in the measurement of the first sample.

After the samples had been chosen, we devised a measurement scheme which would provide a broad overview their reflective properties. In order to also observe in what way printing augmented the reflective properties of the sheets, two specimens from

each sample were produced: one inked and one plain. The inked specimens were generated by printing a large black region onto the samples with typical office-type computer printers. Tests were conducted on the Mountie Matte sample according TAPPI specification T 409 in order to determine its machine direction. Measurements were taken both along and against this direction in order to record any anisotropic tendencies in this specimen's reflectance functions. Perpendicular sets of measurements were also taken for the hand formed specimen for comparison, although no attempt was made to determine its "machine direction." Measurements from all four specimens were taken for a number of incident illumination angles in order to record any effects in the reflectance functions which were related to spatial orientation.

The optical profiling of the specimens were performed by a third party laboratory, and involved measuring the light scattered from the samples when illuminated by a laser. A 670 *nm* laser in an (S)-polarization state was arranged so that the incident beam was at a specified angle with the normal of the specimen. Measurements were then taken by recording the magnitude of the reflected light at discrete locations on the hemi-circle perpendicular to the horizontal plane of the specimen that is formed by sweeping out the angles from -90° to ~+80° with respect to the normal. This type of measurement sweep was performed for a family of incident angles on each specimen. Similar measurements were also taken with the specimens rotated 90° in the horizontal plane, in order to record any anisotropies in their reflectance functions. These latter measurements were only performed on the non-inked samples.

Reflectance functions for a family of incident angles on the first specimen is shown in Figure 26. The most prominent characteristic of these functions is the marked peak located around the mirror reflection direction. This effect was expected since the sample was somewhat glossy in appearance. The inked samples display a lower overall
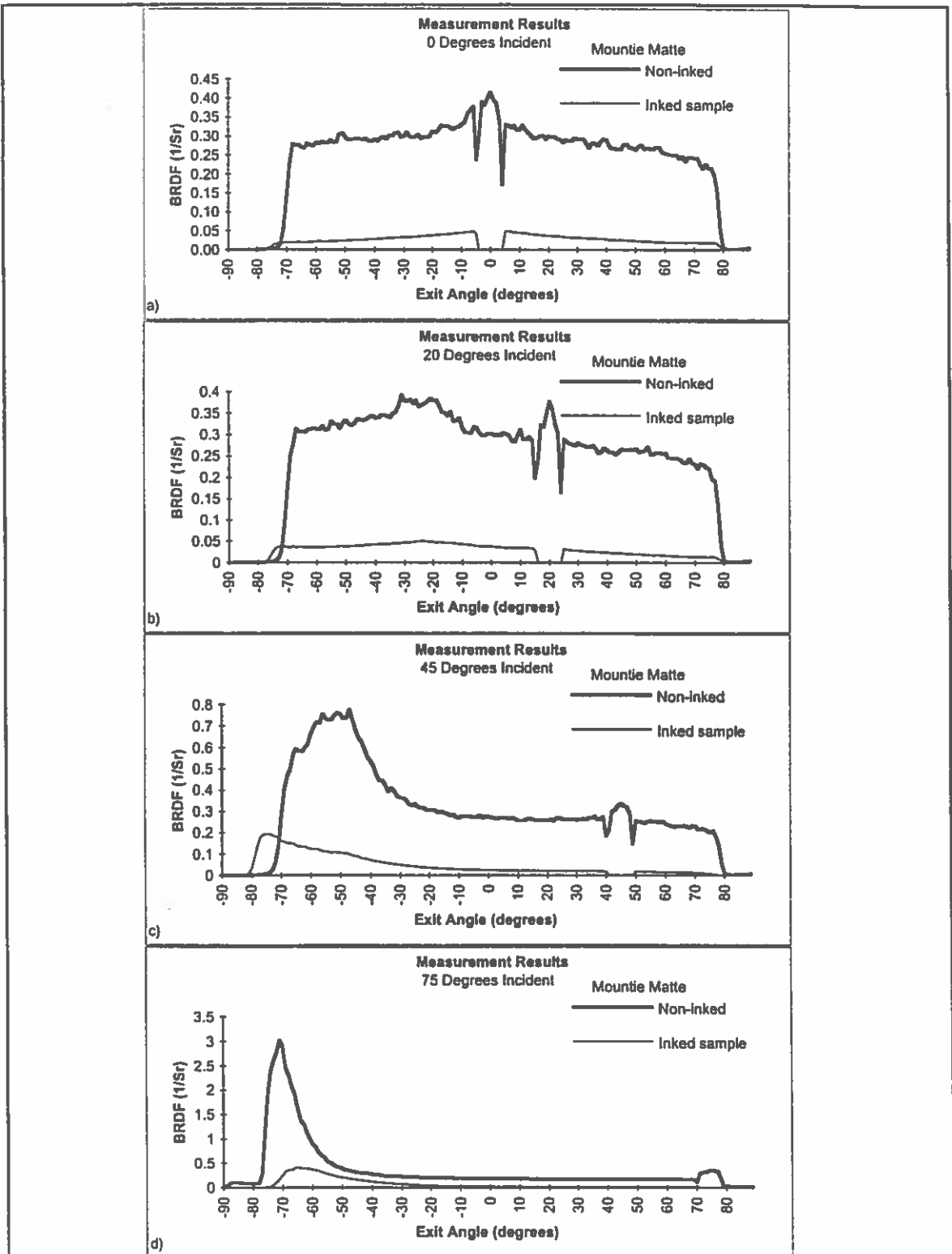
Figure 26: The measured reflectance functions for the Mountie Matte sample, both inked and non-inked. a) 0° incident illumination. b) 20° incident illumination. c) 45° incident illumination. d) 75° incident illumination.
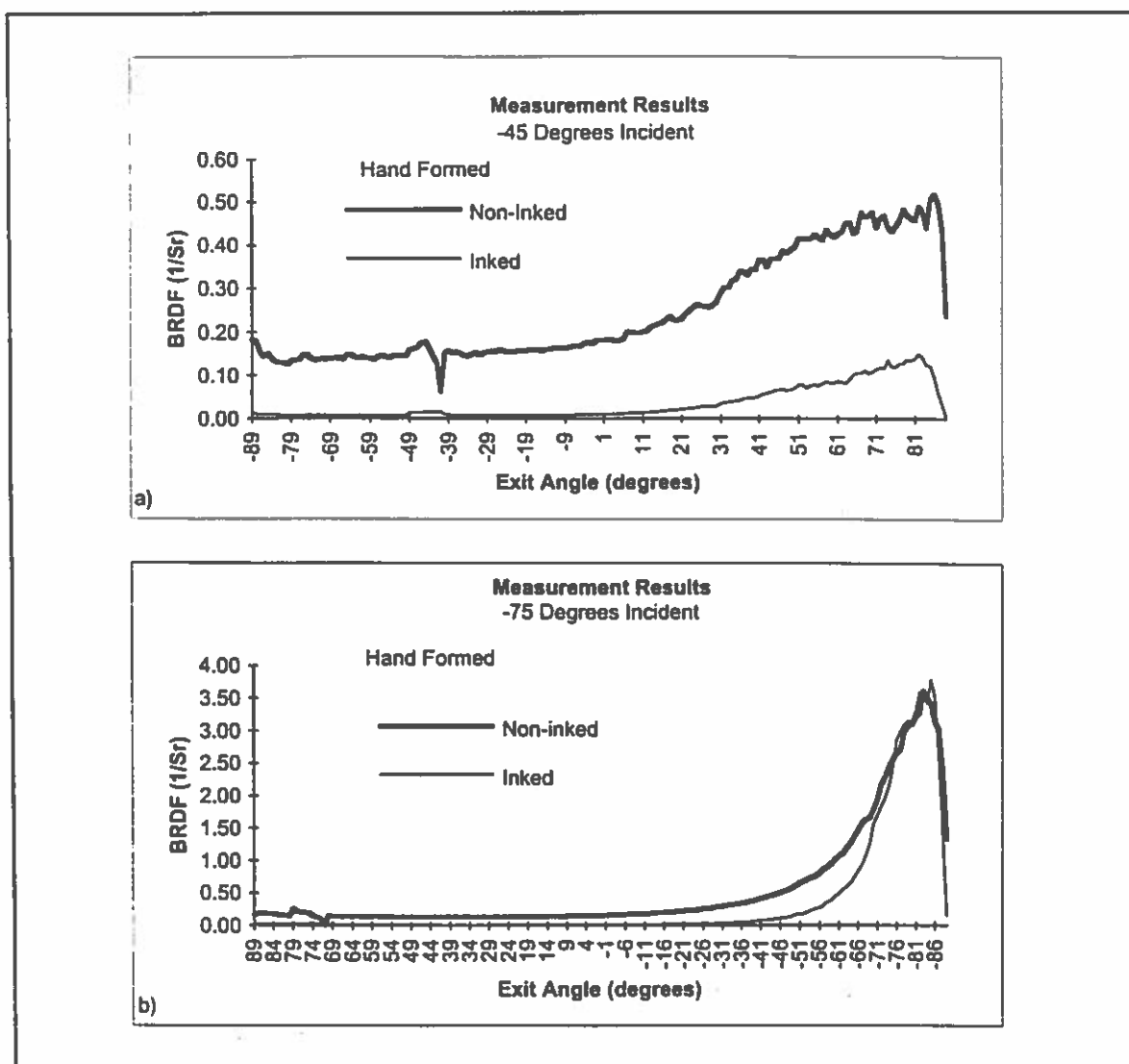
Figure 27: The measured reflectance functions for the hand made sample, both inked and non-inked. a) -45° incident illumination. b) -75° incident illumination.

reflectance in all cases, which was also expected, however there are some anomalies present at glancing exit angles for these cases. The reflectance of the inked samples do not seem to drop off as rapidly as the non-inked samples at these extreme exit angles. In all cases except for 75° incident, the reflectance curves for the inked samples crosses over those of the non-inked at an exit angle of approximately -72°.

We can only speculate as to the cause of this anomaly, however it may be related to an increase in surface reflection caused by the introduction of the ink. Another unexpected result was the significant back-scatter, or reflectance around the angle of incidence. There is a noticeable rise in the reflectance curves around the retro-reflection angle in all cases for the non-inked specimen, and, for 20° incident (curve b), the back-scatter is actually of the same magnitude as the specular reflection. (The discontinuities in the curves at the edges of these back scatter "peaks" are an artifact of the laboratory's experimental set up.) We found this feature in the reflectance functions surprising since such phenomenon was not mentioned in our literature survey. It was only after detecting this feature in the initial measurements that we decided to focus on this issue with further measurements.

The measurement for the hand made samples are shown in Figure 27. These reflectance functions display a more diffuse response than the previous case. The presence of back-scatter is also much less prominent in these curves. The curious aspect in these functions is the relative parity in the magnitude of the specular peak for both the inked and non-inked samples in their -75° incident measurements. Again this result is puzzling and may be due to Fresnel effects which dominate the reflection at these glancing angles.

Modeling the Effects of Formation on Reflectance

Recall from our discussion previously in this chapter that formation is a measure of the degree of non-uniformity in a sheet's distribution of mass. Because of the random nature in the construction of the fiber web, all sheets will exhibit some degree of non-uniformity in this distribution. The optical consequences of formation are readily seen by viewing transmitted light through a typical sheet. The blotchy appearance of the light is

due to the point-to-point variance in mass across the sheet. Since there is a non-linear relationship between mass, or basis weight, and reflectance/opacity, the effects of formation complicate the application of theoretical theories to real sheets. Sub-regions of a sheet that contain below average mass have lower reflectance values than what is compensated for by the regions of above average mass. This results in a discrepancy between values predicted by the theories and reflectances measured for real sheets, because the mass is not uniformly distributed in the latter case. Corrections to the theories which accounted for these discrepancies were developed by various researchers, as was reviewed previously in this chapter. By paralleling the development of one of these modified theories as our first investigation into the modeling paper, we will show that our simulations can produce reflectance functions that agree well with theoretical results.

For our initial attempts at modeling a sheet, we choose to duplicate the morphological model developed by Scallan and Borsch. A sheet is represented in this model as a series of alternating layers which correspond to the bonded cell walls of the fibers and the air spaces of their cores/interstices. This model provided an excellent introductory case for our investigation since its geometry is relatively easy to reproduce and because we could directly confirm the resulting reflectance functions with the theoretical predictions of the Scallan and Borsch formulations. We were also able to parallel in our simulations the extensions made by Scallan and Borsch to account for non-uniform mass distribution.

The original Scallan and Borsch formulations for the reflectance of a sheet were derived by using established optical relationships such as the Fresnel equations and the Bouger-Beer laws to determining the predicted reflectance from the multiple layers of their model. These formulations are discussed in earlier in this chapter and are listed as
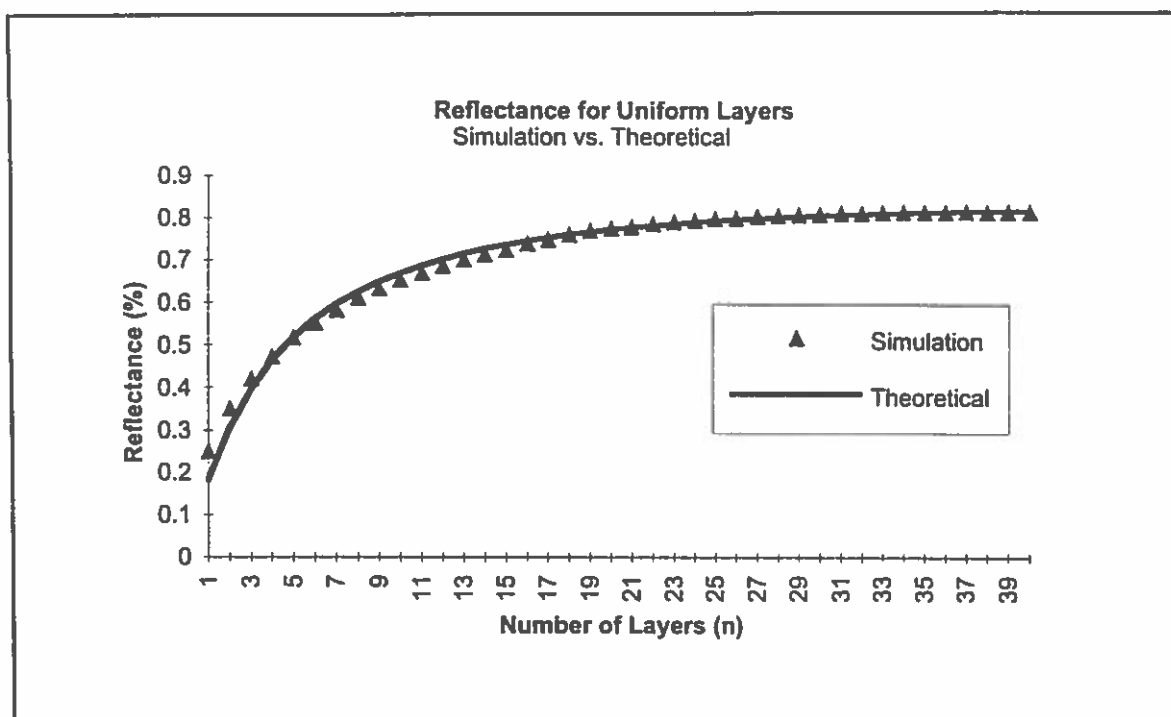
Reflectance for Uniform Layers
Simulation vs. Theoretical

Figure 28: Reflectance as a function of the number of layers n. Simulation results vs. theoretical predictions of Scallan and Borsch formulations.

equations III.13-III.16. The foundations of the virtual goniophotometer are the same established optical relationships used by Scallan and Borsch to develop their theory, thus it is reasonable to directly compare the results from each source. The primary parameters of the Scallan and Borsch formulations include: the number of layers in the sheet, the thickness of these layers, and the index of refraction of the cell wall material. By using the same values in the construction of our model, we were able to generate almost identical reflectance functions to those predicted by their theory.

Our model consisted of uniform alternating layers of cell wall material and air. The cell walls had an index of refraction of 1.56, and the thickness of these layers was set to 5 *mm*, which corresponds to values reported by Scallan and Borsch for typical pulp mixtures. A series of simulations were run on subsequent models, each with an increasing number of layers, and the results are shown plotted against theoretical calculations for
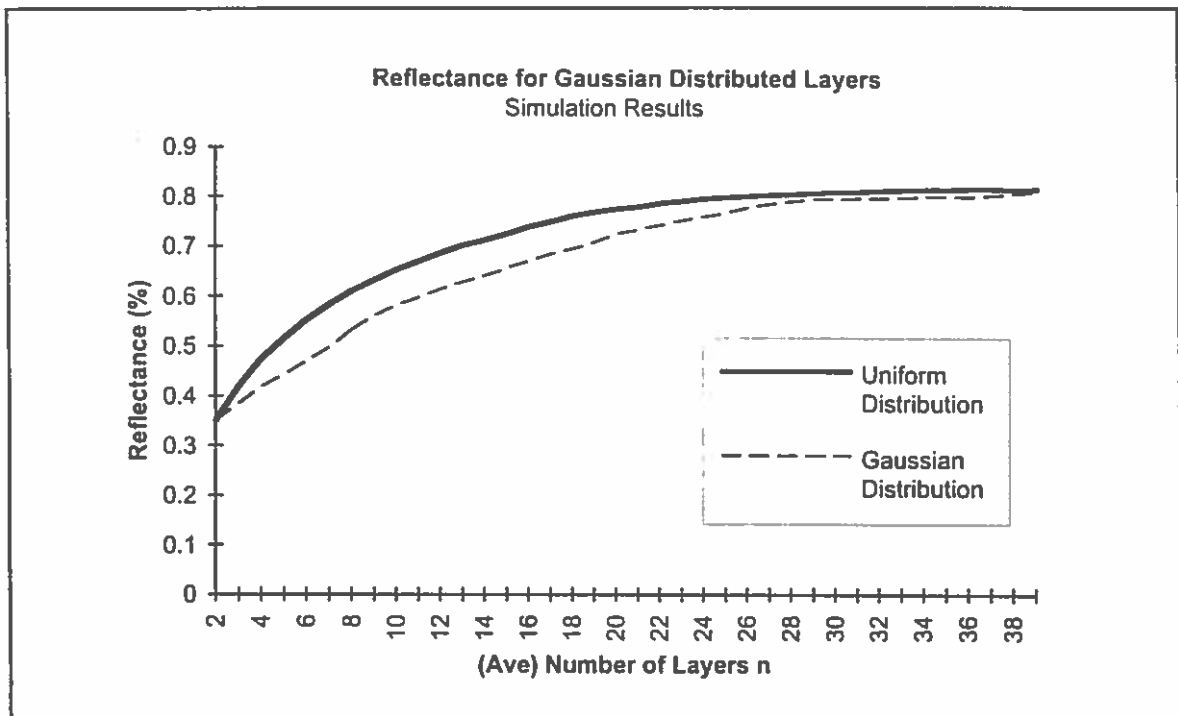
Reflectance for Gaussian Distributed Layers
Simulation Results

Figure 29: Reflectance as a function of the (average) number of layers n. Simulation results for the uniform model and the Gaussian distributed model.

identical parameters in Figure 28. As we can see the two curves show excellent agreement.

In order to account for the effects of formation on the reflectance of a sheet, Scallan and Borsch developed a separate set of equations from their original formulations. While they did not explicitly specify a new geometric model in connection with these corrections, a model was easily derived from their new formulas for our study. The primary difference in their new approach was that the sheet was no longer viewed as having a uniform distribution of mass, and the overall reflectance was now calculated by integrating the local area reflectances over the area of the sheet. This variation in mass manifests itself in the n parameter of the original equations, so the new equations were derived by allowing n to vary. Using a Poisson distribution function for this variance, equation III.19 was derived, as discussed previously.
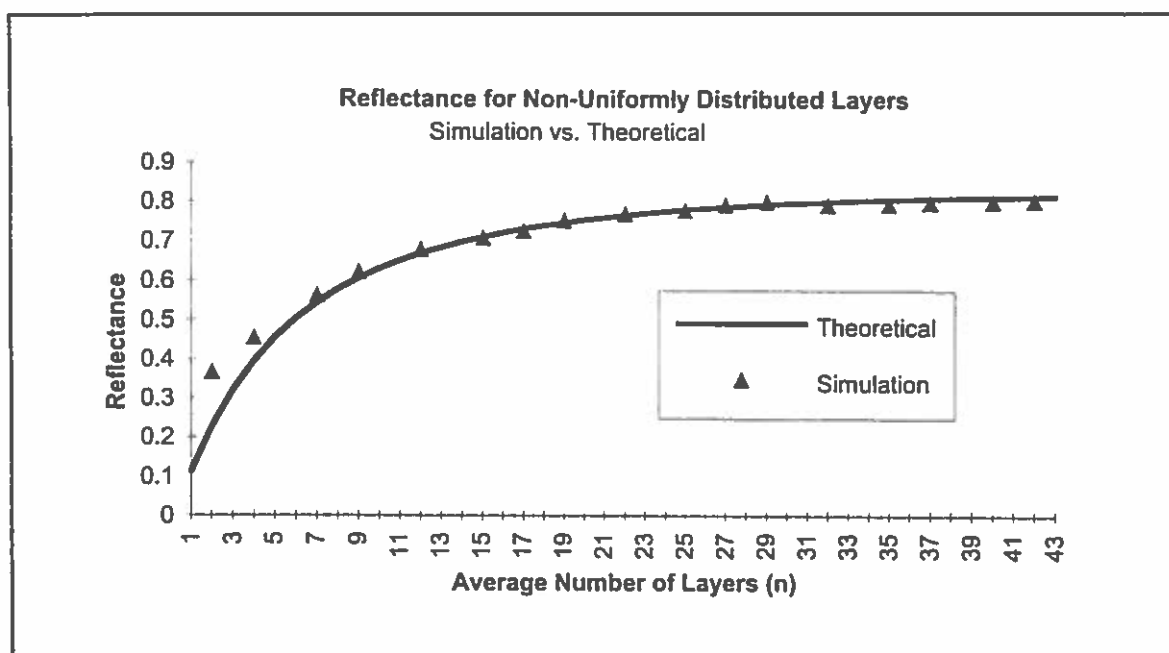
Reflectance for Non-Uniformly Distributed Layers
Simulation vs. Theoretical

Figure 30: Reflectance as a function of the (average) number of layers n. Simulation results for the Gaussian distributed model compared with predicted theoretical results with analogous parameters.

We were able to make an analogous modification to our simulated model. The model was broken up into discrete areas and the number of layers in each area was allowed to vary in a similar fashion as the n parameter of the theoretical formulations. The new model was constructed by an array of 50 by 50 mm rectangular areas with the number of layers in each area randomly assigned according to a Gaussian distribution function. All the other parameters of this model were identical to those of the preceding one. A series of simulations were run using this model with subsequently increasing numbers of (average) layers. The reflectance functions generated for these non-uniform sheets were consistently lower than their uniform counterparts as shown in Figure 29. Similar results are also predicted by the augmented Scallan and Borsch theory as was shown in Figure 28. Comparison of the simulation results for the modified model and the analogous Scallan and Borsch predictions also reveal a high degree of agreement as shown in Figure 30.

Anisotropic Reflection Functions due to Fiber Orientation

A high degree of correlation between the simulation and theoretical reflectance functions was shown in the preceding examples, however, this investigation did not exploit the virtual goniophotometer's ability to distinguish *spatial* detail in the reflectance functions. The theories and simulations that dealt with formation effects only considered the overall diffuse reflectance of a sheet and did not cover any of the spatial aspects of the scattered light. One effect that would manifest itself spatially, and thus would not be evident from inquiries like the preceding one, is the effect that the orientational preferences exhibited by fibers would have on a sheet's reflectance functions. Anisotropies in the mechanical properties of a sheet have been associated with such phenomenon, and would be expected to be similarly present in the optical characteristics of a sheet. The optical effects of such phenomenon have not been documented in any of the literature we reviewed; in fact, there was not much focus on any spatial aspects of scattered light from paper in this previous research.

Fibers that are mechanically deposited on the wire during formation of the base stock will tend to align themselves parallel to the direction the wire is moving. The direction of this orientation is called the *grain* or *machine* direction, and its effects on various mechanical properties are well documented, as was discussed previously in this chapter. In addition to the mechanical properties that this angular preference influences, studies have also linked this phenomenon to the degree of non-uniformity in the distribution of mass, or the formation index of sheets. However, no research has been done regarding the optical consequences this phenomenon might have. Despite these oversights, there is still reason to believe that fiber orientation introduces anisotropy in the optical properties of sheet similar to those encountered in the mechanical properties.
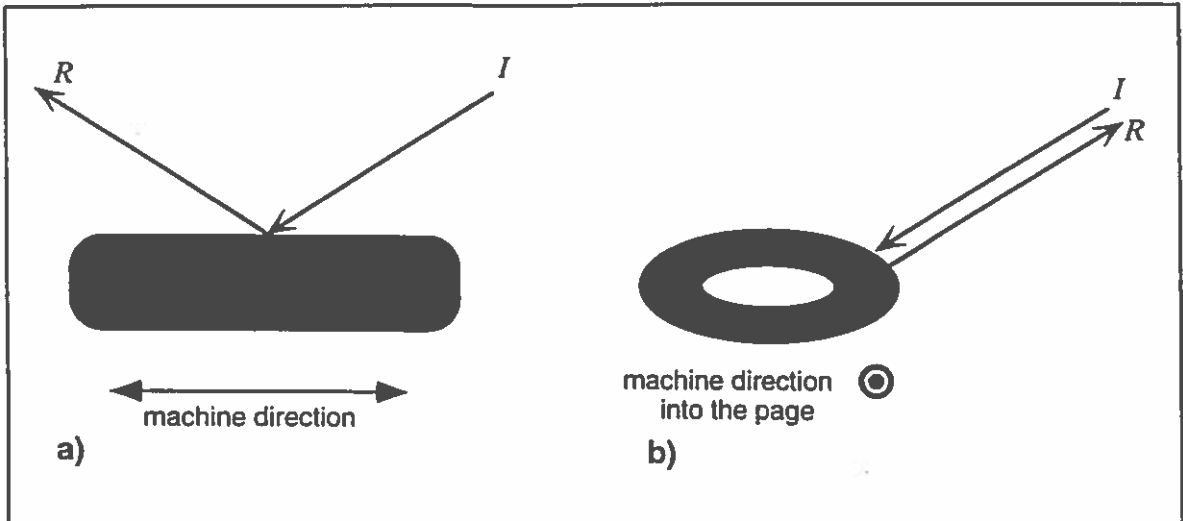
Figure 31 : Geometry of reflected light from a single oriented fiber. a) Incident light in the machine direction. b) Incident light in the cross-machine direction.

Because of the geometry of the fibers in the web, incident light that is parallel to the machine direction should reflect light in a more specular fashion than identical light incident in the cross direction. Figure 31 shows these situations for a single fiber oriented in the machine direction. This phenomenon would manifest itself only in a full spatial profile of the reflected light.

Prior to sending it to the laboratory for measurements, tests were conducted on the Mountie Matte paper sample in order to determine its machine and cross-machine directions. These tests were conducted according to TAPPI test specification T 409 and are detailed in the Appendix. Separate measurements were taken for incident illumination parallel to both these directions. The resulting reflectance functions show a greater specular peak for light incident along the machine direction than for identical illumination in the cross direction. This confirmed that anisotropy exists in the reflectance functions at least for this sheet. Figure 32 clearly shows this effect for 75° incident illumination. The effect was less pronounced for other incident illumination angles. Given that this paper was machine manufactured, we were surprised to find that this anisotropy was not as dramatic as we had expected.
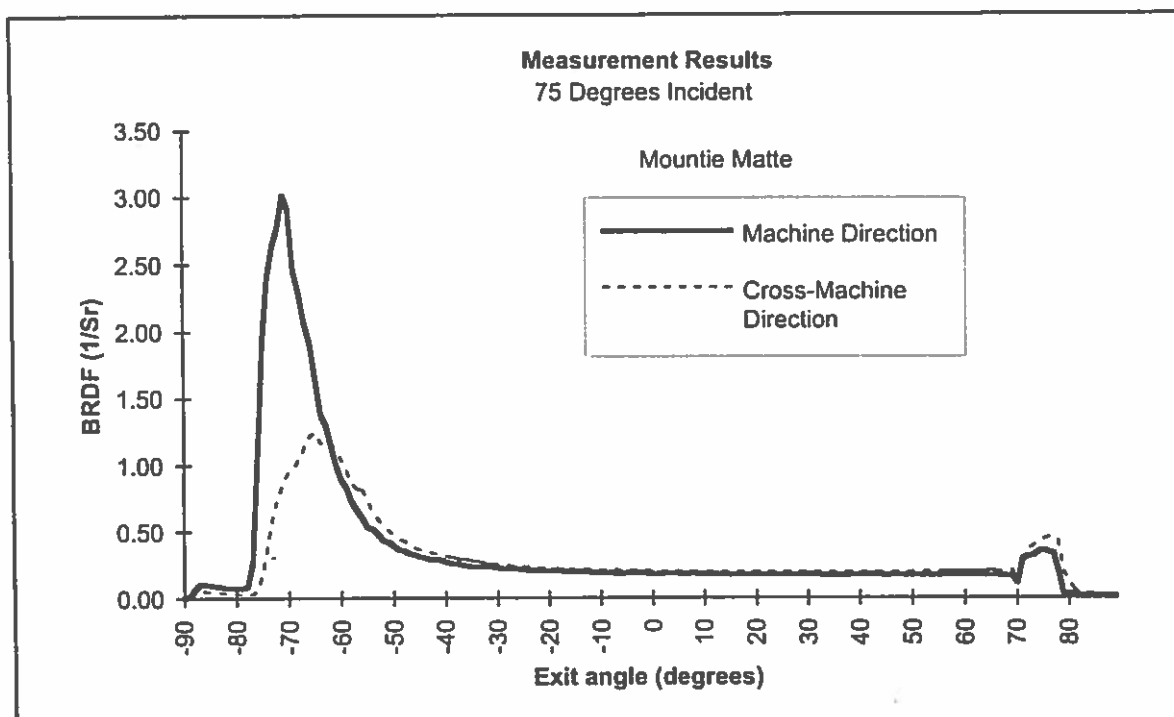
Figure 32: Measured reflectance of the Mountie Matte sample for 75 degree incident illumination. Curves shown represent illumination parallel to both the cross- and machine directions.

The anisotropic tendencies of this sample may have been subdued because of its coating. The geometry of the coating particles for this sample are relatively isotropic in the horizontal plane of the sheet, and thus would not contribute to any anisotropic effect in the reflectance function. The presence of these particles in the top surfaces of the sheet may somewhat mask the anisotropy inherent in the web substrate below. Similar measurements conducted on uncoated, machine manufactured paper could confirm this speculation, but was not attempted in this study. Regardless of the degree to which it is present, there is clearly some anisotropy to the reflectance functions of this sample, and exhibited by Figure 32.

In order to reproduce this anisotropic effect in our simulations, we had to abandon the layer model used in the previous exploration, and model the actual fiber web. The base stock web of a sheet is composed of a collection of slender transparent fibers which

resemble hollow cylinders, and are oriented somewhat randomly in the horizontal plane of the sheet. We choose to use concentric cylinders to represent a fiber for our model. In the pulping and web formation process, fibers may undergo deformations and come to resemble thin ribbons. Studies have shown that fibers will generally deform in predictable ways according to such factors as the fiber source, pulping technique, and method of construction (Jayme and Hunger 62, Wrist 67). For the purposed of our study, we choose a to model a simple deformation that compressed (scaled) the fibers in one direction perpendicular to their long axis. We set the dimensions of our cylinders to be 2 *mm* long, .02 *mm* in diameter for the outer cylinder, and 0.01 *mm* diameter for the inner cylinder. These numbers correspond to the dimensions of typical wood pulp fibers (Dodsen and Fekih 91).

Our first model of the web was a "fully oriented" sheet. 1000 of the deformed cylinders were placed side by side, oriented parallel to the machine axis to form one layer of fibers for our modeled sheet. Ten of these layers were then stacked atop each other to complete the model. The reflectance functions generated by this model are shown in Figure 33. As we can see from this figure, there is clearly a difference in the reflectance functions corresponding to the grain direction. The characteristics of these curves are similar in nature to the measurement results which were shown in Figure 32.

This fully oriented model is sufficient for illustrative purposes, however, no real sheet would have such a uniform configuration. In order to create a better representation of the web, the angular orientation of the cylinders that make up the model must be allowed to vary with a certain degree of randomness. By introducing randomness, we are able to model the fiber orientation more accurately; however, the optimal packing arrangement
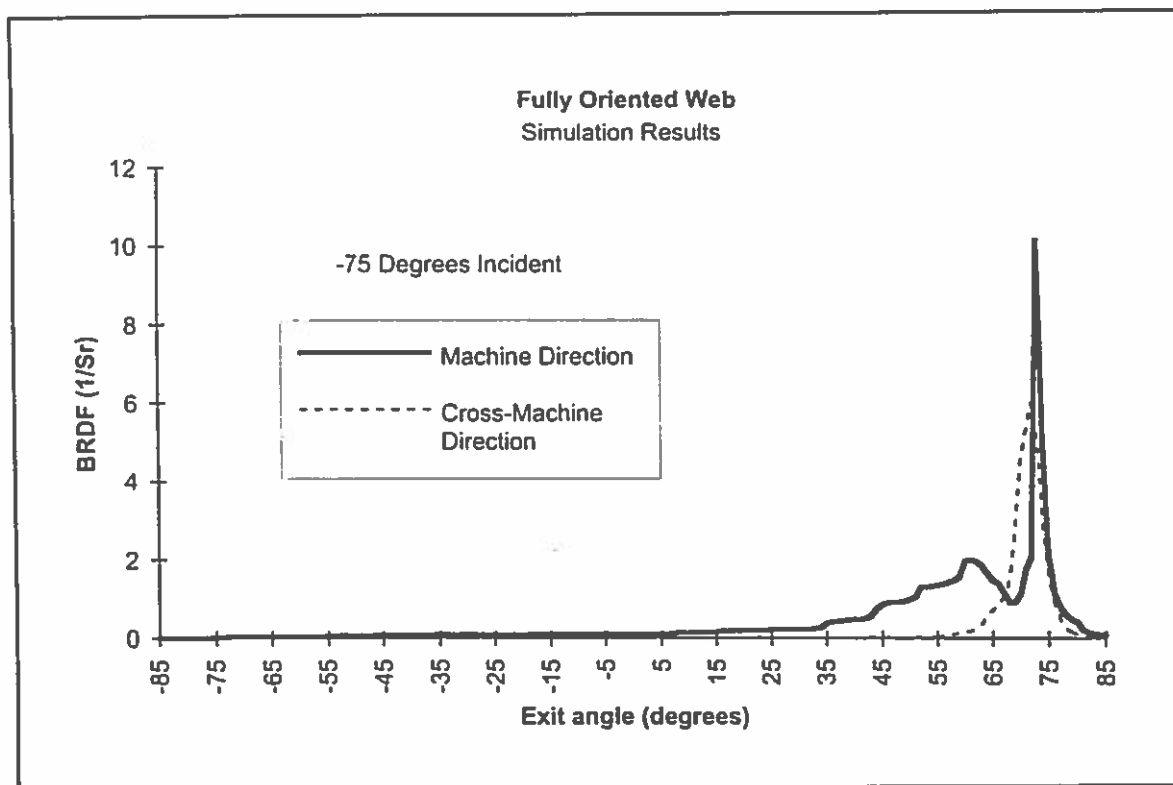
Figure 33: Reflectance functions for the fully oriented paper web model.

of these cylinders is no longer a trivial matter. The packing of geometric primitives is known to be computationally difficult (Gardner 68, Boyd 73). For the purposes of constructing our model, we relaxed one of the other parameters in order to facilitate control over the orientation. To maintain the statistical accuracy of the fiber orientation that we required for the study, we allowed the Z dimension of the model to vary such that the web was allowed to grow unconstrained along this direction during its construction. This translates into a discrepancy between the overall thickness, or caliper, of our modeled sheet and what would be found in real sheets with equivalent amounts of fiber mass. We felt this simplification was justified since we were interested in the optical effects of strictly fiber orientation and not the density of their packing.
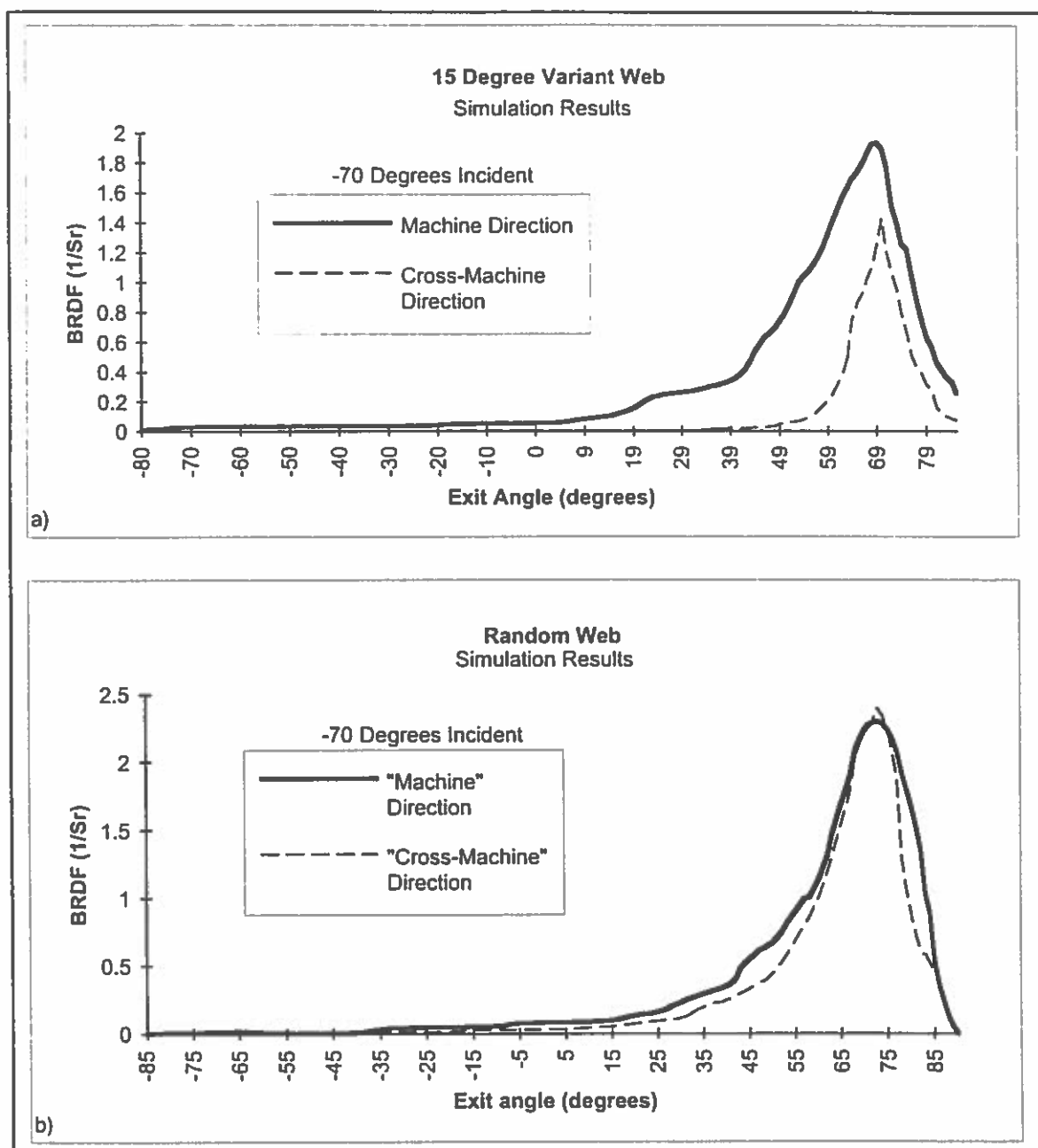
Figure 34: Reflectance functions for the randomly oriented paper web models. a) Web modeled with 15 degree mean variance from machine direction. b) Web modeled with totally random angular distribution. (no machine direction)

Using the same number of fibers as the fully oriented sheet, a random web was constructed to have a mean angular variance of 15° from the machine direction. This variance corresponds to a highly oriented web, but is more realistic than the previous

model. The algorithm used to construct this web attempted to pack the cylinders as densely in the horizontal plane as possible in order to produce adequate coverage across the area of the sheet. However, during the construction we allowed subsequent cylinders to "slide down" the Z axis so that they did not intersect with cylinders already in the web. This algorithm did not produce a particularly dense fiber packing, but did maintain the angular distribution of the fibers.

The reflectance functions produced by the simulations on this model are shown in Figure 34a). There is still a significant anisotropy exhibited in the reflections functions of this model. While the fibers of this model were highly oriented along the machine direction, the overall geometry is more similar to real sheets than was the case for the fully oriented model. Figure 33b) shows the results of simulations on a similar model that had *no* orientational preferences. From the results we can see that the anisotropic effects disappear for a web that has fibers oriented in an entirely random fashion.

Simulation of Retro-Reflectance

Like the anisotropic effect studied in the previous section, we did not encounter any references to the phenomenon of retro-reflectance in our literature survey. However, while we expected to find anisotropy in the measurements, we were somewhat unprepared for the significant amount of retro-reflection exhibited in these same results. The origins of this back-scatter effect are somewhat puzzling, however, we theorize that it is partially a consequence of the geometry of the coating used in this sample.

One of the most notable characteristics found in the measurement results of the Mountie Matte specimen was the significant amount of retro-reflection it displayed over all incident angles. In examining the curves shown in Figure 26, we notice a distinct local

peak in the reflectance around the back-scatter angle in all cases. (For 0° incident, the mirror and back-scatter angle are identical.) None of the geometries we had modeled up to this point had produced reflectance functions with features that in any way resembled this retro-reflection peak. One aspect missing in these models, but present in the Mountie Matte specimen, was a coating.

The aspect of a coating that has the most influence on the spatial distribution of scattered light is the shape of the particles used in the coating. We concentrated on this aspect of the coating since retro-reflectance is a spatial phenomenon. Clay and calcium carbonate are the two primary components of the coating mixture used in the Mountie Matte specimen. As was discussed previously, the geometry of these two substances have different effects on the spatial distribution of light that is scattered from coatings that are composed of them. The platelet-like structure of clay tends to enhance the specular reflection of the scattered light. Calcium carbonate is more spheroidally shaped, and thus tends to scatter light in all directions. The spherical geometry of calcium carbonate may also be contributing to the observed back-scatter in the reflectance functions of the Mountie Matte specimen. This line of reasoning was further explored by the construction a model of calcium carbonate which was used in the virtual goniophotometer to generate back-scatter reflectance functions.

A model of Calcium Carbonate was constructed by creating a volume filled with small transparent spheres. These spheres had a radius of 500 *um*, and their index of refraction was set to be 1.6 corresponding to values reported in (Johns, 77). The spheres were packed in a volume which measured 250 x 250 x 170 *mm* deep by a simple random insertion algorithm. This method is identical to the one employed by Gondek et al. (1994) to model pigmented plastics. Since the geometry of spheres will produce relatively diffuse scattering, significant amounts of energy in the reflectance functions
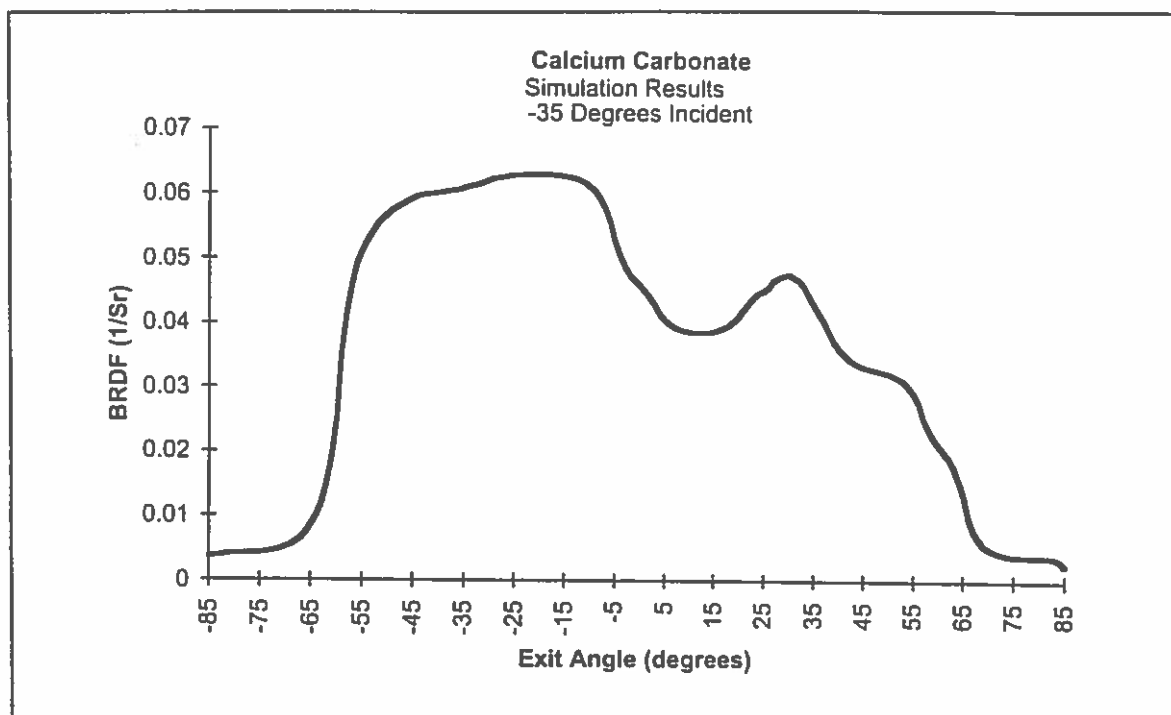
Figure 35: Reflectance function for the Calcium Carbonate model.

generated by this model were in the retro-reflectance direction. Figure 35 shows the peak of this function to be in the retro-reflection direction; it is *not* a specular peak. The dominance of the back-scattering effect in the reflectance functions of this model are not surprising given the nature of its geometry; but these functions are not very suggestive of the ones found in the measurement results.

A second model was developed in which the calcium carbonate coating was placed on top of a simulated base stock web. Since real coatings have a binder applied to them in order to secure them to the substrate, the spheres in this new model were partially embedded in a medium with an index of refraction of 1.1 which represented the binder. Simulations were re-run on this second model, and the results are shown in Figure 36. These reflectance functions show similar characteristics to those of the measured sample. There is both a specular peak, and a retro-reflectance peak present in the curve. Simulations run on a similar web without the coating reveal that this effect is not present
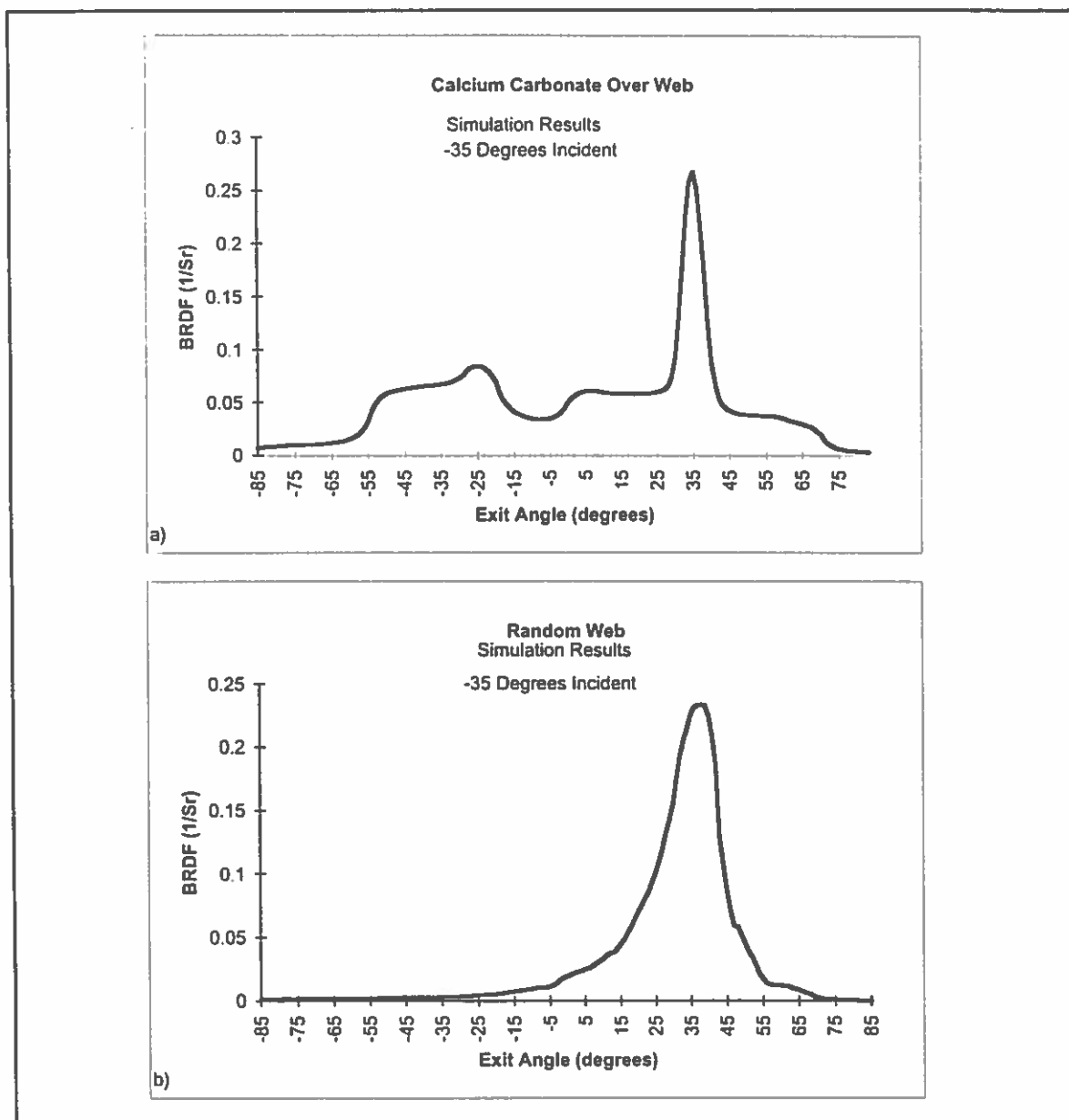
Figure 36: The effects of simulated calcium carbonate.   a) Reflectance functions for the calcium carbonate over simulated web model. b) Similar web without coating.

in the absence of the coatings as shown in b) of Figure 11. The measurement results on the handmade sample also support this claim.   These results are compared with the Mountie Matte in Figure 37 and it is clear that the uncoated sample has much less significant back-scatter than the coated sample.
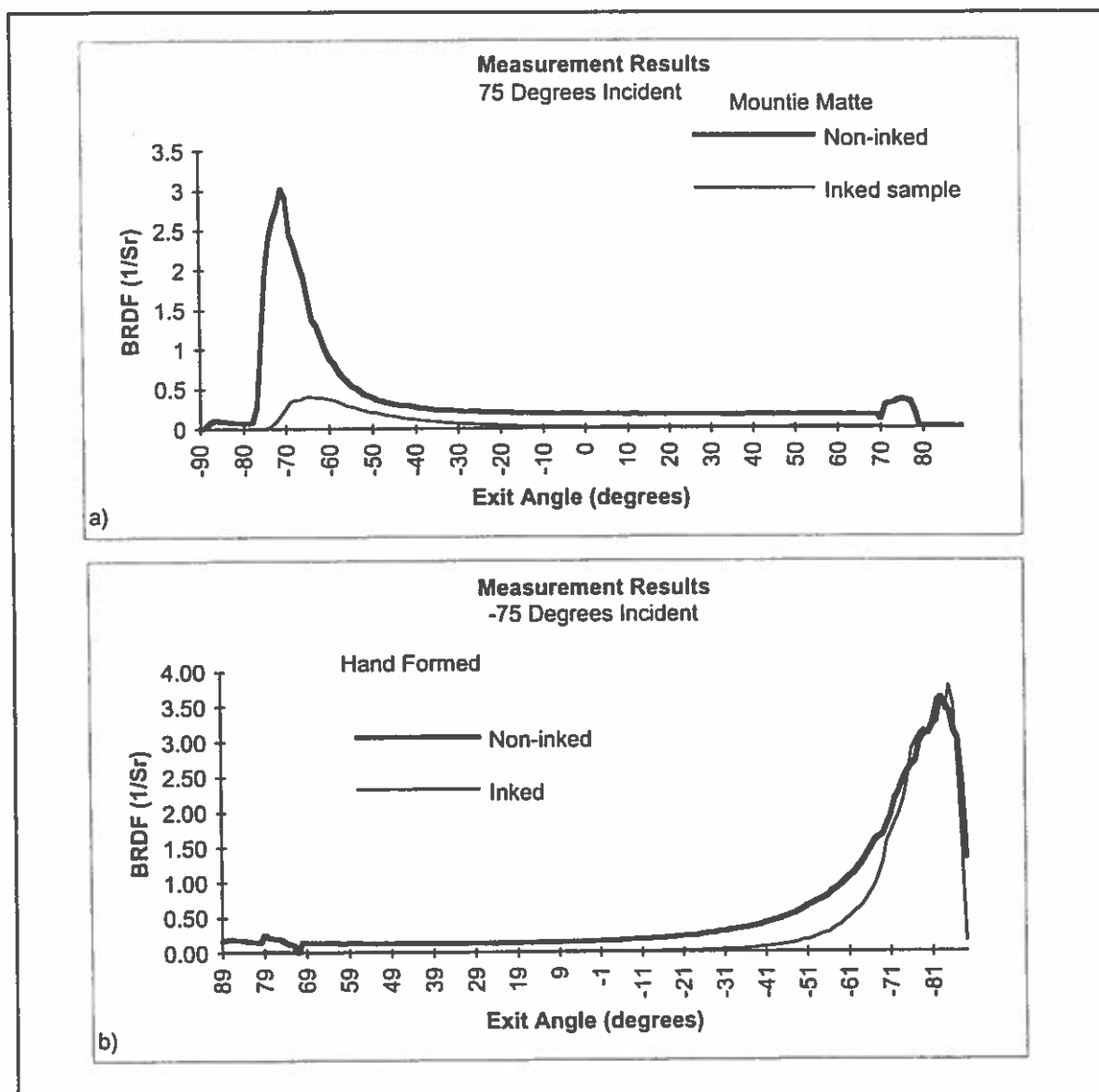
Figure 37: Comparison of measurement results for coated and uncoated paper samples. a) Mountie Matte specimen, coated. b) Hand-formed sample, uncoated.

While these results support the theory that the geometry of the calcium carbonate contributes to the observed retro-reflectance, it must be noted that the models used in these simulations represented a simplified version of the geometry of calcium carbonate. There is reason to believe that the geometry of a pigment plays some role in the observed

back-scatter phenomenon. However, with only these preliminary results, it would be premature to conclude that this is the primary source of this effect.

CHAPTER IV

CONCLUSIONS

The purpose of this study has been to explore the reflective properties of two materials, iridescent hummingbird feathers and paper sheets, in order to gain a better understanding of how their morphology affects their overall optical characteristics. We have also shown that by accurately modeling the microstructure of these materials computer simulations can be used to generate reflectance functions that agree well with both theoretical and measured results. These models and simulations provide valuable insight into some of the more complex reflective properties exhibited by these materials.

The first chapter of this thesis was concerned with reviewing the research done on surface reflectance functions in the field of computer graphics. The evolution of local reflectance models was described and culminated in the description of the virtual goniospectrophotometer developed by Gondek et al. for use in determining realistic surface reflectance functions. The approach used in this software consists of simulating the interaction of light with models of the microstructures of the surfaces under consideration. This tool was used in the work presented here to further explore the modeling of complex structures in generating accurate surface reflectance functions.

The first structure studied was the biologically occurring hummingbird feather. The iridescent colors displayed by some species of hummingbirds have long been thought to be the result of thin film interference. Electron microscopy has shown that iridescent feathers do in fact have a structure similar to multiple thin films. However, studies of the reflectance functions of iridescent feathers have shown that their spectral response curves

deviate from those of corresponding ideal thin films. The hummingbird feathers did not exhibit the characteristic secondary peaks found in multiple thin films, and their primary peak was also attenuated with a sharper bandwidth than predicted for corresponding thin films. Theoretical approaches to account for these deviations were developed by Greenwalt et al. around the hypothesis that they were the result of microfeatures of structures embedded in the barbules of the feather. These theoretically calculated reflectance functions were shown to agree well with empirical observations.

An attempt was made to model the microstructure of an iridescent feather in order to generate reflectance functions that had similar characteristics to those that had been measured and to those predicted by the Greenwalt theory. The first model constructed was composed of ideal thin films. It agreed well with theoretical ideal thin film calculations but did not exhibit the unique characteristics found in the actual structure. More complex models were constructed consisting of: broad plates, brick-like arrays, and flattened spheres respectively. The reflectance functions generated by the broad plates were essentially identical to the ideal thin films. Simulations on the brick-like array model produced reflectance functions which started to exhibit some of the deviations from ideal thin films that had been associated with the actual feathers. While these results were promising, the regular structure of the bricks did not approximate the actual platelet structure of the feather very well. A more complex model was constructed by employing a genetic algorithm that packed flattened spheres with a similar statistical orientation as found in the actual structure. The resulting model had appeared to be a much better structural analog to the actual feather, but its reflectance functions were disappointing. It was found through further observation that the curvature of the spheres used in the model prevented significant reinforcement from occurring because rays exiting the model were not parallel. A similar model composed of flattened cylinders may produce better results.

The next surface which was modeled was the manufactured structure of paper sheets. The visual characteristics that are of interest in the paper industry include: color, gloss, brightness, whiteness, opacity and reflectance. We began by discussing these properties and their meaning within the paper industry. We also reviewed a number of methodological and measurement standards that have been adopted by the industry in order to empirically compare these qualities. The two properties that are most important for a wide variety of applications are opacity and reflectance. The slightly different versions of these metrics that are used in various applications within the industry were explained along with the methods used to measure them.

Theoretical treatments that have been developed in order to predict optical characteristics based on the composition of the paper sheet were also reviewed in Chapter 3. These theories are used mainly in predicting the opacity and reflectance of composite sheets. The various parameters used in these formulations were described as well as the strengths and weaknesses of the different approaches. The next section of this chapter was devoted to discussing how several factors in the composition and production process affect the final appearance of a paper sheet. The previously discussed theoretical approaches can account for some of these effects. However, their predictive power is limited to only a certain class of characteristics. While these theories are useful in predicting the diffuse reflective properties of scattered light, they do not tell us anything about the spatial distribution of this scattering. None of the theoretical treatments we found in our literature survey dealt specifically with the spatial characteristics of scattered light from paper. We were able to explore this aspect of light scattering through a series of carefully planned measurements and by the use of our virtual goniophotometer tool.

Focusing on a few phenomena of interest, optical measurements were conducted on chosen sample sheets and light scattering simulations were performed in order to explore the mechanics of these effects. These phenomena included:

- the impact of formation (mass distribution) on overall reflectance,
- anisotropic reflectance functions caused by fiber orientation,
- retro-reflectance in the incident direction (back-scatter).

In each case computer models were developed and simulations were performed. The results were then compared to analytical results from the literature or measurements that were performed by a third-party laboratory.

In focusing on the effect that formation has on the reflectance of paper, we adopted a geometric model based on the theoretical work done by Scallan and Borsch. We confirmed that the results of simulations performed on this model were almost identical to theoretical results computed with equivalent parameters. We were then able to successfully reproduce the effect of mass distribution on reflectance by creating models which paralleled the development of later mass dependent theoretical treatments by Scallan and Borsch. Simulations run on this augmented model also agreed well with results obtained from their corrected formulas.

Anisotropies associated with fiber orientation have been documented with reference to the mechanical properties of a sheet. However, no previous work was found regarding the optical consequences of this phenomena. Our measurement results revealed that there were anisotropic properties in the reflection functions that are correlated with fiber orientation. Simulation results on webs modeled with varying degrees of orientational preference confirmed this relationship. Reflectance functions generated with these oriented models exhibited consistently higher specular peaks in the machine

direction than the cross-machine direction. This difference disappeared in simulations run on models with webs having no orientational preference.

The most surprising result found in our measurements was the presence of significant amounts of back scatter in certain cases. This effect was unexpected and had not been discussed anywhere in the paper literature we had reviewed. Comparisons of our models with the structure of the measured samples suggest that it is the result of the geometry of the coatings used on the paper. A model of this coating was constructed and was shown to generate reflectance functions with considerable back-scatter. The model coating was then combined with a simulated web and reflectance functions were generated that exhibited characteristics similar to the measured reflectance functions of the coated samples. Subsequent measurements on an uncoated sample showed much less retro-scatter, thus confirming our simulation results.

APPENDIX

SELECTED TAPPI TEST SPECIFICATIONS

Full text of these specifications can be found in TAPPI Test Methods 1994-1995, TAPPI Press, Item No. 0104 TM94, 1994.

•TAPPI T 94: Spectral Illuminate Specification
T 94 specifies the wavelength composition of standard illuminates that are used in visual (color) comparisons of sample sheets. This standard also includes procedural guidelines for the geometric viewing conditions: normal incident illumination and 45° viewing angle.

•TAPPI T 409: Machine Direction of Paper and Paperboard
This method describes several procedures for determining the grain, or machine direction of paper. A number of these tests were performed on the Mountie Matte sample in order to determine its machine direction. The first test involved cutting small squares of the sample which were placed atop water and observing their axis of curl. This axis is the machine direction. The second test involves observing the bend in two long strips of the paper which have been cut perpendicular to each other. The strip that was cut along the machine direction will show a greater tendency to bend under its own weight than the cross-machine strip. The final test involved tearing portions of the sample in perpendicular directions. Tears along the machine direction are more straighter. When performed on the Mountie Matte sample, all three tests indicated the same machine direction.

•TAPPI T 480 and T 653: Gloss Determination
Procedure T 480 is used for sheets that have low to moderate glossiness and involves measuring the specular reflection of incident light at 75° off-normal. The second method, T 653, is used for high gloss sheets and uses a measurement at 20° off-normal for reference. In both cases the specular reflection is referenced against measurements taken from an ideal standard of polished black glass with an index of refraction of 1.540. The specular reflection of this ideal standard is assigned 100 Gloss Units. Sampled measurements are then related to this standard in order to derive the Gloss Units for sampled sheets.

•TAPPI T 452: Brightness Determination
The methodology for measuring a sheet's brightness is described in TAPPI T 452. According to this standard, a pad of sheets is illuminated at a 45° incident angle and the

reflected light is captured at 0° (normal to the surface.) The reflected light is filtered so that a majority of the light captured is centered around a wavelength of 457 nm.

•TAPPI T 525: Diffuse Brightness Determination

This method describes the measurement procedures for the *diffuse brightness*, where the illumination is at 0° and the reflected light is captured for all exit directions in an integrating sphere. The ISO standard method for brightness determination is similar to this. Since the specimen is diffusely illuminated, this method is less dependent on surface characteristics such as grain orientation, and is the primary method used outside the United States. Other related test specifications are T 534 and T 646 which describe the methods for measuring diffuse and directional brightness on clay and other mineral pigments. For all of these cases special measuring instruments exist to determine the brightness.

BIBLIOGRAPHY

Blinn, J.F.   Models of Light Reflection for Computer Synthesized Pictures. *SIGGRAPH 94*. 1977. 192-198.

Borsch, J. and Scallan, A. M. An Interpretation of Paper Reflectance Based on Morphology: The Effects of Mass Distribution. *Tappi* Vol. 59 #10 Oct. 1976. 102-105.

Boyd, D. The Residual Set Dimensions of the Appolonian Packing. *Mathematika* Vol. 20. 1973. 130-135.

Bui-Tong, P. Illumination form Computer Generated Pictures. *Comminications of the ACM*. Vol. 18. June 1975. 311-317.

Bureau, W. H. *What the Printer Should Know about Paper*. Graphics Arts Technical Foundation. 1989.

Cabral, B.N. Max, N. and Springmeyer, R. Bidirectional Reflectance Functions from Surface Bump Maps. *SIGGRAPH 87*. Vol. 21 1994. 213-220.

Clark, H.B. and Ramsay, H. L.   Predicting Optical Properties of Coated Papers.   *Tappi* Vol. 48 #11 Nov. 1965. 609-612.

Cook, R.L and Torrance K.E. A Reflectance Model for Computer Graphics. *ACM Transaction on Graphics*. Vol. 1   1984. 7-24.

Dodson, C.T.J., and Fekih, K. The Effect of Fibre Orientation of Paper Formation. *Journal of Pulp and Paper Science* Vol. 17 #6 Nov. 1991. 203-205.

Gardener, M., Packing of Circles and Spheres. *Scientific American*. Vol. 218. 1968. 130-135.

Gondek, J. Wavelength Dependent Reflectance Functions. M.S. Thesis. University of Oregon. Eugene, 1994.

Gondek, J., Meyer, G. and Newman, J. Wavelength Dependent Reflectance Functions. *SIGGRAPH 94*. 1994. 213-220.

Greenwalt, C.H. *Hummingbirds*. Doubleday. Garden City, New York, 1960.

Greenwalt, C.H., Brandt, W., and Friel, D. Iridescent Colors of Hummingbird Feathers. *Journal of the Optical Society of America*. Vol. 50 #10 Oct. 1960. 1005-1013.

Haase, C. Modeling Pigmented Materials For Realistic Image Synthesis. M.S. Thesis. University of Oregon. Eugene, 1991.

Harrison, V. G. W. Optical Properties of Paper. *Formation and Structure of Paper Vol. 1*. William Clowes and Sons. London, G.B. 1962. 467-486.

Hect, E., and Zajac A. *Optics*. Addison-Wesley Publishing. Reading Mass. 1979.

Howard, G. J. The Influence of Polymers on the Light Scattering of TiO_2 Pigment in Paper. *Tappi* Vol. 66 #6 June 1983. 87-90.

Hunter, R. S. and Harold, R. W. *The Measurement of Appearance*. John Wiley and Sons. New York, New York, 1987.

Jayme, G. and Hunger, G. Electron Microscope 2- and 3-Dimensional Classification of Fibre Bonding. *Formation and Structure of Paper Vol. 1*. William Clowes and Sons. London, G.B. 1962.135-171.

Johns, W.D. Relationships Between Crystal Structures and Physical Properties. *Physical Chemistry of Pigments in Paper Coating*. TAPPI Press. Atlanta, Georgia, 1977. 20-50.

Jordan B.D. Predicting the effect of Formation on Opacity and Scattering Coefficient. *Journal of Pulp and Paper Science* Vol. 13 #6 Sept. 1987. 56-59.

Judd, D. B. Optical Specification of Light-Scattering Materials. *Tappi* Jan. 1938. 5-12.

Judd, D. B. and Wyszecki, G. *Color in Business, Science, and Industry*. John Wiley and Sons. New York, New York, 1975.

Kajiya, J. T. *Anisotropic Reflectance Models. SIGGRAPH 85*. Vol. 19. 1985. 15-29.

Kubelka, P. and Munk, F. *Z. Tech. Physik*. Vol. 12: 593 1931.

Land, M.F. The Physics and Biology of Animal Reflectors. *Progress in biophysics and Molecular Biology*. Vol. 24 1972. 77-106.

Mitton P. B. Opacity, Hiding Power, and Tinting Strength. *Pigments Handbook.* T. C. Patton ed. John Wiley and Sons. New York, New York, 1973. 289-339.

Murray, P. of Unisourse Worldwide Inc., Eugene Oregon. Personal Correspondence 2/95.

Pauler, Nils. Opacity and Reflectivity of Multilayer Structures. *The History of Papermaking.* 1983. 203-224.

Peterson, L. of Potlatch Industries Cloquet, Minnesota Personal Correspondence 3/95.

Ramsay, Howard L. Simplified Calculation for Predicting Optical Properties of Coated Board. *Tappi* Vol. 49 #12 Dec. 1966. 116-118.

Robinson, James V. A summary of reflectance equations for application of the Kubelka-Munk theory to optical properties of paper. *Tappi* Vol. 58 #10 Oct. 1975. 152-153.

Saunderson. Calculating of the Color of Pigmented Plastics. *Journal of the Optical Society of America* Vol. 32 1942. 727-736.

Scallan, A. M. and Borsch, J. An Interpretation of Paper Reflectance Based on Morphology: Initial Considerations. *Tappi* Vol. 55 #4 April 1972. 583-588.

Scallan, A. M. and Borsch, J. An Interpretation of Paper Reflectance Based on Morphology: General Applicability. *Tappi* Vol. 57 #5 May 1974. 143-147.

Simon, H. *The Splendor of Iridescence.* Dodd, Mead, & Co. New York, 1971.

Starr R. E., and Young R.H. A Study of the Light Scattering Coefficients of various Pigments using the Kubelka-Munk Analysis. *Tappi* Vol. 59 #12 Dec. 1976. 103-106.

Starr R. E., and Young R.H. Paper Coating Formulations: A study of the limitations involved in the determinations and use of the Kubelka-Munk constants. *Tappi* Vol. 61 #6 June 1978. 78-80.

Steele, F.A. The Optical Characteristics of Paper: 1. The Mathematical Relationships between Basis Weight, Reflectance, Contrast Ratio, and other Optical Properties. *Tappi* #12 March 1935. 37-52.

TAPPI Test Methods 1994-1995. TAPPI Press. Atlanta, Georgia, 1994.

Van Den Akker, J. A. Scattering and Absorption of Light in Paper and Other Diffusing Media: A note on the Coefficients of the Kubelka-Munk Theory. *Tappi* Vol. 32 #11 Nov. 1949. 498-500.

Van Den Akker, J. A. Optical Aspects of Coating Pigments. *Physical Chemistry of Pigments in Paper Coating*. TAPPI Press. Atlanta, Georgia, 1977. 337-364.

Van Den Akker. Optical Properties of Paper. *Handbook of Paper Science 2 The Structure and Physical Properties of Paper*. H.F. Rance ed. Elsevier Scientific Publishing Co. New York, New York, 1982. 127-174.

Westin, S.H. Arvo, J.R. and Torrance, K.E. Predicting Reflectance Functions from Complex Surfaces. *SIGGRAPH 90*. Vol. 26 1990. 255-264.

Wrist, P. E. Flow Properties of Fibrous Suspensions. *Surfaces and Coatings Related to Paper and Wood*. Marchessault and Skaar ed. Syracuse University Press. Syracuse, New York, 1967. 67-95.

Yuhara, T., Hasuike, M., and Murakami, K. Fibre Orientation Measurements with the Two-Dimensional Power Spectrum of a High-Resolution Soft X-Ray Image. *Journal of Pulp and Paper Science* Vol. 17 #4 July 1991. 110-114.